Fall 12-18-2015

The Role of Tumor Suppressor Co-Chaperone CHIP/STUB1 in ERBB2-Mediated Oncogenesis

Haitao Luan
University of Nebraska Medical Center

THE ROLE OF TUMOR SUPPRESSOR CO-CHAPERONE CHIP/STUB1 IN ERBB2-MEDIATED ONCOGENESIS

by

Haitao Luan

A DISSERTATION

Presented to the Faculty of

The University of Nebraska Graduate College

In Partial Fulfillment of the Requirements

For the Degree of Doctor of Philosophy

Genetics, Cell Biology & Anatomy
Graduate Program

Under the Supervision of Professor Hamid Band, M.D., Ph.D.

University of Nebraska Medical Center
Omaha, Nebraska

December 2015

Supervisory Committee:

Vimla Band, Ph.D.	Runqing Lu, Ph.D.
Xu Luo, Ph.D.	Amarnath Natarajan, Ph.D.

Acknowledgement

First of all, I would like to thank my advisor Dr. Hamid Band for his guidance and support. I greatly appreciate his mentoring and incredible patience, and I am very fortunate to have had the opportunity to learn from him. We have had many interesting and thought-provoking discussions that have encouraged and motivated me. He has been everything I could have hoped for in an advisor, and more.

I would like to thank the members of my supervisory committee, Dr. Vimla Band, Dr. Runqing Lu, Dr. Xu Luo and Dr. Amarnath Natarajan, for their valuable insight, suggestions, and support.

I would like to thank the current and former members of the Band lab for their help and support. They always are there when you need discussions or cheers or anything you want. Especially I thank Dr. Srikumar Raja and Dr. Tameka Bailey for their hand-to-hand help when I just entered the lab. I appreciate their kindness and help, without which, the road would be much more difficult in the beginning.

I would like to give my family the most thanks for their support and understanding for years. My dad Yuping Luan and my mom Xiaozhen zhou, they always stand by me. My wife, Xiangxue Lu, she gives me all the spiritual support during my whole graduate study. Thanks to you, now we are a family.

Lastly, I would like to thank the China Scholarship Council for the support of my four-year graduate study.

I dedicate my thesis to my family!

THE ROLE OF TUMOR SUPPRESSOR CO-CHAPERONE CHIP/STUB1 IN ERBB2-MEDIATED ONCOGENESIS

Haitao Luan, Ph.D.

University of Nebraska, 2015

Supervisor: Hamid Band, M.D., Ph.D.

The epidermal growth factor receptor (EGFR) family member ErbB2 (Her2) is overexpressed in 20 -30% of invasive breast cancers and this overexpression correlates with poor prognosis and shorter overall as well as disease-free survival. Aberrant expression of ErbB2 through gene amplification, transcriptional deregulation and/or altered endocytic trafficking results in overexpression of ErbB2 at the plasma membrane and biases ErbB2 from primarily ligand-driven hetero-dimerization under normal expression conditions to increased ligand-independent homo-dimer and hetero-dimer formation and consequent activation. C-terminus of HSC70-Inteeracting protein (CHIP)/STIP1-homologous U-Box containing protein 1 (STUB1) is an HSP90/HSC70 interacting negative co-chaperone known to promote ubiquitination and degradation of unfolded proteins, playing an essential role in protein quality control. HSP90/HSC70 are required for the stability and function of a variety of signaling proteins, including a number of protein kinases and their downstream signaling components. It is now known that CHIP can function as an E3 ubiquitin ligase towards such HSP90/HSC70 clients to induce their ubiquitination and degradation. ErbB2 is a prominent receptor tyrosine kinase that is dependent on its continuous association with HSP90 for its stability and function as an oncogene. Thus, CHIP, acting as an E3 ubiquitin ligase towards ErbB2 and its downstream signaling proteins has been hypothesized to function as a tumor

suppresser. Consistent with this idea, recent work indicates that CHIP mRNA and protein expression is reduced in a subset of breast cancers, primarily those that are estrogen-receptor negative and belonging to ErBB2+ and triple-negative subsets. How CHIP functions as a tumor suppressor in breast cancer in general and in ErbB2+ breast cancer in particular, has not been fully elucidated. In this thesis, we identify two inter-connected and novel mechanisms by which CHIP suppresses ErbB2-mediated breast oncogenesis. First, we demonstrate that CHIP targets newly synthesized HSP90/HSC70-associated ErbB2 for in the Endoplasmic Reticulum and Golgi for ubiquitin/proteasome-dependent degradation to negatively control the levels of cell surface ErbB2. Second, by analyzing CHIP expression in tissue microarrays from a large and well-annotated cohort of breast cancer patient samples, we identified a series of transcription factors whose cognate DNA-binding activity is up- or down-regulated by CHIP. We identify Myeloid Zinc Finger 1 (MZF-1), a transcription factor that transcriptionally upregulates the expression of extracellular matrix degrading enzymes cathepsin B and cathepsin L (CTSB/L) as a target of direct CHIP-dependent ubiquitination and degradation as well as indirect inhibition through reduced transcription. Small hairpin RNA (shRNA)-mediated depletion of CHIP in ER+ breast cancer cells or ectopic overexpression of CHIP in ErbB2 in ErbB2+ and triple-negative breast cancer cells demonstrated that loss of CHIP in the two latter subtypes of breast cancer is a principal determinant of MZF1-dependent upregulation of CTSB/L expression and activity, increased cell migration, invasiveness and matrix degradation, anchorage-independent growth in soft agar, and xenograft tumor formation and metastasis in vivo. Targeting of CTSB using specific chemical inhibition lead to statistically-significant tumor growth inhibition with reduced angiogenesis, correlating with inhibition of matrix degradation in vitro, suggesting altogether a potentially new therapeutic avenue to improve metastatic breast cancer treatment by targeting those tumors with reduced

CHIP expression for cathepsin inhibitor therapy in conjunction with conventional and ErbB2-targeted therapeutics.

Table of Contents

Chapter 1: Introduction

1.1 Protein maturation

1.1.1. Protein folding in the Endoplasmic Reticulum (ER)

Proteins destined for secretion or residence in the plasma membrane, Golgi apparatus, lysosomes, or ER are first translocated into the ER. Translocation of most polypeptides into the ER lumen occurs through the Sec61 protein channel (1). Targeting of soluble ER proteins and Type I membrane proteins is achieved by an N-terminal signal sequence. As these polypeptides enter the ER lumen co-translationally in an extended conformation, chaperones start to function and help them fold correctly. Binding immunoglobulin protein (BiP), also called glucose-regulated protein 78 (Grp78), is a member of the Hsp70 family of proteins and the major ER luminal chaperone. Like cytoplasmic chaperones, BiP maintains the polypeptides in a folding-competent conformation and prevents their aggregation. It is one of the first proteins that meets nascent polypeptides entering the ER along with other chaperones that are pre-assembled into a complex. This complex is poised to interact with the polypeptides being translocated into the ER and prevents the nascent chain from slipping backwards into the cytoplasm. Proteins containing the N-linked glycosylation consensus sequence (asparagine-X-serine/threonine, where X is any amino acid except proline) are recognized by the oligosaccharide transferase (OST) complex as the polypeptide exits the translocon on the luminal side. Glycosylation increases the protein's solubility, helps folding, and increases the stability of folded protein. The OST complex catalyzes the transfer of pre-assembled Glc3Man9GlcNAc2 (Glucose3, Mannose9, N-acetylglucosamine2) from dolichol pyrophosphate onto the asparagine residue of the glycan acceptor of the polypeptide. Once glycans are covalently attached to polypeptides, the two outer glucose residues are removed by Glycosidase I and II. This produces a Glc1Man9 GlcNAc2 glycan structure which is preferentially bound by the lectin chaperones calnexin and calreticulin. Calnexin and calreticulin recruit ERp57, an

enzyme that catalyzes one of the rate-limiting steps of protein folding, the disulfide bond formation. Binding of calnexin and calreticulin to polypeptide chains also provides time for polypeptides to fold and serves as an ER retention mechanism. When calnexin releases the glycan, glycosidase II removes the third and final glucose moiety. If the glycoprotein is correctly folded by this time, it is allowed to continue its progression through the secretory pathway. If the polypeptide has failed to fold correctly, it will be either given another chance to attempt folding or will be marked for removal from the ER and be degraded through ubiquintin-proteasome system (UPS). Re-entry into the calnexin/calreticulin cycle is achieved by re-glycosylation of the glycan by UDP-glucose: glycoprotein glycosyltransferase (UGGT)(2, 3)(Figure 1.1).

Once the proteins are correctly folded, native conformers enter ER exit sites. Vesicles that are coated with the coatomer protein (COP) II coat bud off and traffic through the ER-Golgi intermediate compartment (ERGIC) to the cis-face of the Golgi complex (4). In certain cases, the retrieval of misfolded proteins from the Golgi complex by COP I vesicles has been observed (5). The Golgi complex does not contain molecular chaperones and does not seem to support protein folding. Once the proteins pass through the cis-Golgi, they proceed through the trans-Golgi network (TGN) to the plasma membrane or beyond (Figure 1.2).

1.1.2. Endoplasmic Reticulum Associated Degradation

Terminally misfolded or unassembled proteins that are unable to acquire their native structure must be degraded to prevent fruitless folding attempts and the accumulation of misfolded polypeptides in the ER. This degradation process is known as ER-associated degradation (ERAD), which occurs in three primary steps: (1) recognition and targeting (substrate recognition within the ER and targeting to the retro-translocon),

(2) retro-translocation (substrate delivery from the ER to the cytosol), and (3) degradation (ubiquitin–proteasome dependent degradation)(6).

The recognition of misfolded or mutated proteins depends on the detection of substructures within proteins such as exposed hydrophobic regions, unpaired cysteine residues, and immature glycans. In mammalian cells, there exists a mechanism called glycan processing. In this mechanism, the lectin-type chaperones calnexin/calreticulin (CNX/CRT) provide immature glycoproteins the opportunity to reach their native conformation. They can do this by way of re-glucosylating these glycoproteins by an enzyme called UDP-glucose-glycoprotein glucosyltransferase. Terminally misfolded proteins, however, must be extracted from CNX/CRT. This is carried out by EDEM (ER degradation-enhancing α-mannosidase-like protein) and ER mannosidase I. The mannosidase removes one mannose residue from the glycoprotein and the latter is recognized by EDEM. Eventually EDEM will target the misfolded glycoproteins for degradation.

Because the ubiquitin–proteasome system (UPS) is located in the cytosol, terminally misfolded proteins have to be transported from the endoplasmic reticulum back into cytoplasm. The protein complex Sec61 is a possible channel for the transport of these misfolded proteins, however it is an unlikely candidate as retro-transport through the complex is difficult. It is unknown which other membrane protein(s) is responsible for this transport. Further, this translocation requires a driving force that determines the direction of transport. Since poly-ubiquitination is essential for the export of substrates, it is likely that this driving force is provided by ubiquitin-binding factors. One of these ubiquitin-binding factors is the Cdc48p-Npl4p-Ufd1p complex in yeast. Humans have the homolog of Cdc48p known as valosin-containing protein (VCP/p97)

with the same function as Cdc48p. VCP/p97 helps transport substrates from the endoplasmic reticulum to the cytoplasm using its ATPase activity.

1.1.3. Ubiquitin proteasome system

Ubiquitin itself is a highly conserved 76 amino acid protein which covalently attaches to substrate proteins through the formation of an isopeptide bond between ubiquitin's C-terminal carboxyl function and in most studied cases the ε-amino group of a lysine residue within the substrate protein. In eukaryotes, ubiquitin is abundant with levels around 0.1-5% of total cellular proteins (7). Ubiquitin forms a globular structure and is very stable. The transfer of a single ubiquitin to a substrate, a reaction referred to as mono-ubiquitylation, typically alters interactions, localization or activity of the modified substrate. Conversely, the attachment of multiple ubiquitin molecules results in polymeric chains, which, depending on their connectivity, could have unique functions. Ubiquitin chain formation can occur through seven lysine residues (K6, K11, K27, K29, K33, K48 and K63) or the N-terminus of ubiquitin (M1), leading to the assembly of multiple chains with distinct topology; the use of different lysine residues leads to more complex ubiquitin topologies. All linkage variants have been detected in cells and their abundance changes during the cell cycle or cell differentiation (8, 9).

Most ubiquitination reactions occur through the subsequent actions of an adenosine triphosphate (ATP)-dependent enzymatic cascade consisting of ubiquitin activating enzymes (E1), ubiquitin conjugating enzymes (E2) and ubiquitin ligases (E3). Two ubiquitin specific E1s exist in vertebrates called UBA1 and UBA6. The human genome contains about forty E2s. More than six hundred distinct E3s ensure the regulated modification of specific substrates within human cells (10).

As shown in Figure 1.3, the initial step in the ubiquitination cascade is the binding of Mg•ATP and ubiquitin to E1. Next, ubiquitin is adenylated at its C-terminus by E1 with

release of pyrophosphate (PPi). E1's catalytic cysteine sulfhydryl group attacks the ubiquitin adenylate bond leading to discharge of adenosine monophosphate (AMP) and the formation of a thioester between E1 and ubiquitin's C terminal carboxyl group. Another round of ubiquitin adenylation leads to a complex of E1 bound to the activated ubiquitin adenylate and the thioester ubiquitin intermediates. This single E1 bound to two activated ubiquitin species binds E2s with nanomolar affinities. Ubiquitin is then transferred to the catalytic site cysteine residue of the respective E2 in a trans-thio-esterification reaction. The ubiquitin charged E2 dissociates from E1, which now can undergo another cycle of ubiquitin thioester and subsequent ubiquitin adenylate formation. An E3 will bind an E2 loaded with ubiquitin and catalyze ubiquitin transfer from the E2's active site onto the substrate forming a stable isopeptide bond between ubiquitin's C terminal carboxyl group and a ε-amino group of a lysine residue of the respective substrate (11). This process can be repeated multiple times resulting in the formation of polyubiquitin chains on a substrate; engagement of the substrate already modified with ubiquitin by an E3 causes the addition of another ubiquitin moiety from an E2 leading to formation of a covalent bond between the C-terminus of E2 bound ubiquitin and a lysine residue of the substrate attached ubiquitin (12). E3 binding sites in substrates are called degrons if the E3 promotes substrate degradation. The determinants of E2/E3 pairing are further elaborated below. E3s can be divided in two major classes: really interesting new gene (RING) and homologous to E6-AP carboxy terminus (HECT) ligases. Ubiquitin ligases that further ubiquitylate oligoubiquitylated substrates are called E4s.

The human 26S proteasome is responsible for ubiquitin-dependent protein degradation in the ubiquitin proteasome system (UPS) (13). It consists of the proteolytic 20S core particle (CP) and a 19S regulatory particle (RP). The CP consists of 28 subunits encoded by 14 different genes and is shaped like a barrel in a symmetrical

manner (14, 15). The interior of the barrel is coated with six peptidase active sites, which together are able to hydrolyze a wide range of proteins into oligopeptides (14, 15). Entry into the inner chamber of the CP is regulated by the RP (13). The RP consists of 19 subunits in yeast and can be further subdivided into base and lid. Six different ATPases responsible for CP-RP complex formation, two scaffold proteins and two ubiquitin binding proteins, the 26S proteasome regulatory subunits Rpn10/S5a and Rpn13 (also called ubiquitin receptors), make up the base. ATP binding to the ATPases is necessary for proper assembly of the complex formations. ATP hydrolysis is required for protein unfolding and translocation of the unfolded polypeptide via a channel into the proteolytic chamber of the CP (13). The only assigned function for one of the nine lid subunits is the deubiquitinase (DUB) activity of Rpn11, which is important for proteasome activity cleaving off a ubiquitin chain in one step at the proximal ubiquitin. Consequently, the concerted actions of CP and RP enable the 26S proteasome to bind a ubiquitylated protein via its ubiquitin receptors, to unfold the protein with its ATPases, to cleave off ubiquitin with its DUB and to translocate the unfolded protein into the inside of the CP, where its peptidases hydrolyze the proteins. Several other proteins bind the proteasome, regulating its function. The ATP-driven chaperone valosin-containing protein/p97 (p97) has been implicated in targeting ubiquitylated proteins to the proteasome as well (16, 17). In complex with its cofactors, which have ubiquitin binding domains, p97 is able to interact with ubiquitylated proteins (17, 18). Using its so-called “segregase” activity, p97 can extract proteins from the ER or the mitochondrial membrane as well as chromatin for proteasomal degradation; it has also been shown to be involved in the clearance of intracellular protein aggregates, in autophagy and in endosomal trafficking (19).

1.2 Molecular Chaperones

1.2.1. Hsp70 family

The Hsp70 family is one the most ubiquitous and conserved classes of chaperones, existing in almost all living organisms. The sequence identity between prokaryotic Hsp70, DnaK, and its eukaryotic homologues is around 60% (20). In eukaryotes, Hsp70s are found in the cytosol, mitochondria (mtHsp70), chloroplasts (cpHSC70), and ER (Grp78/Bip) (21). In mammals, there are two isoforms of cytosolic Hsp70, constitutively expressed Hsc70 and stress-inducible Hsp70. Hsp70 is composed of three structural domains, a 44 kDa N-terminal ATPase domain followed by an 18 kDa substrate binding domain (SBD) and a 10 kDa C-terminal domain (22). Clients interact with the hydrophobic pocket in the SBD, and the interaction is profoundly affected by the interaction between Hsp70 and nucleotides. In the ATP bound-state, Hsp70 has a low affinity but fast exchange rate, while the ADP bound-state shows high client affinity but slow exchange rates (22, 23). Moreover, the position of the C-terminal lid is different. In the ADP-bound state, the lid moves closer to the SBD, which prevents the release of client protein (24, 25). Hsp70s facilitate not only the protein folding or refolding, but also the degradation and translocation. To achieve these functions, Hsp70 works together with J-proteins (Hsp40s) and nucleotide exchange factors. These co-chaperones regulate the Hsp70 machinery by either conferring client specificity or affecting the interaction with nucleotides.

The Hsp70 chaperone machine does not always act alone, but also cooperates with other chaperone machines. For example, in the folding of nascent polypeptides, Hsp70 interacts with unfolded clients and then transfers them to the Hsp90 chaperone machinery through the adaptor protein Hop (Hsp70-Hsp90 Organizing Protein) for final maturation and activation (26). Hsp70 forms an early complex with client proteins, Hop binds to the open conformation of Hsp90 and acts as the attachment site for Hsp70 bound client protein. Hop facilities the transfer of the client protein from Hsp70 to Hsp90 and the intermediate complex is formed. Hsp90 converts to the closed conformation

after binding of ATP and p23. After the hydrolysis of ATP, p23 and the folded client protein are released from Hsp90 (25, 27).

1.2.2. Hsp90 family

Hsp90 is a highly conserved molecular chaperone that is essential in eukaryotes (28, 29), and is one of the most abundant proteins, even in unstressed cells (30, 31). It contributes to various cellular processes including signal transduction, protein folding, intracellular transport, and protein degradation.

Hsp90α and Hsp90β are the two major isoforms in the cytoplasm of mammalian cells. Hsp90α is the major form which is inducible under stress conditions, while Hsp90β is constitutively expressed (32, 33). Hsp90 analogues also exist in other cellular compartments such as Grp94 in the endoplasmic reticulum and Trap-1 in the mitochondrial matrix.

One thing of note is that Hsp90 is highly overexpressed in cancer cells (34, 35). They utilized the Hsp90 machinery to protect mutationally-activated and overexpressed oncoproteins from misfolding and degradation, thereby contributing to tumor survival.

1.3 The ErbB family of receptor tyrosine kinases

1.3.1. Structure of ErbB receptors

The Epidermal Growth Factor Receptor (EGFR) family of receptor tyrosine kinases (RTK) consists of four members: EGFR (ErbB1, HER1), ErbB2 (HER2; Neu in rat), ErbB3 (HER3), and ErbB4 (HER4). They are all Type I class of receptors, sharing similar structural characteristics including an extracellular ligand binding domain, a single pass hydrophobic transmembrane domain, a highly conserved catalytic protein tyrosine kinase (TK) core followed by a carboxyl terminal stretch containing several critical

tyrosine residues (36). The extracellular region of the ErbB family of RTKs is comprised of four distinct subdomains: two homologous ligand-binding domains (I and III) and two cysteine-rich domains (II and IV). One function of subdomains II and IV is to maintain an auto-inhibited configuration through intramolecular contacts, thereby forcing subdomains III and I into a relative orientation that prevents high-affinity binding of a ligand. Once a ligand binds to sub domains I and III, this alters the configuration of the extracellular region and exposes a dimerization arm located in sub domain II, thus allowing it to make intermolecular links with an adjacent receptor and driving dimerization (37). The tyrosine kinase domain is responsible for the transfer of a phosphate group from an ATP molecule to a tyrosine residue on a protein substrate. As mentioned above, the most highly conserved region within all ErbB family members, as is the case with most other RTKs in general, is the tyrosine kinase domain. One exception however is the ErbB3 protein. This receptor shares the least sequence identity with the other ErbB receptors, including residues that are critically conserved throughout all protein kinases, thus rendering it catalytically inactive (38). The carboxyl-terminal tail sequences are among the most divergent between ErbB receptors (39). Sequence alignment comparing the carboxyl-terminus shows the highest level of conservation between the EGFR and ErbB2 receptors, particularly in the several tyrosine autophosphorylation sites that have previously been mapped in the carboxy-terminus of the EGFR and ErbB2. It is these phosphorylated residues that are recognized and bound by specific intracellular proteins, thereby initiating a highly coordinated signal cascade (40). All ErbB receptors other than EGFR are endocytosis-resistant after ligands binding (41).

1.3.2. Activation of ErbB receptors

Typically, ErbB receptors are activated by a number of ligands, adding to the potential and diversity of ErbB signaling responses (42). Each ligand, now commonly

referred to as EGF-like peptide, has an EGF-like domain that is sufficient to confer unique specificity for its receptor substrate and they have the ability to modulate the catalytic activity of the receptor. Most of these ligands act over short distances as autocrine or paracrine factors and their availability or expression pattern in a tissue-specific or developmental stage-specific pattern offer a level of control over their signaling potential. The EGF-like peptides are divided into three groups based on their specificity: epidermal growth factor (EGF), amphiregulin (AR) and transforming growth factor-a (TGF-a) specifically activate EGFR (43); betacellulin (BTC), heparin-binding EGF (HB-EGF) and epiregulin (EPR) exhibit dual specificity for EGFR and ErbB4 (40); and the neuregulins (NRG) bind to both ErbB3 and ErbB4 (44). No direct soluble ligand for ErbB2 has been identified to date and it remains an orphan receptor. In fact, structural analyses of the ectodomain of ErbB2 suggest that it may not require ligand binding and remains in a conformation that is conducive to oligomerization. However, there have been reports suggesting that a member of the Mucin family known as Muc4/sialomucin may act as an unconventional intramembrane ligand for ErbB2 (45-47). Interestingly, Muc4/sialomucin contains EGF-like domains that are similar in sequence to the EGF-like domains in the NRG ligands (48) and is capable of activating ErbB2 leading to limited ErbB2 phosphorylation as well as inducing the translocation of ErbB2 from the basolateral surface to the apical surface in polarized epithelial cells (49, 50). Also, ErbB2 is the only receptor that needs Hsp90 binding for its stability even in its fully mature state and at the cell surface.

1.3.3. ErbB2 and breast cancer

Elevated expression of the ErbB receptors has been observed in clinical studies of a significant number of sporadic breast cancers (51). Indeed, overexpression of EGFR in mammary carcinomas inversely correlates with patient outcome (52). Furthermore, a

limited number of studies relating the ErbB3 receptor with human breast cancer have concluded that approximately 22% of cases involved elevated levels of ErbB3, however there was no evidence that this was the result of gene amplification. Other studies suggest that ErbB3 may be a culprit along with ErbB2 in breast cancer by relating the coincidental elevated co-expression of ErbB2 and ErbB3 in mammary tumors (53) or the requirement for both ErbB2 and ErbB3 to drive breast tumor cell proliferation.

To this end, a number of clinical studies have estimated that amplification and overexpression of the erbB2 is involved in about 20-30% of human breast cancer (54-58). The consequences of this have been correlated with a poor clinical prognosis for the patient with increased chance of relapse and death (54, 55, 59-61). Consistent with other receptors, activating mutations seem to only play a minor role in ErbB2-related human cancers. It should be noted however that despite the identification of the V664E activating mutation in the sequence of the rat Neu transmembrane region (62), a comparable mutation has not been found in human ErbB2. Instead, mutations, when found, are within the kinase domain. Thus, it appears that expression of erbB2 to elevated levels either through gene amplification or deregulated expression of wild type erbB2 is the primary mechanism of ErbB2-driven oncogenesis. Notably, an alternatively spliced isoform of ErbB2 was detected in human breast tumor samples and this mutant receptor displays elevated catalytic activity in vitro (63). The alternate splicing results in an ErbB2 receptor that is strikingly similar to the activating deletion mutations identified in Neu-induced murine tumors, which have a higher propensity to dimerize (53, 64). However, the exact role and function of the alternatively spliced ErbB2 receptor in the normal mammary gland and/or in mammary oncogenesis is not clear at this point..

1.4 Carboxyl terminus of Hsp70-interacting protein (CHIP)

1.4.1. Structure of CHIP

CHIP, also known as STUB1 (STIP1-homologous U-Domain-containing protein 1; STIP1 is an alternative name for Hop) was discovered in an attempt to identify novel TPR-containing proteins in the human heart. In these studies, a fragment of the human CyP-40 (cytochrome P-40) cDNA, corresponding to its TPR domain-encoding nucleotides 721 to 1150, was radiolabeled with [α-^{32}P] dCTP and used to screen a phage library of human heart cDNAs at low stringency (65). CHIP cDNA encodes a 34.5-kDa protein. Evolutionarily, CHIP is a well-conserved protein with an amino acid sequence similarity of ~98% with mouse and ~60% with the fruit fly (66). Intracellularly, CHIP was found to primarily localize to the cytoplasm under quiescent conditions (65) although a fraction of CHIP was later found to be present in the nucleus as well (67).

CHIP is an E3 ubiquitin ligase, has two characteristic domains, one the tetratricopeptide repeats (TPRs) at its amino terminus, which serves as the protein-protein interaction domains, interacting in particular with heat shock proteins (Hsp70, Hsc70 and Hsp90) through binding to their conserved c-terminal “EEVD” motifs. Another important and unique domain is the U-box domain at the carboxyl-terminus region. The U-box domain was first recognized in yeast Ufd2 protein, which perform “E4” activities. Moreover, the tertiary structure of U-box resembles that of the RING finger domain, which is responsible for E3 activities for a large family of ubiquitin ligases (68). Also, CHIP participates in ubiquitinated substrate delivery to the proteasome by interacting with the S5a proteasome subunit. Therefore, CHIP protein mediates interactions between the chaperone system and the ubiquitin-proteasome system (69-72).

1.4.2. CHIP in protein quality control

The classical role of chaperones was initially regarded as those of folding and salvaging proteins. However, it became clear that each and every newly synthesized polypeptide that engages with chaperones for its folding could not reach a native state,

and thus there must be a link between the chaperones and the degradation pathways. CHIP provides that link. CHIP was shown to inhibit the forward cycle of chaperones. However, the actual role of CHIP became clarified when it was shown to have intrinsic E3 ligase activity owing to the C-terminal U-box. Experimental studies with increased cellular levels of CHIP found a marked shift towards degradation of the HSP90/HSC70 clients, glucocorticoid receptor (GR) (65, 73), ErbB2 (74, 75), serum-and glucocorticoid-regulated kinase (SGK1) (76) and CFTR (77, 78). Definitive evidence for a quality control role of CHIP was provided when it was shown to selectively promote the ubiquitination of thermally denatured luciferase (and not the native form) when captured by Hsc70 and Hsp90 (70, 71, 79). That CHIP may participate in protein turnover was hinted by initial observations depicting a relatively higher expression of CHIP mRNA in tissues with a large proportion of terminally differentiated, non-proliferating cells and high levels of metabolic activity such as skeletal muscle, heart, and brain (65). The physiological importance of CHIP came into light with the observations that ~20% of CHIP null (CHIP − /−) mice die at embryonic stages and 100% fail to survive thermal stress (80).

CHIP was previously shown to cooperate with the UbcH5 family of E2s to catalyze Lys-48-linked poly-ubiquitination. UbcH5 is a stress-associated E2. UbcH5~Ub conjugates have been shown to adopt both infinite spiral and linear staggered (backside interaction) arrangements. Interestingly, CHIP can directly interact with four (or more) UbcH5~Ub conjugates allowing wide conformational flexibility during poly-ubiquitination of substrates (81). One consequence of this is the possibility of formation of forked ubiquitin chains.

Later, Xu and coworkers (82) reported CHIP to interact with the dimeric ubiquitin E2 complex Ubc13-Uev1A, which catalyzes the synthesis of Lys-63-linked poly-ubiquitination. They analyzed crystal structures of mouse CHIP U-box in complex with

Ubc13-Uev1a and found a common “Ser-Pro-Ala” motif present in UbcH4, UbcH5, and Ubc13 that mediates, and is necessary for, their interaction with the CHIP U-box. Although the catalysis of K63-linked poly-ubiquitination is an inherent structural feature of Ubc13-Uev1A, it is not clear at present how the binding of CHIP to Ubc13-Uev1A facilitates the process. Interestingly, CHIP only stimulates the formation of free K63-poly-ubiquitin by Ubc13-Uev1a and thus may have to interact sequentially with other E2 enzymes to attach K63-linked poly-ubiquitin chains on substrates. CHIP binds 3- to 5-fold more strongly to uncharged Ubc13 than UbcH5a. It remains to be seen whether CHIP displays similar relative binding affinities towards ubiquitin charged E2s.

1.4.3. CHIP in breast cancer

Kajiro et al. (83) showed that CHIP mRNA and protein expression was reduced in a small fraction of breast cancer patient tumors that were predominantly estrogen receptor (ER)-negative. In vitro and xenograft studies with cell lines expressing high or low CHIP indicated that CHIP is an important negative modulator of breast tumor progression. Subsequently, a number of studies have connected CHIP expression differences to breast and other cancers. Interestingly, there seems to be a dispute regarding the oncogenic or tumor suppressive role of CHIP. It was reported that tumor growth and metastasis were negatively correlated to CHIP levels in a nude mouse xenograft model of breast tumor. CHIP also seemed to regulate the levels of a number of well-known oncogenic proteins like the steroid receptor coactivator SRC- 3 and inhibit anchorage-independent cell growth and migration. Supporting this finding, some of the later studies reported CHIP to negatively regulate breast tumor promoting proteins like TRAF2, NF-kB, PTK6, and MIF (macrophage inhibitory factor). These studies also documented inhibition of various oncogenic properties of breast tumor cells such as MCF7 and MDA-MB-231 (84-86). Further supporting its role as a tumor suppressor,

CHIP has been reported to degrade a number of other critical oncoproteins such as pAkt (87, 88), c-Myc (89), HIF-1 (90, 91) and ErbB2 (74, 75, 92) in various cancers. Patani et al. (93) assessed the mRNA expression of CHIP in normal and malignant breast tissues and correlated with clinico-pathological characteristics. They found a striking decrease of CHIP expression with increasing malignant grades (TNM stages). Further, the overall patient survival for low CHIP-expressing tumors was significantly lower than high CHIP-expressing tumors. This study identified CHIP as an important favorable prognostic marker (93). However another study suggested that expression of CHIP was a negative prognostic factor for breast cancer (92). It is known that chaperones (Hsp70 and Hsp90) are overexpressed in cancers and many cancer are addicted to these proteins. Indeed, many phase III clinical trial drugs are specific inhibitors of chaperones (35, 94). The co-chaperones HOP Hop and CHIP compete with each other for chaperone binding and exert mutually opposite effects on chaperone function. While CHIP tilts the balance toward pro-degradation pathway, Hop favors a pro-folding outcome. Consequently, an understanding of the relative levels of co-chaperones Hop and CHIP is of importance. Another group observed higher expression of Hsp70, Hsp90, and Hop in colorectal cancer. They demonstrated that like Hsp70 and Hsp90, Hop (but not CHIP) is a transcriptional target of HSF1 which itself is upregulated in cancers, thus forming a positive feedback pro-carcinogenic circuit. Further, the ratio of Hop to CHIP was suggested to be a better prognostic marker than individual levels of either protein. Seemingly, the downregulation of CHIP is an independent event necessary for the realization of this circuit (95). In yet other interesting study, mRNA and protein levels of CHIP were found to be significantly lower in more than 75% of gastric tumors relative to normal tissue which are in line with previous reports in other cancers (96).

Thus far, the molecular mechanism in which CHIP regulates oncoproteins and suppresses oncogenesis is still largely unknown. In particular, there is paucity of

information on key CHIP-regulated molecular pathways that contribute directly to oncogenic traits and can be targeted for therapy. Studies presented in this study were aimed to elucidate the role of CHIP in ErbB2+ breast cancers with a focus on identifying therapeutically-targetable pathways.

Figure 1.1. Schematic of protein maturation in the ER.

(A) Protein folding in the ER. (B) The ER to Golgi apparatus trafficking.

Adapted from Ellaaard L. and Helenius A., (97) .

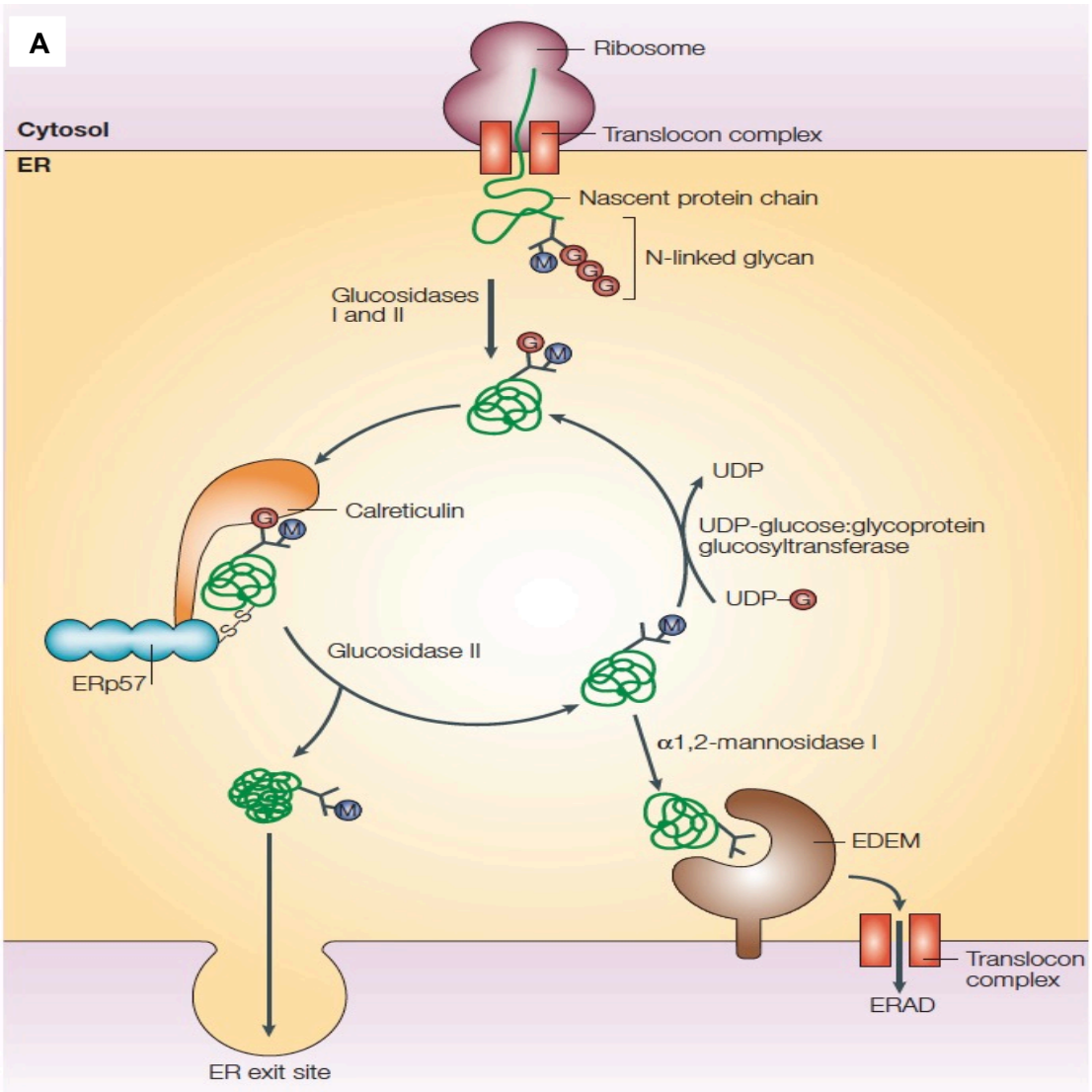
A
Ribosome
Cytosol
Translocon complex
ER
Nascent protein chain
N-linked glycan
Glucosidases I and II
UDP
Calreticulin
UDP-glucose:glycoprotein glucosyltransferase
UDP-G
Glucosidase II
ERp57
α1,2-mannosidase I
EDEM
Translocon complex
ERAD
ER exit site

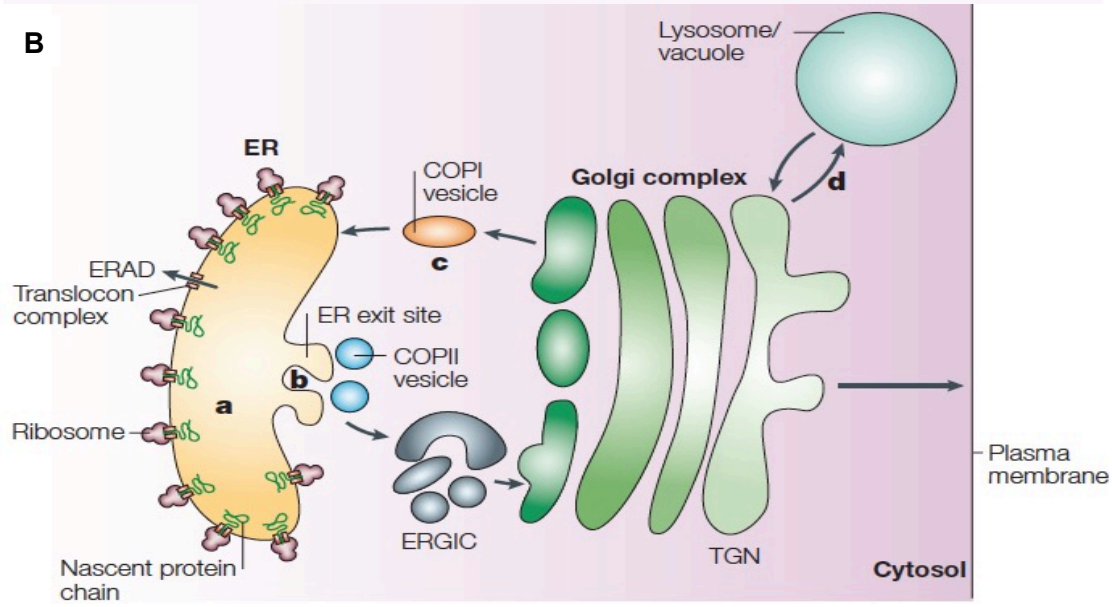
B
Lysosome/ vacuole
ER
COPI vesicle
Golgi complex
d
c
ERAD
Translocon complex
ER exit site
COPII vesicle
b
a
Ribosome
Plasma membrane
ERGIC
TGN
Nascent protein chain
Cytosol

Figure 1.2. Schematic of ubiquin cascade and proteasome-mediated protein degradation

Ubiquitination is carried out in three main steps; activation, conjugation and ligation. Ubiquintin-tagged substract is transported to proteasome for degradation. Adapted from Yoshida Y. et al., (98).

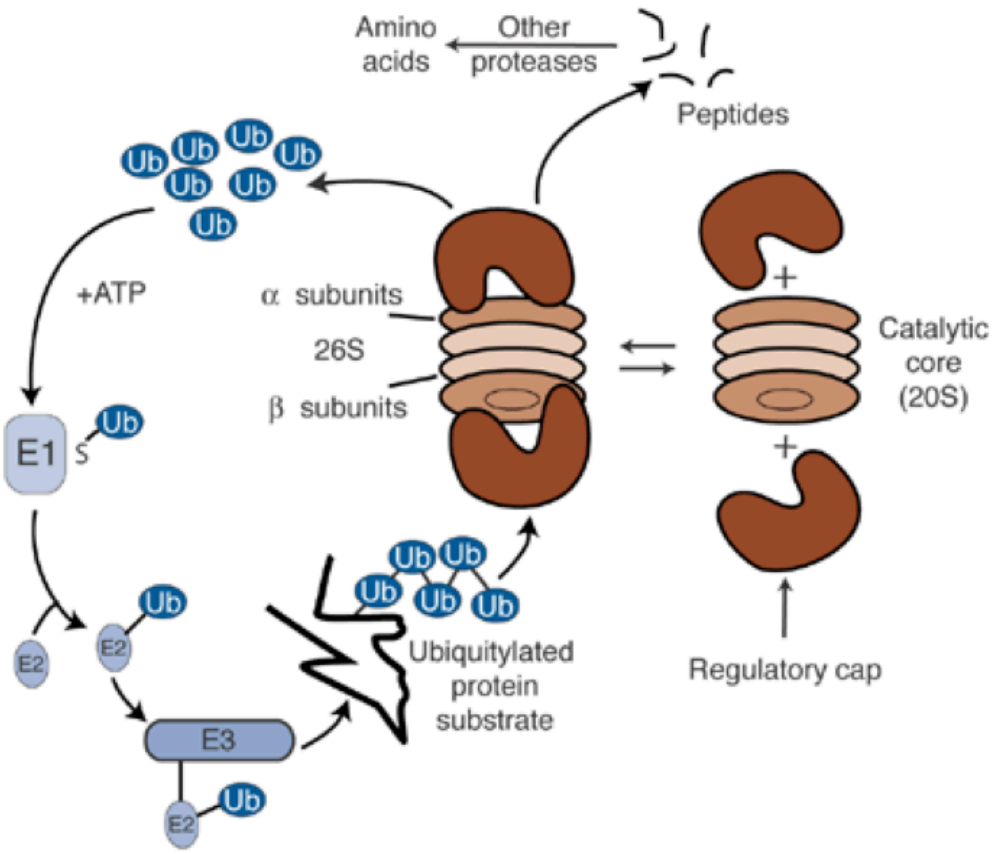
Amino acids
Other proteases
Peptides
Ub
+ATP
α subunits
26S
β subunits
Catalytic core (20S)
E1
E2
E3
Ubiquitylated protein substrate
Regulatory cap

Chapter 2: Materials and methods

2.1 Cell lines and medium

ErbB2-overexpressing breast cancer cell lines SKBR3 and BT474 were cultured in complete α-MEM medium with 5% fetal bovine serum, 10 mM HEPES, 1 mM each of sodium pyruvate, nonessential amino acids and glutamine, 50 μM 2-ME, and 1% penicillin/ streptomycin (Life technologies, Carlsbad, CA). ErbB2-overexpressing breast cancer cell line 21MT1 cells, obtained from Dr. Vimla Band, was cultured in α-HE medium (α-MEM medium supplemented with 1 μg/mL hydrocortisone and 12.5 ng/mL epidermal growth factor (Sigma-Aldrich, St. Louis, MO)) (99). The lentiviral packaging cell line TSA-54, the ER+ breast cancer cell line MCF7 and the ErbB2-negative and estrogen receptor/progesterone receptor-negative (triple-negative) breast cancer cell line MDA-MB-231 was cultured in complete DMEM medium with 5% fetal bovine serum, 10 mM HEPES, 1 mM each of sodium pyruvate, nonessential amino acids and glutamine, 50 μM 2-ME, and 1% penicillin/ streptomycin (Life technologies, Carlsbad, CA).

2.2 Antibodies and reagents

The following antibodies were used for immunoblotting: Ubiquitin – monoclonal antibody P4D1 from Cell signaling, Denver, PA; ErbB2 – monoclonal antibody (Cat. 554299) from BD-Pharmingen, San Jose, CA; Phospho-tyrosine - 4G10 monoclonal antibody from EMD Millipore, Billerica, MA; Hsc70 - B-6 antibody from Santa Cruz Biotechnology, Santa Cruz, CA; CHIP – Rabbit anti-serum made in the laboratory through Covance Research Products, Denver, PA (75). CHIP IHC staining was performed using polyclonal rabbit antibody from Thermo Scientific, Waltham, MA. ErbB2-specific phosphorylation was assessed using anti-phospho-ErbB2-Y1248 antibody from Cell Signaling Technology, Danvers, MA. Secondary reagents used for immunoblotting included horseradish peroxidase (HRP)-conjugated Protein A and Rabbit anti-Mouse HRP (Invitrogen, Carlsbad, CA). ErbB2 immuno-staining was carried out

using the AF1129 antibody from R&D Systems, Minneapolis, MN, or Alexa Fluor-488 or 647-conjugated mouse anti-human ErbB2 (CD340) monoclonal antibodies (clone 24D2; cat. 324410 and 3244412, respectively) from Biolegend Inc., San Diego, CA, and Alexa Fluor -488 or 647 mouse mAb IgG1 (MOPC-21) controls (cat. 400129 and 400130) also from Biolegend. Secondary antibodies for immunostaining included Alexa Fluor 488 donkey anti-goat IgG for ErbB2 and Alexa Fluor 594 donkey anti-rabbit IgG for phospho-ErbB2-Y1248 from Invitrogen Molecular Probes, Eugene, OR. 17-AAG was obtained from Biomol, Plymouth, PA, and stocks prepared at 10 mg/ml or higher in DMSO. Trastuzumab (obtained from UNMC pharmacy) was dissolved in Phosphate Buffered Saline (PBS). Brefeldin A (Sigma-Aldrich, St. Louis, MO) was dissolved in DMSO. Cathepsin B-specific inhibitor CA074 (Sigma-Aldrich, St. Louis, MO) was dissolved in 1% DMSO in PBS.

2.3 Protein lysis and quantification

Cells were either lysed in Radio-Immuno-Precipitation Assay (RIPA) lysis buffer (50 mM Tris pH 7.5, 150 mM NaCl, 1% Triton-X-100, 0.05% deoxycholate, 0.1% Sodium Dodecyl Sulfate (SDS)) with or in Triton-X-100 lysis buffer (50 mM Tris pH 7.5, 150 mM NaCl, 0.5% Triton-X-100), 1 mM PMSF, 10 mM NaF, and 1 mM sodium orthovanadate. Lysates were rocked at 4°C for a minimum of 1 hour, centrifuged at 13,000 rpm for 20 minutes at 4°C in a bench-top micro-centrifuge and supernatants were transferred to fresh tubes. Protein concentrations of samples were estimated using the Bicinchoninic acid (BCA) assay kit (Thermo Fisher Scientific, Rockford, IL) or the Bradford assay reagent (Bio-Rad Laboratories, Hercules, CA) using bovine serum albumin (BSA) as a standard.

2.4 Immunoprecipitation (IP) reactions

Cells were lysed in RIPA buffer. Following the total protein estimation of the lysate samples, the optimized ratio of total lysate and antibody was allowed to incubate on a rocker overnight at 4°C. 200 µL of 10% Protein A Sepharose (PAS, GE Healthcare, Chalfont St. Giles, UK) beads (washed with RIPA buffer) were added to each IP sample and rocked at 4°C overnight. Following this incubation, the samples were centrifuged for 5 minutes at 13,000 rpm at 4°C, the supernatant was removed to a separate tube, and the beads were washed five times with 1 m1 of RIPA buffer. Then, 100 µL of 2X sample buffer (10% glycerol, 3% SDS, 0.02% bromophenol blue, 0.5X Upper Tris [4X Upper Tris -0.5 M Tris pH 6.8, 0.4% SDS]) was added to each sample, heted at 95^{o}C for 3-5 min, resolved by SDS-Polyacrylamide (Biorad) Gel Electrophoresis (PAGE), transferred to Polyvinylidene fluoride (PVDF) membrane (Bio-Rad Laboratories, Hercules, CA) and subjected to Western Blotting(75).

2.5 Confocal immunofluorescence microscopy

Cells were grown on glass coverslips inside the wells of a 24-well tissue culture plate. After the completion of an experiment cells were fixed in 4% paraformaldehyde (PFA) in PBS for 20 minutes. The PFA solution was removed and the cells were permeabilized for 20 minutes in immunofluorescence (IF) buffer (10% FBS, 0.2% BSA, and 0.05% saponin in PBS). The cells were then stained with primary antibodies for overnight at 4 °C followed by three 10-minute washes in PBS. The cells were then incubated with the appropriate secondary antibodies for 1 hour (diluted 1:500 in the IF buffer), followed by three 10-minute washes in PBS. In preparation for confocal microscopy, PBS was removed and the coverslips were carefully removed and inverted onto glass microscope slides with Vectashield mounting medium (Vector Laboratories, Burlingame, CA), which contained 4′, 6-diamidino-2-phenylindole (DAPI) to stain DNA in the nucleus of the cell. The coverslips were allowed to adhere to the surface and dry for

5 minutes or more, and then images were captured using a Nikon C1 confocal microscope.

2.6 Transfection and plasmids

XtremeGENE 9 transfection reagent was from Roche Applied Science (Indianapolis, IN); siRNA smartpools and Dharmafect I transfection reagent were from Dharmacon division of Thermo-Fisher (Pittsburgh, PA). Fluorescent Golgi marker plasmid Pm-Turquoise2-Golgi was purchased from Addgene (plasmid No. 36305).

2.7 ^{35}S-methionine/cysteine pulse-labeling followed by chase (pulse-chase)

Cells were grown in 10-cm dishes until sixty to seventy percent confluent. The medium was removed, cells were washed three times with PBS, and incubated with methionine- and cysteine-free DMEM medium [cat. 21013-024, Life technologies, Carlsbad, CA]) for 30 minutes at 37 °C. 35S-labeled methionine/cysteine mixture (EXPRE35S35S Protein Labeling Mix, cat. NEG772, from Perkin Elmer, Waltham, MA) was added to a final concentration of 0.5 mCi/ml. After 20 minutes, cells were washed three times with cold PBS and chased with complete DMEM medium supplemented with 100 fold extra unlabeled methionine and cysteine for various time points with or without brefeldin-A treatment.

2.8 Analysis of cumulative proliferation

Cells were grown in 6-well plates at a density of 5,000 cells per well. The cells were counted after seven-day culture and re-plated in fresh 6-well plates at the original plating density for a total of five serial cultures. The cumulative cell numbers were calculated based on the fractions of each harvest used for replating and plotted as a function of the times cells were re-plated.

2.9 Anchorage-independent growth on soft agar

2,500 cells were seeded in 0.35% soft agar on top of 0.6% soft agar layer in 6-well plates. After two weeks, cells were stained with crystal violet and imaged under a phase contrast microscope. The colonies were enumerated using the Image J (NIH, MD).

2.10 Trans-well migration and invasion assays

The migration and invasion assays were performed in trans-well chambers separteed by 8 μm pore size nitrocellulose filters (Corning). The membranes for the invasion assay were coated with 1:2 diluted matrigel (BD Biosciences) solutions. The cells were added in the top chamber in serum-free medium. Medium containing 10% FBS served as a chemoattractant in the lower chamber. After incubation for 24 h, the cells from the upper side of the membrane were removed by scraping with cotton swabs. The cells on the lower side of the filter were fixed with methanol and then stained with crystal violet and counted from 10 random fields. All the experiements have 3 replicates, and repeated for three times.

2.11 In vivo xenograft tumorigenesis

10 million cells mixed with 0.2 ml Matrigel (BD Biosciences) were implanted in the mammary fat pad of 4-6 week old non-pregnant female NSG mice (The Jackson Laboratory). Three days prior to cell implantation, the mice were primed with s/c estrogen pellet (0.72 mg/ 60 day pellets; Innovative Research of America, Sarasota, FL). Tumor growth was monitored weekly for 10 weeks. Tumor dimensions were measured with Vernier calipers and tumor volume calculated as length x width x depth/2. At the end of the experiment the tumors along with livers and lungs are taken out for fixation

and further analyses. Mice were euthanized when control tumors reached 2 cm^3 in volume or showed signs of ill health, as per institutional IACUC guidelines.

2.12 Protein/DNA array based screen of DNA-binding activity of 345 transcription factors

Protein/DNA arrays were used to simultaneously screen 345 transcription factors for DNA-binding activity. This was carried out by using the protein/DNA combo-array kit (cat. MA1215, Affymetrix, Santa Clara, CA). In brief, 4 µg of total nuclear protein (prepared using the Panomics Nuclear Extraction Kit [Cat. AY2002, Affymetrix, Santa Clara, CA]) were incubated with biotin-labeled DNA-binding probe mix provided by the vendor (TranSignal Probe Mix) to allow the formation of complexes of transcription factors (TFs) in the lysates with cognate DNAs in the probe mix. The protein-DNA complexes were separated from free probes by electrophoresis in agarose gels. The probes present in the complexes were eluted, denatured and hybridized to the TranSignal membrane dotted with corresponding non-labeled probes, and the signals were detected by chemi-luminescence.

2.13 Electrophoretic mobility shift assay (EMSA)

EMSA was carried out by using the EMSA kit (cat. 20148, Life Technologies, Waltham, MA). The binding reactions were performed by adding 1 µg of nuclear extract protein to a mixture containing 20 fmol of 5'- biotin end-labeled double-stranded DNA probes in 20 µl of binding buffer. Competition reaction mixtures contained a 200-fold molar excess of non-biotin-labeled oligonucleotides. The DNA-protein complexes were separated on pre-cast native 7.5% polyacrylamide gels (cat. 456-1021, Bio-Rad, Hercules, California) at 100 V and then transferred onto a PVDF membrane. The

positions of the biotin end-labeled oligonucleotides were detected by a chemiluminescent reaction according to the manufacturer's instructions.

2.14 Cathepsin B (CTSB)/Cathepsin L (CTSL) activity assay

CTSB/L activity was performed using Magic Red CTSB/L Activity Kit (Cat. 937 & 941, Immunochemistry Technologies, Bloomington, MN) according to the manufacturer's protocol. Cells were seeded on coverslips and incubated with Magic Red CTSB substrate for 1 h at 37 °C. The cells were washed with PBS, and fixed with 0.1% formaldehyde. The coverslips were mounted with medium containing DAPI staining. Images were taken under fluorescence microscope. The fluorescence intensity was further analyzed using Image J (NIH).

2.15 Extracellular matrix degradation assay

This assay was carried out using QCM™ Gelatin Invadopodia kit (Cat. ECM670, EMD Millopore, Billerica, MA) according to the manufacturer's protocol. FITC-labeled gelatin was coated onto glass coverslips and crosslinked with 0.5% glutaraldehyde in PBS for 30 minutes. Coated coverslips were then washed three times each with PBS and 50 mM glycine in PBS. Cells were cultured for various time points to allow ECM degradation, seen as focal loss of fluorescent signal ("holes") in the labeled gelatin layer. The fluorescence intensity was further analyzed using Image J (NIH).

2.16 Patient population and tissue microarrays

Tissue microarrays (TMAs) were prepared from formalin-fixed, paraffin-embedded tissue specimens that include a series of primary operable (stage I and II) breast carcinoma cases of age <70 presented consecutively between 1988 and 1998 at the University of Nottingham Hospital Breast Unit with tumors of less than 5 cm diameter

(100). This is a well-characterized series (900 cases) that includes clinical and pathological data. These tissue arrays were provided by Dr. Emad Rakha, Pathologist at University of Nottingham Hospital. The breast cancer specific survival (BCSS) is defined as time (in months) from the date of primary surgery to the date of breast cancer-related death. Distant metastasis free survival (DMFS) is defined as duration (in months) from the date of primary surgery to the appearance of distant metastasis. The median age of patients was 55 years (range 18–70 years) with a median BCSS of 129 months (range 4–243 months) and median time of DMFS of 114 months (range 5–241 months). Distant recurrence occurred in 249 cases (31 %); 228 (29 %) patients died from breast cancer, while 435 (56 %) patients were alive at the end of follow-up. Adjuvant systemic therapies were provided according to the Nottingham Prognostic Index (NPI) group. Systemic therapy was prescribed to the Excellent (NPI B 3.4) and Good (NPI 3.41–5.4) prognostic Groups. The Moderate I group received hormonal therapy for ER+ tumors. The Moderate II, Poor, and Very Poor Groups received hormone therapy for ER+ tumors and cytotoxic therapy for ER- patients. Of the informative cases (n = 801) 360 have received hormone therapy (45 %) while 201 cases received chemotherapy (25 %). None of the patients received neoadjuvant therapy or anti-HER2 targeted therapy.

2.17 Scoring of TMA

Of the cores of the 900 breast cancer samples were analyzed as TMAs, sufficient tissue was available to perform scoring in 803 cases and these form the basis of analyses presented in this study. Normal controls included 25 normal human breast tissue specimens. The tissue arrays were stained using immunohistochemistry with anti-CHIP antibody as described previously (101).

Semi-quantitative assessment of staining intensity utilized a modified histochemical score (H-score) that includes the intensity of staining and the percentage

of stained cells. The intensity of staining was scored on a scale of 0 to 3 corresponding to negative (0), weak (1), moderate (2), and strong (3) staining. Percentage of positive cells was visually estimated. Multiplication of the two indices (intensity and percentage positive cells) provided final scores that range from 0 to 300. The pattern of expression was visually recorded as nuclear, cytoplasmic, or combined nuclear and cytoplasmic or no nuclear/cytoplasmic staining. Any nuclear expression (>1) was considered positive, while cytoplasmic expression was considered positive if it exceeded a cut-off of an H-score of 110, which is based on histogram distribution of the cases as well as X-Tile computer software analysis. All cases were scored by a trained pathologist without prior knowledge of the clinic-pathological parameters or outcome data. The samples with cytoplasmic staining were considered cytoplasmic positive regardless of nuclear-negativity or positivity; similarly nuclear positive cases included nuclear positive staining regardless of cytoplasmic staining status.

2.18 Statistical analysis

Statistical analysis of tissue microarray IHC staining was performed using the SPSS 16.0 statistical software (SPSS Inc., Chicago, IL, USA). Optimal cut-offs for CHIP expression were determined using the X-tile bioinformatics software (version 3.6.1, 2003–2005, Yale University, USA). Analysis of categorical variables was performed with $\chi 2$ test. Survival curves were analyzed using the Kaplan–Meier method with significance determined by the Log Rank test. Multivariate analysis was performed using the Cox hazard analysis. Group comparison analysis was performed using student's t test. A p value (two-sided) of <0.05 was considered significant.

Chapter 3: CHIP functions as a negative regulator of ErbB2 by promoting its ER-associated degradation (ERAD)

3.1 Introduction

The ErbB family (ErbB1-4) of trans-membrane receptor tyrosine kinases (RTKs) plays critical physiological roles (102-104). ErbB1 (EGFR) and ErbB2 (Her2/Neu) drive oncogenesis in a number of human malignancies. ErbB2 overexpression, as a result of gene amplification and/or increased transcription, drives oncogenesis in over a quarter of human breast cancer patients (105){{109 Emde,A. 2012}} and also specifies poor overall patient survival (105, 106). ErbB2 overexpression has been successfully exploited for therapeutic targeting with humanized monoclonal antibodies (e.g., Trastuzumab, Pertuzumab) and more recently with small molecule kinase inhibitors (e.g., Lapatinib), resulting in significant improvement of treatment outcomes when added to conventional chemo-radiotherapy (107, 108). De novo as well as rapidly acquired resistance, however, has emerged as a major limitation to ErbB2-targetd therapy (109, 110). Newer avenues to promote more effective and durable responses to targeted therapy of ErbB2-driven breast and others cancers are therefore urgently needed.

Overexpression of ErbB2, most often due to gene amplification, is a diagnostic attribute of ErbB2-driven breast cancer and also a predictor of initial response to targeted therapy. ErbB2 is a transmembrane (TM) glycoprotein synthesized in the ER, and as such is subject to ER quality control, which ensures that the newly synthesized proteins do not exit the ER until they are determined to be correctly folded and/or fully assembled. Increase in the abundance of misfolded proteins triggers an unfolded protein response, one arm of which carries out the dislocation of misfolded/unassembled TM proteins into the cytosol for ubiquitin-dependent proteasomal degradation, a conserved process of ER-associated degradation (ERAD) (111). A subset of ER-synthesized proteins, which include the ErbB family member ErbB3, also undergo an ER “quantity” control, which targets otherwise correctly folded proteins to ERAD to maintain their physiological levels (112, 113). The folding of luminal domains of TM proteins is

mediated by ER luminal Hsp90-family chaperones, such as Hsp94, while the folding of cytoplasmic domains is mediated by the Hsp90-Hsc70 chaperone (Hsc70 will be used to collectively refer to both constitutive and inducible members of Hsp70 family) (114). Both of these pathways are hyperactive in ErbB2-overexpressing breast cancers, and appear critical to maintain the oncogenic drive (111). Hsp90-Hsc70 chaperone complex is a dual-purpose machine that promotes folding, but Hsc70 can also attain a pro-degradation conformation (regulated by co-chaperones) to facilitate degradation of client proteins whose mis-folding is sensed to be beyond restoration (106, 115). Studies of cystic fibrosis trans-conductance regulator (CFTR) as a model TM protein illustrate this process and have established that ER quality control of the cytoplasmic domains of TM proteins requires the Hsp90-Hsc70 chaperone, with the associated ubiquitin ligase (E3) CHIP functioning to promote a degradation state of Hsc70, leading to CFTR ERAD (62, 67, 77).

Newly-synthesized RTKs, including EGFR and ErbB2, associate with Hsp90-Hsc70 on the ER, and inhibition of Hsp90 with geldanamycin (GA) or its analogues (such as 17AAG) promotes rapid RTK degradation, indicating a requirement for Hsp90-Hsp70 complex to promote folding of newly synthesized RTKs (116-118). Distinct from other RTKs, however, ErbB2 remains Hsp90-associated even after its exit from the ER. As others and our laboratory have shown, the inhibition of Hsp90 promotes rapid ubiquitination and degradation of mature ErbB2 protein (74, 75, 118). Notably, Hsp90 inhibitors exhibit selectively higher antitumor effects against ErbB2-overexpressing breast cancer cells and these effects are synergistic with ErbB2-targeted therapeutics, trastuzumab or lapatinib (119). Thus, increased Hsp90-Hsc70 chaperone function in ErbB2-overexpressing breast cancers is a co-driver of oncogenesis and a therapeutic target. Indeed, the Hsp90 inhibitor and trastuzumab combination is currently undergoing clinical evaluation in breast cancer (www.clinicaltrials.gov) (120). Understanding how

Hsp90-Hsc70 complex protects ErbB2 and how Hsp90 inhibitors promote its degradation are therefore critical biological and clinically-relevant questions.

Since treatment of ErbB2+ breast cancer cells with Hsp90 inhibitors promotes rapid ubiquitination and proteasome-dependent degradation (117), identification of the ubiquitin ligase (E3) CHIP (C-terminus of Hsc70 Interacting Protein) as a binding partner and inhibitor of the folding function of Hsc70 (65) suggested that it may serve as mediator of Hsp90 inhibitor-induced ErbB2 degradation. Consistent with this idea, others and our laboratory observed that overexpression of CHIP in ErbB2-overexpressing breast cancer cell lines enhanced the GA- or 17AAG-induced ubiquitination and degradation of ErbB2 (74, 75). However, ErbB2 degradation upon Hsp90 inhibition was unaffected in CHIP-null mouse embryonic fibroblasts (MEFs) (74) and upon CHIP shRNA KD in distinct ErbB2-overexpressing breast cancer cell lines(Figure 3.1). Thus, these studies clearly established that CHIP was not a mediator of acute degradation of mature ErbB2 (which is predominantly at the cell surface) upon Hsp90 inhibition. However, despite a lack of involvement of CHIP in ErbB2 degradation induced by Hsp90 inhibitors, several recent lines of evidence support a critical involvement of CHIP in the regulation of ErbB2-driven oncogenesis. In this chapter, we demonstrate that newly synthesized ErbB2 is a direct target of CHIP-mediated ubiquitination and degradation, through a modified ERAD pathway.

3.2 CHIP regulates cell surface ErbB2

To examine the molecular mechanisms underlying CHIP-mediated ErbB2 degradation, we first developed stable CHIP knock-down (KD) ErbB2+ breast cancer cells. We observed that cell surface ErbB2 level increased in the 21MT1 CHIP KD cells comparing with 21MT1 control cells when analyzed by FACS analysis (Figure 3.2A, left

panel). This result was consistent with higher surface ErbB2 staining in CHIP KD cells analyzed by immunofluorescence imaging (Figure 3.1 B).

Next, we constructed stable ErbB2+ breast cancer cells with Myc-tagged CHIP overexpression to check the impact on ErbB2 levels. As we expected, surface ErbB2 level was decreased in CHIP overexpressing cells comparing with control cells (Figure 3.2A, right panel). The CHIP level in ErbB2+ cells was verified by western blotting (Figure 3.1B).

As CHIP is a E3 ubiquitin ligase, we asked if ErbB2 was a direct target of CHIP without any stimuli such as Hsp90 inhibition. Previous reports demonstrated that CHIP could regulate the protein quality control both in the ER, with CFTR as a well-studied example, and in the cytoplasm (67). We therefore asked if CHIP plays an important role in ErbB2 quality/quantity control since overexpression creates opportunities for increased mis-folding of the newly synthesized ErbB2 proteins.

3.3 CHIP ubiquitinates ErbB2 for degradation

To confirm the surface ErbB2 level change was due to CHIP involvement in ErbB2 ubiquitination, we performed immuneprecipitation assays in CHIP-overexpressing vs. parental ErbB2+ BT474 breast cancer cells. CHIP overexpression increased basal ErbB2 ubiquitination even without proteasome inhibitor bortezomib treatment while control cells did not show any ubiquitination signals. Proteasome inhibition further elevated ubiquitination of ErbB2 in CHIP overexpressing cells compared to control cells (Figure 3.3), suggesting that proteasome degradation was an essential pathway for ErbB2 degradation. These data demonstrated that CHIP itself functions as an E3 ubiquitin ligase targeting ErbB2 for proteasome degradation in the absence of Hsp90 inhibition. However, the total ErbB2 level was not changed dramatically when CHIP was overexpressed in ErbB2+ cells. One possible explanation was that in these ErbB2

overexpressing cells ectopic-CHIP expression was not high enough to clear all the ErbB2 protein and that CHIP only targeted a small pool of ErbB2. Given our results described below on CHIP localization, we reason that it is the newly-synthesized pool of ErbB2 that is targeted by CHIP.

3.4 CHIP destabilizes immature form of ErbB2

Since we showed that alterations in CHIP expression predominantly impacted the cell surface ErbB2 expression, we undertook analyses of the impact of CHIP expression on ErbB2 during its maturation process. We performed ^{35}S-methionine/cysteine-labeling pulse-chase experiments to investigate if CHIP overexpression could affect the stability and maturation of newly synthesized ErbB2. As shown in Figure 3.4A, two bands of ErbB2 appeared after radiolabeled pulse and chase. The low-molecular-weight immature form (precursor) appears after pulse-labeling, while the higher molecular-weight mature form appears after chase and reflects the post-ER glycosylated form that is eventually transported to the cell surface (74). CHIP-overexpressing 21MT1 cells had a similar maturation pattern as the control cells; however, the intensity of the mature ErbB2 form in CHIP overexpressing 21M1 cells was reduced relative to the intensity of the initial precursor form compared to the pattern in control 21MT1 cells (Figure 3.4B). In the control 21MT1 cells, almost 70% of the immature form converted to the higher molecular weight form, consistent with a proportion of the newly-synthesized ErbB2 being degraded through ERAD as part of the protein quality control. In CHIP-overexpressing 21MT1 cells only 50% of immature form converted into the higher molecular weight form, consistent with a larger proportion of newly-synthesized ErbB2 undergoing ERAD. These results provide a plausible explanation for reduced export of ErbB2 to the cell surface in CHIP-overexpressing cells.

Next, to test whether CHIP promoted the instability of the immature form of ErbB2, we performed ^{35}S-methione/cysteine pulse-chase experiments without or with brefeldin A (BfA), an inhibitor of the transport of newly-synthesized membrane proteins from ER to Golgi apparatus. Under BfA treatment, newly-synthesized ErbB2 would be expected to remain in an immature form in the ER instead of maturing in the Golgi for transport to the cell surface. As expected, BfA treatment for 4 hours efficiently blocked the appearance of the mature form of newly-synthesized ErbB2, as there was no signal of high-molecular-weight band detected (Figure 3.4C). Indeed, we observed that CHIP overexpressing 21MT1 cells showed a faster loss of the immature radiolabeled ErbB2 compared to the kinetics of loss f signal in control 21MT1 cells (Figure 3.4D). This result further supports the conclusion that CHIP targets the immature form of ErbB2 for degradation at the ER. Thus, extending previous findings (68), our results show that newly-synthesized ErbB2 targeted for ERAD by CHIP.

3.5 CHIP overexpression promotes intracellular retention of ErbB2 in ER and Golgi

Since CHIP overexpression was observed to promote the destabilization of ER-localized ErbB2, likely reflecting its targeting to ERAD pathway, we hypothesized that CHIP may function at the ER or Golgi to prevent incorrectly-folded, newly-synthesized ErbB2 from being exported to the cell surface and preparing it for ERAD. To further explore this idea, we performed immunofluorescence imaging studies to asses the localization of ErbB2 in CHIP-overexpressing vs. parental SKBR3 cells. As shown in Figure 3.5, ectopically-overexpressed CHIP-GFP in ErbB2+ SKBR3 cells colocalized with markers of ER and Golgi (Figure 3.5A, calnexin staining represents ER; Figure 3.5B, GM130 staining represents cis-Golgi), suggesting that CHIP can function in both ER and Golgi apparatus. Importantly, cells with ectopic CHIP-GFP overexpression exhibited substantially reduced levels of surface ErbB2 staining, consistent with our conclusion

that CHIP function at ER and Golgi negatively regulates ErbB2 transport to the cell surface.

We further looked at the ErbB2 staining in stably CHIP-overexpressing vs. control ErbB2-overexpressing 21MT1 cells. In CHIP overexpressing 21MT1 cells, we observed increased intracellular ErbB2 while no intracellular ErbB2 was seen in control cells (Figure 3.6 and Figure 3.7). Under these conditions, the intracellular ErbB2 did not co-localize with an ER marker calnexin (Figure 3.6); instead, it co-localized with a Golgi apparatus marker GM130 (Figure 3.7A). To further validate the Golgi localization of intracellular ErbB2, we transfected SKBR3 cells with a plasmid coding for a Golgi-localized pmTurquoise fluorescent probe (from Addgene). Ectopic pmTurquoise Golgi marker also co-localized with intracellular ErbB2 in CHIP-overexpressing cells while no co-localization was observed in control cells (Figure 3.7B). The quantification of Golgi and ErbB2 co-localized cells confirmed that intracellular ErbB2 were stuck in the Golgi in most of the CHIP overexpressing ErbB2+ cells (Figure 3.7C).

The classical ‘ERAD’ is thought to take place at the ER organelle (6). Since we observed the CHIP-mediated destabilization of immature ErbB2 in stably CHIP-overexpressing cells, yet intracellular ErbB2 was only seen in Golgi in these cells, the CHIP-dependent control on newly synthesized ErbB2 does not appear to simply involve retention in the ER followed by ERAD. We speculate that partially unfolded ErbB2, apparently in association with Hsp90, is allowed to progress to the Golgi apparatus. However, association of CHIP with molecular chaperones is likely to prevent its further transport and may promote retro-transport to ER for degradation. Notably, overexpressed ErbB2 is unique among its family members to require Hsp90 for its stability in its mature form, including that present on the cell surface. In contrast, other RTKs, such as EGFR, require Hsp90 only in their newly-synthesized forms (29). In a previous study from our laboratory(75), elevated interaction of ErbB2 and Hsp70 was

found upon U-box mutant CHIP H260Q expression, but ErbB2/Hsp90 complex did not disassociate when cells were treated with an Hsp90 inhibitor 17AAG, a result in contrast to results with parental cells or cells expressing wildtype CHIP. We reason that CHIP acts as a negative co-chaperone for Hsp90/Hsc70 (65) and promotes the release of Hsp90/Hsc70 from ErbB2, thereby exposing the inherent hydrophobic sequences previously identified in ErbB2 to be required for Hsp90 chaperone (118). It is likely that this switch leads to newly-synthesized ErbB2 being sensed as an unfolded protein, promoting its retention in the Golgi/ER and eventual targeting for ERAD. To assess if this model is likely, we carried out IP/Western blotting analysis of ErbB2 association with Hsp90 and Hsc70, upon CHIP KD. As shown in Figure 3.8, CHIP KD increased the interactions of ErbB2 with Hsp90 and Hsp70. Thus, tumor-associated loss of CHIP can be viewed as an adaptive mechanism to relieve ErbB2 of a bottleneck on its transit to the cell surface in association with Hsp90.

3.6 Reduced expression of CHIP promotes ER stress

The needs for protein quality control are elevated in cancer cells as their higher metabolic demands create elevated ROS levels and increased protein synthesis creates additional protein unfolding (121). Since CHIP is known to serve as a key regulator of protein quality control (65, 70), it is reasonable to anticipate that lower levels of CHIP will promote the accumulation of unfolded proteins and elevate ER stress. To test this idea experimentally, we used the treatment with proteasome inhibitor bortezomib, a clinically-used drug known to induce ER stress (122-124). We treated 21MT1 control cells and their CHIP KD derivative cells with bortezomib for various time points and analyzed the expression of ER stress marker CHOP (C/EBP homologous protein) were examined by western blotting. As shown in Figure 3.9, CHOP levels were increased in control cells upon bortezomib treatment but this was seen primarily at later time point (8 hours); in

contrast, basal CHOP levels were elevated in CHIP KD cells copared to control cells and bortezomib treatment led to an earlier increase in CHOP levels, indicating that CHIP is required to mitigate ER stress and that reduced levels of CHIP, as are now known to occur in tumors such as ErbB2+ breast cancer (124), would be expected to increase the basal levels of ER stress.

A high ER stress level is known to trigger the unfolded protein response (UPR) (125). Depending on the duration and degree of ER stress, the UPR could provide either survival signals by activating adaptive and anti-apoptotic pathways, or death signals by inducing cell death programs. The former is thought to occur in tumor cells which activate the UPR gradually and contributes to their ability to survive and exhibit other oncogenic traits under hostile environments such as tissue hypoxia and lack of nutrients (125). Therefore, acute elevation of ER stress or repression of the adaptive UPR mechanisms pharmacologically has been proposed as a means to elevate ER stress to levels that could produce cell growth inhibition or death, and hence produce a beneficial therapeutic effects against cancer (126). We tested whether lower expression of CHIP in tumor cells could indeed sensitize them to acute elevation of ER stress and lead to an anti-tumor effect using anchorage-independent growth in soft agar as well as 2D cell proliferation assays to assess the effects of bortezomib. As shown in Figure 3.10A, CHIP KD SKBR3 cells had elevated colony formation compared to control cells. Treatment with bortezomib led to a dose-dependent inhibition of colony formation. However, when we compared the efficiency of colony formation (Figure 3.10B), boretomib treatment led to a a dramatic decrease in CHIP KD cells as compared with control SKBR3 cells. In 2D proliferation assay, the IC50 for bortezomib in CHIP KD cells was 10$\pm$1.2nM, compared to 15$\pm$ 1.3nM in control cells (Figure 3.10C), consistent with the increased sensitivity of tumor cells with increased ER stress due to loss of CHIP expression to acute pharmacologic elevation of ER stress.

3.7 ER stress inducer synergistically inhibit ErbB2+ cells with Trastuzumab

Trastuzumab (Herceptin, from Genentech, part of Roche) is a standard targeted therapeutic antibody for ErbB2+ breast cancer since 1998. We therefore investigated if elevated ER induction with bortezomib could have a synergistic or additive effect with Trastuzumab ErbB2+ breast cancer cells. We performed proliferation assays on BT474 cells by treating with bortezomib alone, Trastuzumab alone, or a combination of both. As shown in Figure 3.11, BT474 cells showed a dose dependent growth inhibition upon bortezomib or Trastuzumab alone treatment. Analysis of the Combination Index of the effects of combined bortezomib and Trastuzumab treatment as an indicator of their interaction indicated that bortezomib and trasuzumab could synergistically inhibit BT474 cell growth (combination indices between between 0 and 1). These results further establish that CHIP is a key regulator of oncogenic traits and therapeutic sensitivity of tumor cells, and the results described here could form the basis of future efforts to target CHIP-low breast ErbB2+ cancers with a combination of ER stress inducers such as bortezomib together with Trastuzumab to produce a therapeutic improvement for patients with ErbB2+ breast cancer.

3.8 Discussion

In this chapter, we established a novel role of CHIP in regulating ErbB2 through a modified ERAD pathway. Our results suggest that CHIP-dependent alterations in the association of ErbB2 with molecular chaperones are an important mechanism to promote the Golgi to surface transport of newly-synthesized ErbB2 in ErbB2-overexpressing breast cancer cells. Thus, loss of CHIP in a majority of EbB2+ breast cancers may accentuate oncogenesis in part by ensuring that HSP90 remains

associated with ErbB2 and allows this complex to exit ER/Golgi for transport to cell surface where it functions to promote oncogenesis.

As discussed in the introduction, Hsp90-Hsc70 chaperone monitors the folding state of cytoplasmic domains of TM proteins (20, 29). CHIP, as a negative co-chaperone, promotes the pro-degradation state of the Hsp90-Hsc70 chaperone. Studies of model TM proteins, such as CFTR, have demonstrated that misfolding of cytoplasmic domains triggers Hsp90-Hsc70 chaperone-dependent ERAD (67, 77). Overexpressed ErbB2, which lacks any mutations, is persistently bound to Hsp90-Hsc70 chaperone even in its mature state through a unique hydrophobic patch on ErbB2 (118). Inhibition of this association (by Hsp90 inhibitors) leads to rapid degradation of ErbB2 (74, 75). When the aforementioned hydrophobic patch was rendered EGFR-like, the mature form of this mutant ErbB2 is insensitive to Hsp90 inhibitors; under these conditions, Hsp90-Hsc70 still interacted with the cytoplasmic region, but through another undefined region, and Hsp90 inhibition only destabilized the newly synthesized form, indicating that Hsp90-Hsc70 chaperone was separately needed to stabilize the cytoplasmic domain of newly synthesized ErbB2. As shown in this study, CHIP in ErbB2-driven breast cancer played the essential role as an enforcer of ErbB2 ERAD. As CHIP-dependent ERAD was enforced on immature ERbB2 and was accentuated by the retention of this form in the ER using brefeldin-A, it would be consistent with ER quality control roles assigned for CHIP in the context of mutant CFTR. An example of the ER “quantity” control has been presented in which the ER-localized ubiquitin ligase Nrdp1 enforces the ERAD of ErbB3 to control its surface levels (112, 113). It is therefore plausible CHIP-dependent control of the ERAD of ErbB2 could also function as a “quantity” control rather than “quality” control since ErbB2 is transported to the cell surface in a chaperone-associated form and is functional in this form.

It should be noted that acutely overexpressed CHIP co-localized with the ER and Golgi in ErbB2-overexpressing breast cancer cells (Figure 3.5), as previously described previously in other cells (89). It is therefore plausible that CHIP may function at both organelles during the ER quality/quantity control newly-synthesized transmembrane proteins such as ErbB2. R, However, stably overexpressed CHIP localized primarily in the Golgi and not the ER in ErbB2-overexpressing cells. Since our results with pulse-chase labeling clearly show that CHIP regulates the conversion of newly sysnthesized immature to mature form of ErbB2 and that inhibition of ER to Golgi transport of ErbB2 exposed immature ErbB2 to CHIP-dependent degradation (Figure 3.4), we suggest that CHIP function towards ErbB2 and potentially other transmembrane proteins, is more complex than simply ERAD. We speculate that CHIP association with molecular chaperones bound to transmembrane proteins such as ErbB2 promotes ERAD and in addition can expose the targeted proteins for degradation even in non-ER compartments such as Golgi but that such processes may be slower compared to ERAD (thus accounting for a pool of CHIP and ErbB2 being seen in the Golgi but not in the ER in stably CHIP-overexpressing ErbB2+ breast cancer cells). This idea is consistent with recent results in which mutant CFTR was shown to undergo an ERAD-like degradation dependent in part on CHIP even at the cell surface (127). It is also possible that CHIP-dependent ubiquitination of either molecular chaperones (128) or transmembrane proteins such as ErbB2 (74, 75), promotes the retrograde transport from Golgi to ER where the marked proteins are then eliminated by ERAD. Notably, CPY protein has been shown to be retro-transported from Golgi to ER for ERAD (129).

Demonstration of CHIP as an enforcer of ErbB2 ERAD would allow future studies to test therapeutic options that target components of ERAD and the linked unfolded protein stress and UPR response pathways. Recent studies have shown that the proteasome inhibitor Bortezomib, which was approved by the FDA for treating multiple

myeloma (130), has a very potent inhibitory effect on breast cancer cell lines, and clinical trials to test Bortezomib in breast cancer patients are ongoing (122, 123). Our in vitro proliferation data suggests that a combination of Bortezomib and Trastuzumab specifically in ErbB2+ patients that show reduced CHIP expression could produce a therapeutic improvement.

Figure 3.1 CHIP is not required for Hsp90 inhibition induced ErbB2 degradation

(A). 21MT1 control and CHIP KD cells were treated with 17AAG for different time points. Western blot analysis of cell lysate for ErbB2 and CHIP, Hsc70 is the loading control. (B). SKBR3 control and CHIP KD cells were seed on cover slips and treated with 17AAG for 8 hours, cells then were fixed and stained with anti-ErbB2 antibody followed by secondary fluorescent conjugate. Cover slips were mounted with DAPI staining and further taken images under confocal microscopy.

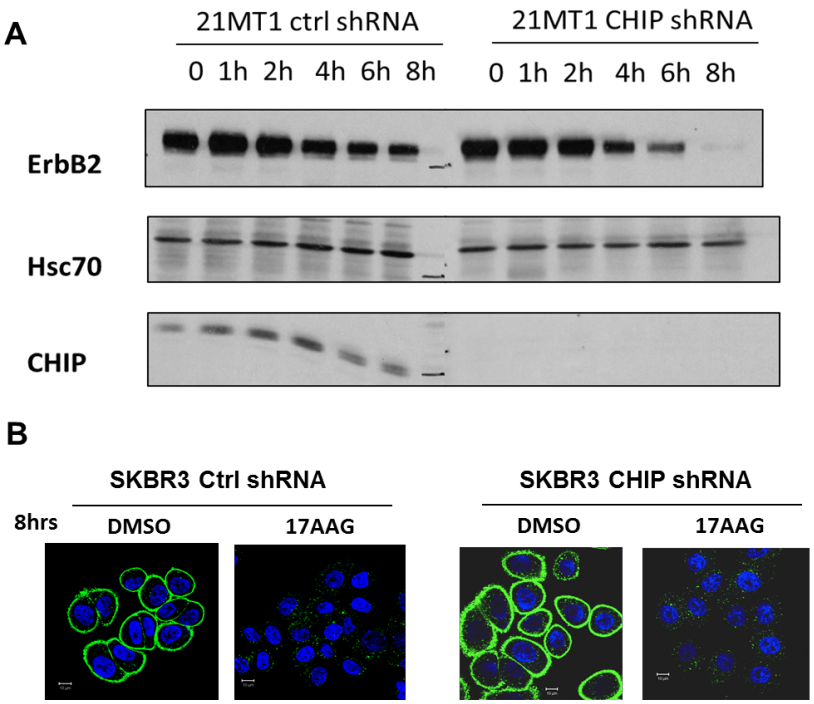
A
21MT1 ctrl shRNA
21MT1 CHIP shRNA
0 1h 2h 4h 6h 8h
0 1h 2h 4h 6h 8h
ErbB2
Hsc70
CHIP
B
SKBR3 Ctrl shRNA
SKBR3 CHIP shRNA
8hrs
DMSO
17AAG
DMSO
17AAG

Figure 3.2 CHIP regulates cell surface ErbB2

(A). 21MT1 cell surfaceErbB2 level is determined by FACS analysis. Knockdown of CHIP increased cell surface ErbB2, overexpression of CHIP further decreased cell surface ErbB2. Data represent mean + S.D., n=6 (B). Western blot analysis of 21MT1 cell lysate for CHIP, Hsc70 is the loading control.

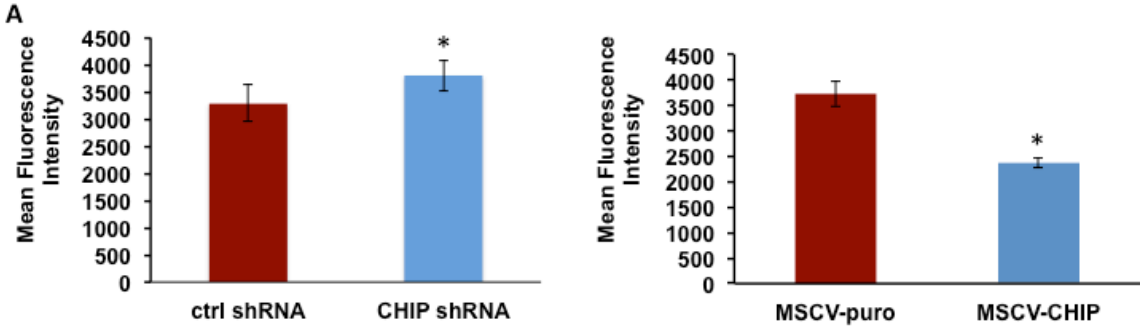
A
Mean Fluorescence Intensity
4500
4000
3500
3000
2500
2000
1500
1000
500
0
*
ctrl shRNA
CHIP shRNA
Mean Fluorescence Intensity
4500
4000
3500
3000
2500
2000
1500
1000
500
0
*
MSCV-puro
MSCV-CHIP

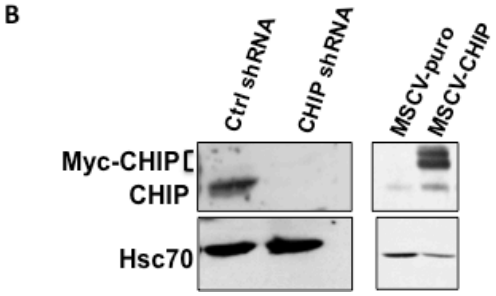
B
Ctrl shRNA
CHIP shRNA
MSCV-puro
MSCV-CHIP
Myc-CHIP
CHIP
Hsc70

Figure 3.3 CHIP elevates basal ubiquitinates of ErbB2

BT474 cells were seed in 10cm dishes and incubated with or without treatment of proteasome inhibitor bortezomib for 4 hours. Cleared lysates from cells harvested were quantified by BCA assay. ErbB2 was immuoprecipitated by using trastuzumab (5ug/ml), ubiquitin and ErbB2 signals were detected in immuoprecipitates (upper panel) and ErB2, and CHIP signals were detected in whole cell lysates (lower panel).

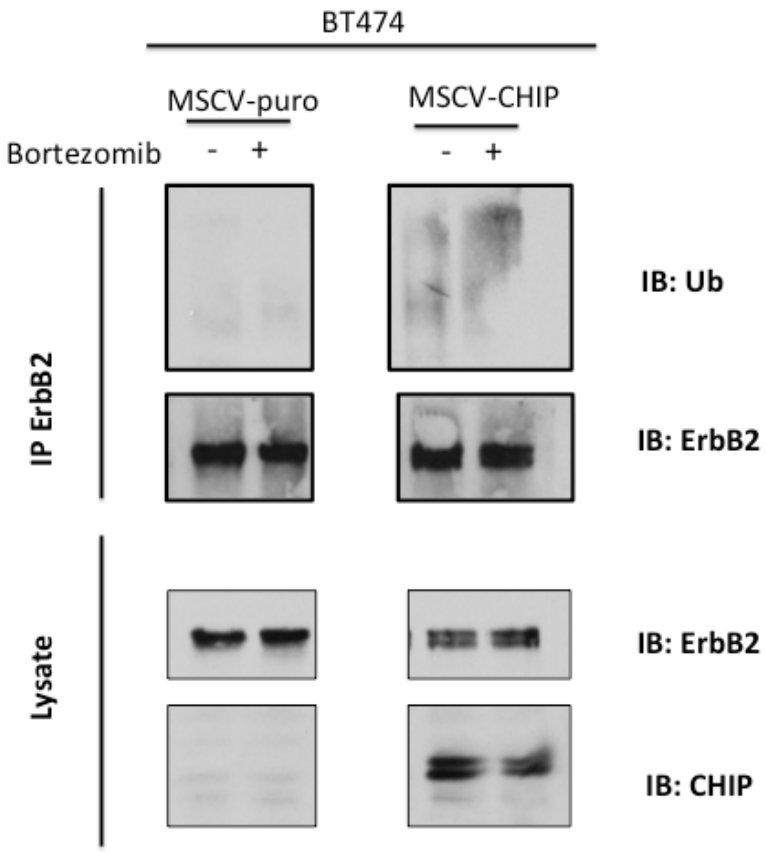
BT474
MSCV-puro
MSCV-CHIP
Bortezomib
- +
- +
IP ErbB2
IB: Ub
IB: ErbB2
Lysate
IB: ErbB2
IB: CHIP

Figure 3.4 Overexpression of CHIP down regulates newly synthesized ErbB2

(A) 21MT1 cells were pulse-labeled for 20 min with [^{35}S] methionine-cysteine and were then chased with excess unlabeled methionine-cysteine medium. Cleared lysates from cells harvested at the indicated times were immunoprecipitated with anti-ErbB2 antibodies and were analyzed by autoradiography. (B) Quantification of ErbB2 signal in A. (C) 21MT1 cells were pulse-labeled for 20 min with [^{35}S] methionine-cysteine and were then chased with excess unlabeled methionine-cysteine medium with Brefeldin A treatment. Cleared lysates from cells harvested at the indicated times were immunoprecipitated with anti-ErbB2 antibodies and were analyzed by autoradiography. (D) Quantification of ErbB2 signal in C.

A

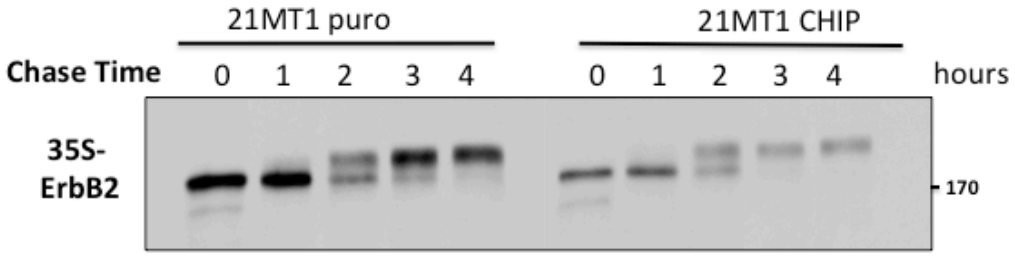
21MT1 puro
21MT1 CHIP
Chase Time
0 1 2 3 4
0 1 2 3 4
hours
35S-
ErbB2
170

B

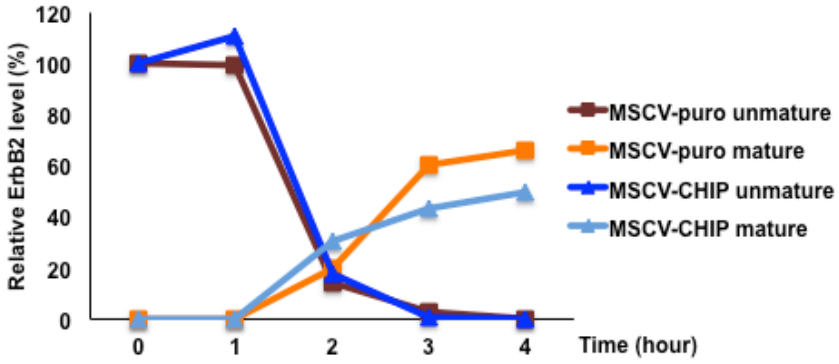
Relative ErbB2 level (%)
120
100
80
60
40
20
0
0 1 2 3 4
Time (hour)
MSCV-puro unmature
MSCV-puro mature
MSCV-CHIP unmature
MSCV-CHIP mature

C

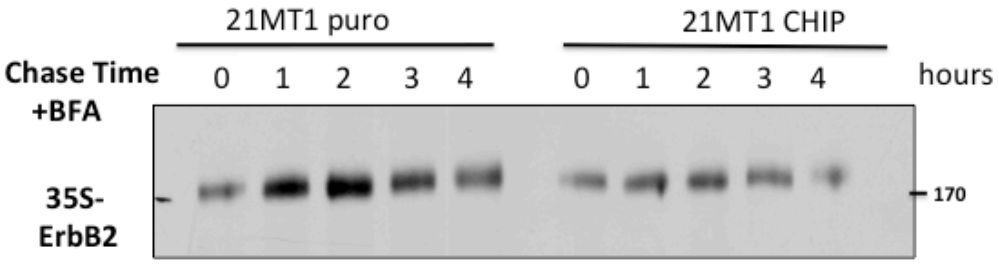
21MT1 puro
21MT1 CHIP
Chase Time
+BFA
0 1 2 3 4
0 1 2 3 4
hours
35S-
ErbB2
170

D

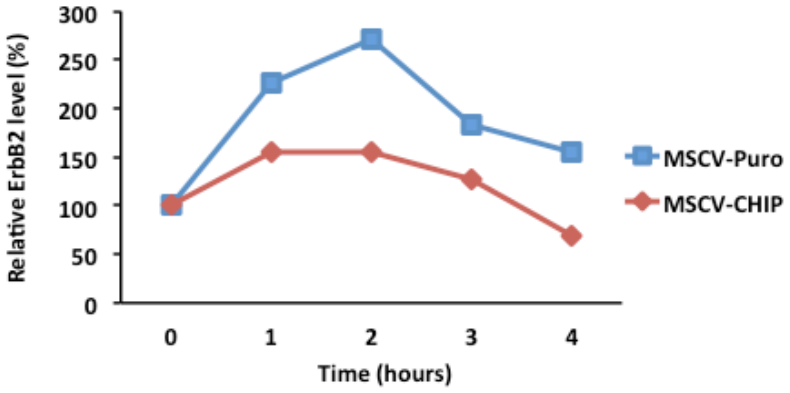
Relative ErbB2 level (%)
300
250
200
150
100
50
0
0 1 2 3 4
Time (hours)
MSCV-Puro
MSCV-CHIP

Figure 3.5 CHIP co-localized with ER and Golgi apparatus

(A) SKBR3 cells were seed on cover slips and transiently transfected with CHIP-GFP vector, cells then were fixed and stained with anti-ErbB2 and anti-calnexin antibody followed by secondary fluorescent conjugate. Cover slips were mounted with DAPI staining and further taken images under confocal microscopy. (B) SKBR3 cells were seed on cover slips and transiently transfected with CHIP-GFP vector, cells then were fixed and stained with anti-ErbB2 and anti-GM130 antibody followed by secondary fluorescent conjugate. Cover slips were mounted with DAPI staining and further taken images under confocal microscopy.

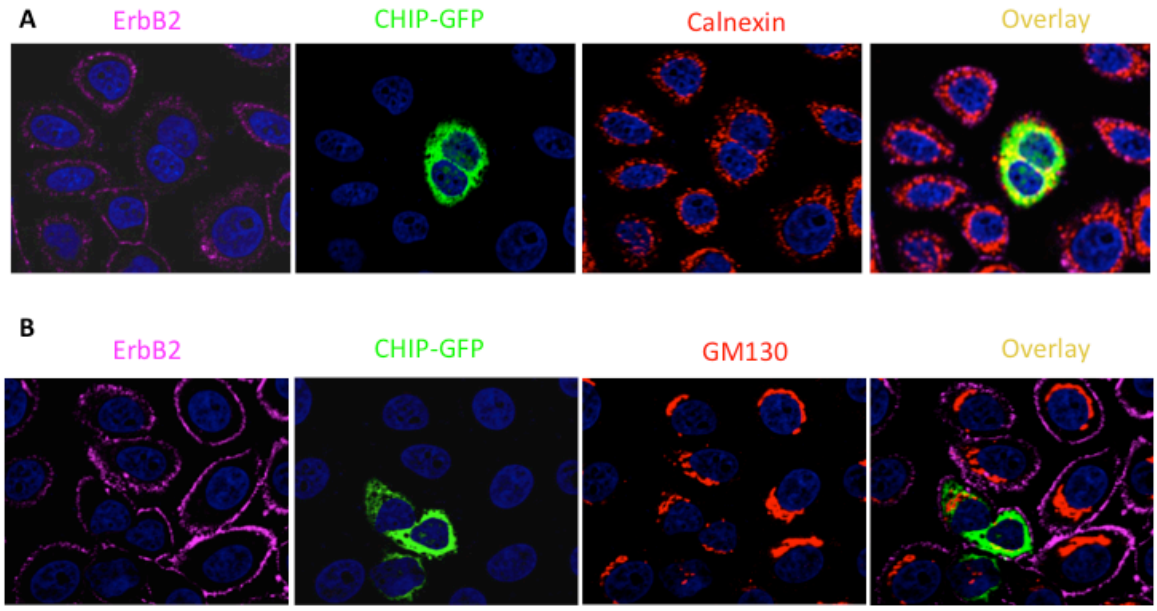
A
ErbB2
CHIP-GFP
Calnexin
Overlay
B
ErbB2
CHIP-GFP
GM130
Overlay

Figure 3.6 ErbB2 does not co-localize with ER in CHIP overexpressing ErbB2+ cells

21MT1 cells were seed on cover slips, then fixed and stained with anti-ErbB2 and anti-calnexin antibody followed by secondary fluorescent conjugate. Cover slips were mounted with DAPI staining and further taken images under confocal microscopy.

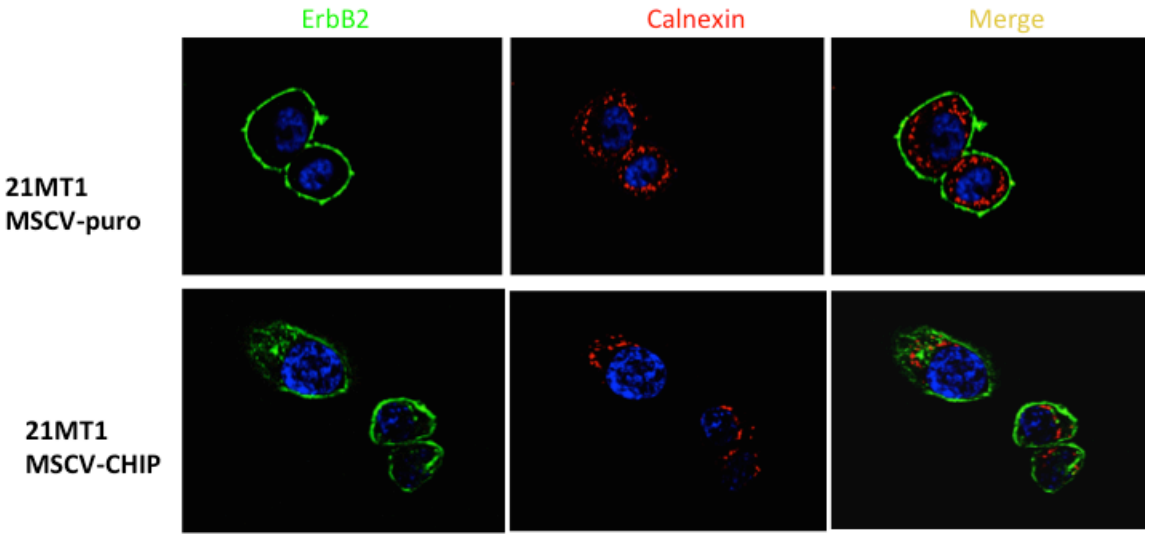
ErbB2
Calnexin
Merge
21MT1
MSCV-puro
21MT1
MSCV-CHIP

Figure 3.7 ErbB2 co-localized with Golgi in CHIP overexpressing ErbB2+ cells

(A) 21MT1 cells were seed on cover slips, then fixed and stained with anti-ErbB2 and anti-GM130 antibody followed by secondary fluorescent conjugate. Cover slips were mounted with DAPI staining and further taken images under confocal microscopy**.** (B) SKBR3 cells were seed on cover slips and transiently transfected with pmTurquoise-Golgi vector, cells then were fixed and stained with anti-ErbB2 antibody followed by secondary fluorescent conjugate. Cover slips were mounted with DAPI staining and further taken images under confocal microscopy. (C) Quantification of Golgi and ErbB2 co-localized cells in A & B.

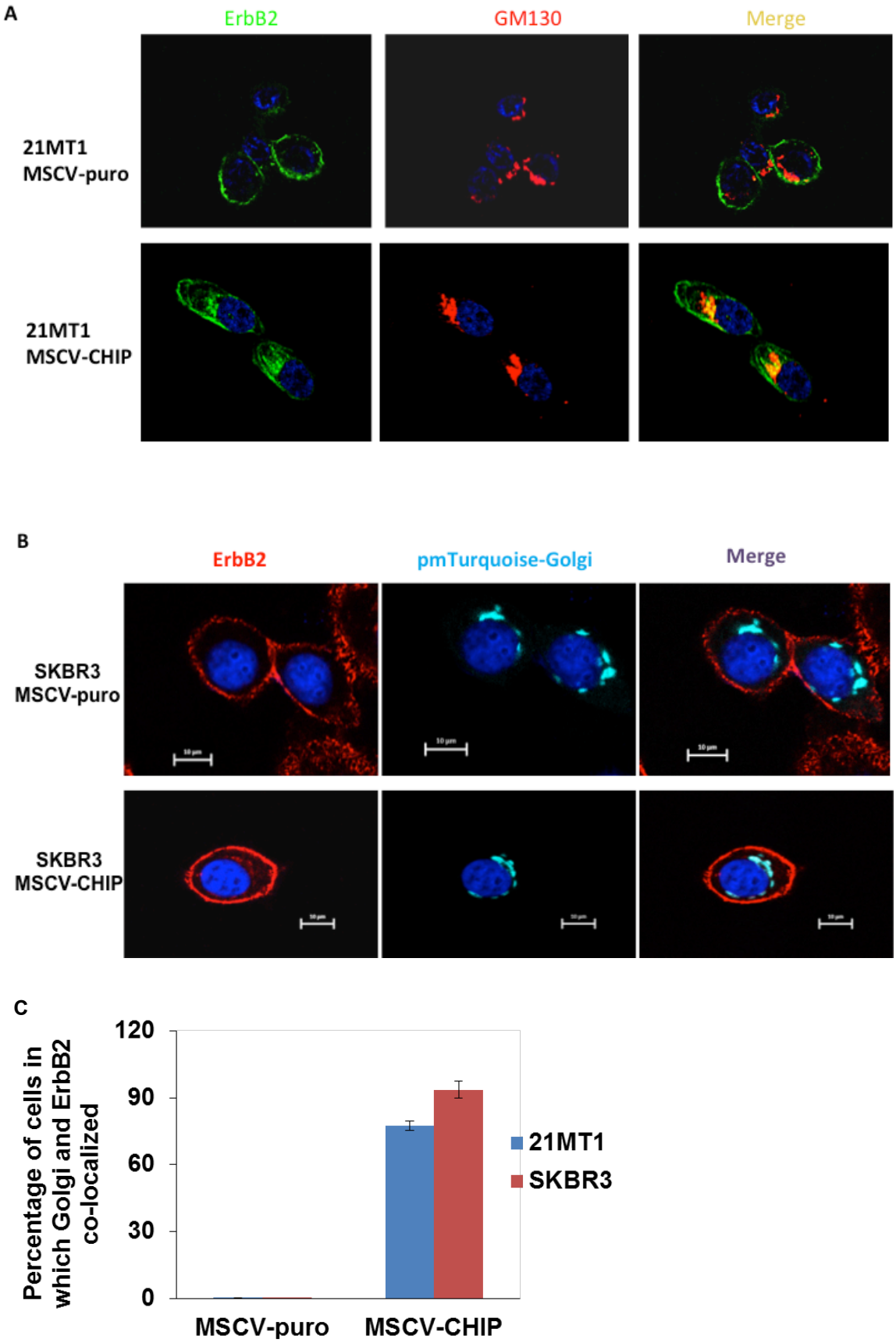
A
ErbB2
GM130
Merge
21MT1
MSCV-puro
21MT1
MSCV-CHIP
B
ErbB2
pmTurquoise-Golgi
Merge
SKBR3
MSCV-puro
SKBR3
MSCV-CHIP
C
Percentage of cells in which Golgi and ErbB2 co-localized
120
90
60
30
0
MSCV-puro
MSCV-CHIP
21MT1
SKBR3

Figure 3.8 Loss of CHIP elevates interaction between ErbB2 and Hsp90/Hsp70

21MT1 Cells were seed in 10cm dishes and incubated with or without treatment of Hsp90 inhibitor 17AAG for 4 hours. Cleared lysates from cells harvested were quantified by BCA assay. ErbB2 was immuoprecipitated by using trastuzumab (5ug/ml), Hsp90, Hsp70 and ErbB2 signals were both detected in immuoprecipitants (right panel) in whole cell lysates (left panel).

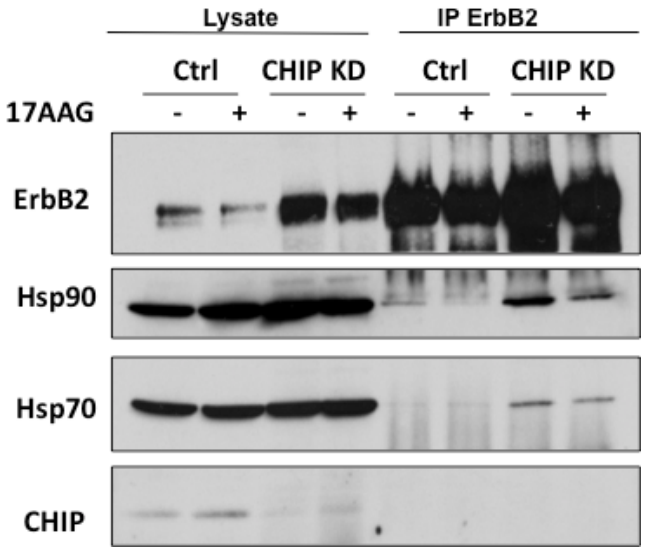
Lysate
IP ErbB2
Ctrl
CHIP KD
Ctrl
CHIP KD
17AAG
- + - + - + - +
ErbB2
Hsp90
Hsp70
CHIP

Figure 3.9 Loss of CHIP induces ER stress

21MT1 Cells were seed in six well plates and incubated with or without treatment of proteasome inhibitor Bortezomib for different time points. Cleared lysates from cells harvested were quantified by BCA assay. ErbB2, CHOP and CHIP signals were detected from western blotting, Hsc70 served as loading control.

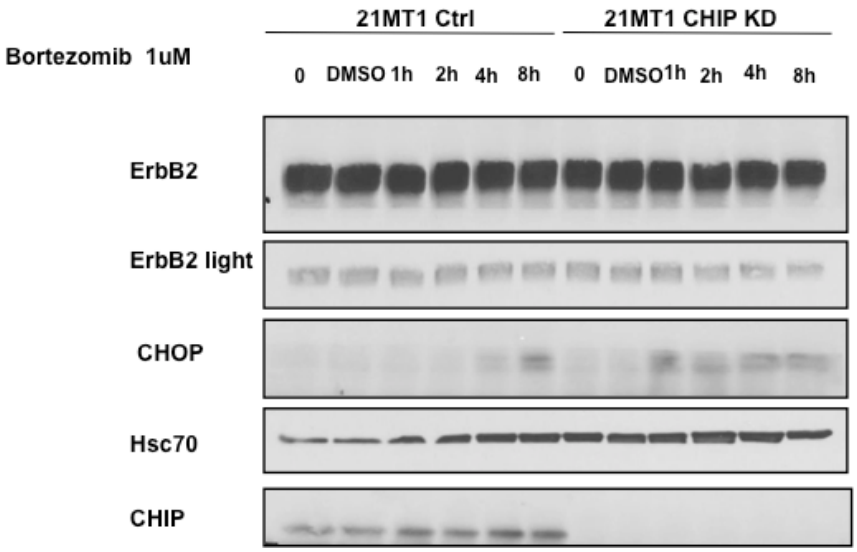
21MT1 Ctrl
21MT1 CHIP KD
Bortezomib 1uM
0 DMSO 1h 2h 4h 8h 0 DMSO 1h 2h 4h 8h
ErbB2
ErbB2 light
CHOP
Hsc70
CHIP

Figure 3.10 Loss of CHIP sensitizes growth inhibition by stress inducer in ErbB2+ cells

(A) SKBR3 cells were seed in soft agar plates (0.6% bottom, 0.35% upper) with the treatment of proteasome inhibitor Bortezomib at different concentrations and incubated for 3 weeks. Colonies were stained, imaged and analyzed under microscope. Data represent mean + S.D., n=3. (B) The colony numbers in A were normalized to the untreated group of control cells. (C) SKBR3 cells were seed in 96 well plates, followed by the treatment of proteasome inhibitor Bortezomib at different concentrations for 5 days. Plates were stained with MTT and read under plate reader. IC50 was calculated by Prism software.

A

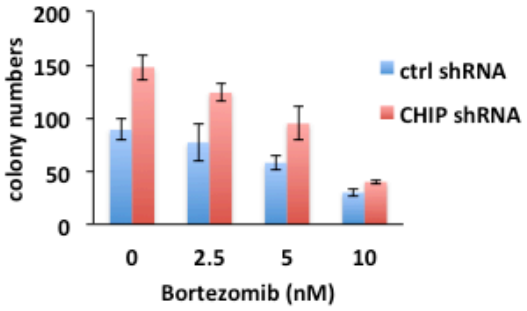
200
150
100
50
0
colony numbers
ctrl shRNA
CHIP shRNA
0
2.5
5
10
Bortezomib (nM)

B

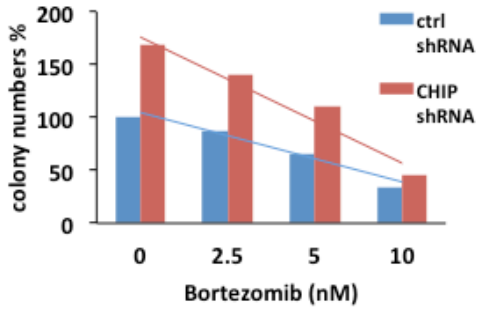
200
150
100
50
0
colony numbers %
ctrl shRNA
CHIP shRNA
0
2.5
5
10
Bortezomib (nM)

C

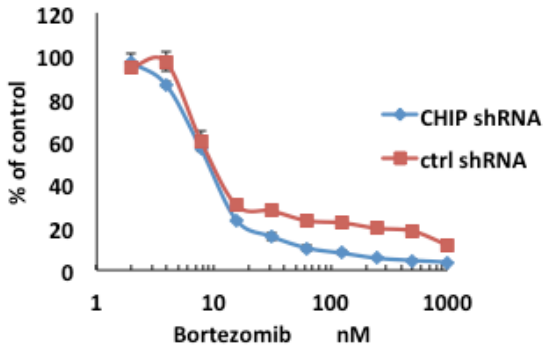
120
100
80
60
40
20
0
% of control
CHIP shRNA
ctrl shRNA
1
10
100
1000
Bortezomib nM

Figure 3.11 Trastuzumab and bortezomib synergistically inhibit BT474 proliferation

BT474 cells were seed in 96 well plates, followed by the treatment of trastuzumab alone (A), Bortezomib and the two combinations (B) at different concentrations for 5 days. Plates were stained with MTT and read under plate reader**.** Data represent mean + S.D., n=3 (C) Combination index was calculated by the software of Prism.

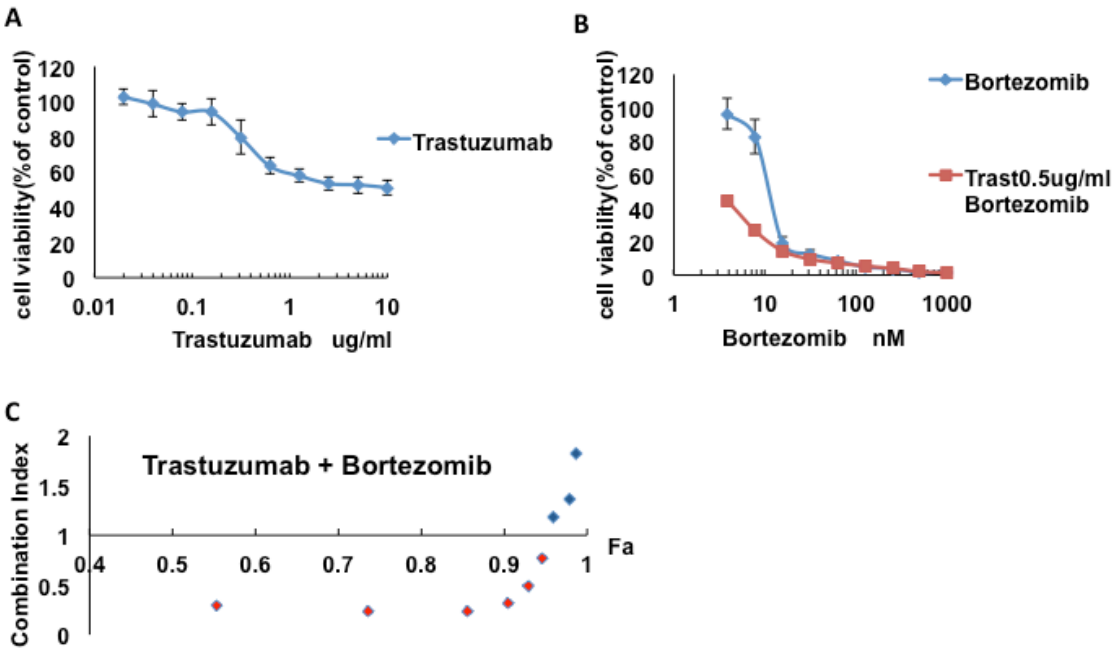
A
cell viability(%of control)
120
100
80
60
40
20
0
0.01
0.1
1
10
Trastuzumab ug/ml
Trastuzumab
B
cell viability(%of control)
120
100
80
60
40
20
0
1
10
100
1000
Bortezomib nM
Bortezomib
Trast0.5ug/ml
Bortezomib
C
Trastuzumab + Bortezomib
Combination Index
2
1.5
1
0.5
0
0.4
0.5
0.6
0.7
0.8
0.9
1
Fa

Chapter 4: Loss of CHIP in breast cancer unleashes a program of tumor invasion and metastasis mediated by the transcription factor MZF1 and its targets, cathepsins

4.1 Introduction

ErbB2 overexpression, as a result of gene amplification and/or increased transcription, drives oncogenesis in about 20%-25% of human breast cancer patients and specifies poor overall survival (131). ErbB2 overexpression and mutations also drive smaller subsets of other cancers, such as aero-digestive and ovarian cancers. Targeting of overexpressed ErbB2 with humanized monoclonal antibodies (e.g., Trastuzumab, Pertuzumab), and recently with small molecule kinase inhibitors (e.g., Lapatinib), in combination with conventional chemo-radiotherapy has led to significant improvements in treatment (107, 108). All treated patients however will eventually develop resistance, through de novo or acquired mechanisms, leading to eventual disease progression and death due to metastatic disease (109, 110). Current antibody-based therapeutics are also ineffective against brain metastases due to their inability to cross the blood-brain barrier (108). Newer avenues whose targeting could improve the existing ErbB2-targeted therapies to impart more effective and lasting responses are urgently needed.

While overexpressed ErbB2 is the driver of oncogenesis in ErbB2+ tumors, substantial rewiring of biochemical pathways in tumor cells, together with alterations in tumor microenvironment are also essential (132). One such pathway is mediated by the Hsp90-Hsc70 molecular chaperone complex, which is essential to facilitate the folding of newly synthesized proteins and assembly of multi-subunit protein complexes (133). A number of signaling proteins, including ErbB2 itself, perpetually remain Hsp90-associated to maintain their mature functional states (134). Specific inhibition of Hsp90 ATPase activity (e.g., with 17AAG) rapidly destabilizes ErbB2, and results in tumor cell killing (119, 135). As our laboratory has shown (119, 135), Hsp90 inhibitors synergize with ErbB2-targted therapeutics and such combinations are now under clinical development although beset with toxicity (120).

At the molecular level, ErbB2+ breast cancers express higher levels and a more active conformation of Hsp90 (136, 137). The Hsp90-Hsc70 chaperone complex is a dual-purpose machine that promotes folding but its Hsc70 component can also attain a pro-degradation conformation (133). These transitions are regulated by co-chaperones that interact with Hsp90/Hsc70. The positive co-chaperone Hop and negative co-chaperone CHIP (C-terminus of Hsc70-interacting protein; also called STUB1) interact with the C-termini of Hsp90 and Hsc70, and mediate an on-off switch (138, 139). Elevated phosphorylation near the C-termini of Hsp90 and Hsc70 was shown to enhance Hop interaction and reduce CHIP interaction, providing one mechanism for upregulation of the active Hsp90-Hsc70 form in breast cancer (26). Loss of CHIP expression has now emerged as another mechanism

CHIP is a U-box-containing ubiquitin ligase (E3) that interacts with Hsp90 and Hsc70 through its TPR domains. The co-chaperone function of CHIP is essential for protein quality control, and a substantial number of cellular proteins have been identified as binding partners and targets of CHIP E3 activity(138, 138, 139, 139, 140, 140). These include ErbB2 itself, as others and we have demonstrated (74, 75), and is further demonstrated by studies presented in Chapter 3 of this thesis. Recent clinical studies support a tumor suppressor function of CHIP in ErbB2+ breast cancers. Two studies of smaller breast cancer cohorts showed that CHIP mRNA or protein expression was reduced in cancer tissues of a majority of ErbB2+ and triple-negative patients, and loss of CHIP expression predicted poor patient survival (83, 92). However, another study came to an opposite conclusion (93). In one study, it was shown that CHIP depletion in ER+ MCF7 cells upregulated the expression of ER coactivator SRC3, which was found to be a CHIP target (83). The significance of this finding to ErbB2+ and triple-negative breast cancers, a majority of which does not express ER, is unclear and oncogenesis-relevant targets of CHIP in these breast cancer subtypes remain unknown.

Here, we undertook an extensive clinical-pathological study using a cohort (>800 patients) of extensively annotated breast cancer tissues (100). Further, we utilized protein/DNA array to identify a novel pathway, mediated by the transcription factor MZF1 and impinging on matrix degrading enzymes cathepsin B and L, that is regulated by CHIP and whose deregulation as a result of loss of CHIP expression contributes to ErbB2+ breast cancer progression. We further show that targeting this pathway could serve as a potential therapeutic avenue for breast cancer.

4.2 Decreased nuclear CHIP expression correlates with clinical characteristics and a poorer survival in breast cancer patients

That CHIP may serve as a tumor suppressor is supported by reports in different solid tumors that show loss of CHIP expression with tumor progression. In our study, immunohistochmical staining of CHIP in tissue microarrays (TMAs) from about 956 breast cancer patients revealed two distinct patterns: cytoplasmic and nuclear staining (Figure 4.1A). The Kaplan-Meier analysis revealed that low nuclear staining pattern was significantly correlated with poorer breast cancer specific survival of all the breast cancer patients while cytoplasmic CHIP staining was not predictive (Nuclear CHIP p=0.003 Vs. cytoplasmic CHIP p=0.469, Figure 4.1B). As shown in Table 4.1 lower nuclear CHIP expression in the cancerous tissues was also significantly correlated with clinic-pathological feathers of tumor progression, such as higher tumor size, tumor grade, pleomorphism and mitosis status. However, the cytoplasmic CHIP expression was not significantly correlated with these features (Table 4.1). Loss of nuclear CHIP expression also showed a significant correlation with high levels of various biochemical markers of tumor progression and metastasis (Table 4.2), such as reduced staining for hormone receptors ER and PR, altered cytokeratins (CK 18, CK19), increased early epithelial-mesenchymal transition markers (N-cadherin, P-cadherin) and EGFR family proteins

(EGFR, ErbB2, ErbB4). However, none of those markers correlated with cytoplasmic CHIP expression except CK 18 (p=0.001) and ErbB2 (p=0.016) (Table 4.3). Thus, our large TMA analysis confirmed previous findings that low CHIP expression is found in larger subsets (about 2/3rd) of ErbB2+ and triple-negative breast cancer patients and a smaller subset (1/3rd) of ER+ patients, but more importantly demonstrated that it is the loss of nuclear staining of CHIP that provides a marker of poor disease-free survival and tumor progression. These latter findings provided a basis for further studies to demonstrate a mechanistic basis of how loss of nuclear CHIP may contribute to breast cancer oncogenesis. Given the overall focus of this thesis on ErbB2-driven oncogenesis as a model to investigate the tumor suppressor function of CHIP, we used ErbB2+ breast cancer cell lines as a primary model. However, key findings related to new mechanistic insights were confirmed in limited experiments in triple-negative and ER+ breast cancer cell line models.

4.3 CHIP suppresses ErbB2+ breast cancer cell growth and tumor formation both in vitro and in vivo

Given our TMA IHC results and previous studies indicating lower CHIP expression in ErbB2+ and triple-negative breast cancers, we examined the mRNA and protein levels of CHIP in a panel of human breast cancer cell lines that included examples of all three major subsets as well as immortal mammary epithelial cell line controls. The CHIP expression levels (both mRNA and protein level) were found to be lower in ErbB2+ and in triple negative cells compared to normal mammary epithelial cell lines and ER+ breast cancer cell lines (Figure 4.1C and 4.1D); analyses of ER+ and triple-negative cell lines are consistent with a previous report (83) but our analyses show clearly that ErbB2+ breast cancer cell lines recapitulate the lower expression of CHIP seen in this subset of breast cancer in patient samples.

We then asked whether the tumorigenic traits of ErbB2-overexpressing breast cancer cell lines were dependent on the relaxed protein quality control expected in these cells as a result of reduced levels of CHIP expression. This was clearly suggested by our experiments (Chapter 3) in which the low CHIP levels in ErbB2+ breats cancer lines were further reduced by CHIP KD, resulting in increased ErbB2 surface expression. For this purpose, we engineered three ErbB2+ cell lines to stably overexpress CHIP ($CHIP^{OE}$, Figure 4.1E)

We used ErbB2-overexpressing 21MT1 cell line CHIP-hi/low cell pair to investigate the role of CHIP in proliferation, anchorage-independent cell growth and invasiveness,, important in vitro traits associated with tumor progression. While no significant difference in proliferation was observed in a single passage, consistent with a similar result upon CHIP overexpression in triple-negative breast cancer cell line MDA-MB231 published previously (83), our analysis of cumulative cell proliferation over multiple passages revealed that $CHIP^{OE}$ cells proliferated modestly but significantly lower compared to control cells (Figure 4.3A). In a more stringent assay of proliferation under anchorage-independent conditions in soft agar, $CHIP^{OE}$ cells exhibited a significantly lower number of colonies compared to control cells (Figure 4.3B), indicating the CHIP overexpression decreased anchorage-dependent cell growth. We next performed trans-well migration and invasion assays using serum growth factors to provide a chemoattractant gradient. These analyses demonstrated that $CHIP^{OE}$ cells show a significantly reduced ability to migrate in trans-well chambers (Figure 4.3C) and a significantly reduced invasion through Matrigel, as shown by the number of cells that penetrated the Matrigel-coated membrane (Figure 4.3D).

Nude mice were orthotopically implanted in the mammary fat pad with BT474 $CHIP^{OE}$ and control cells (6 mice per group). The CHIP-overexpressing BT474 cells formed significantly smaller tumors compared those formed by control cells (Figure 4.2A

and 4.2B). Exogenous CHIP overexpression in tumors was confirmed by western blotting (Figure 4.2C). Histologic examination revealed that, compared with control cells, $CHIP^{OE}$ tumor cells had a lower degree of nuclear atypical and a lower mitotic index (Figure 4.2D). In addition, immunostaining of the proliferative marker Ki67 demonstrated that the ratio of proliferative cells was lower in $CHIP^{OE}$ tumors (Figure 4.2E and 4.2F). However, immunostaining of the apoptotic marker cleaved-caspase 3 did not show any significant difference between control and $CHIP^{OE}$ tumors (Figure 4.2E and 4.2G), suggesting that the impact of CHIP overexpression is primarily cytostatic.

The results of these assays indicated that the oncogenic potential of ErbB2+ cells was significantly decreased by CHIP overexpression and supports the idea that loss of CHIP expression in ErbB2+ breast tumors promotes tumor progression as suggested by our clinical-pathological analyses.

4.4 Identification of potential nuclear targets of CHIP using a screen of cognate DNA-binding activities of nuclear transcription factors

Given our results with breast cancer tissue IHC analyses, which highlighted the loss of nuclear but not cytoplasmic CHIP expression as a predictor of tumor progression and poor patient outcomes, we reasoned that targets of CHIP relevant to its tumor suppressor function may likely function in the nucleus. Transcription factors are an obvious category of such targets that must act inside the nucleus by binding to their cognate DNA elements and regulating the transcription of specific gene sets, often in concert (141). Indeed, previous studies in cancer cells and non-cancer cell systems and in vivo have identified a number of transcription factors as potential targets of CHIP-mediated ubiquitylation and functional regulation. The known transcription factor targets and the tissues/cell types in which these were found are indicated in Table 4.4. These prior examples suggest examples, such as NFkappaB and others, that may be relevant

to the tumor suppressor role of CHIP in ErbB2+ breast cancer. We however opted to carry out an unbiased screen of CHIP-regulated transcription factors by assessing the DNA-binding activities of transcription factors present in a commercially available array. The Combi-Array from Affymetrix has an array of cognate DNA-binding sequences corresponding to 345 transcription factors in a filter format that allows the analysis of the levels of DNA-binding activities of corresponding transcription factors present in a nuclear extract, using a work flow described in Chapter2. Although this assay measures DNA-binding activity, and not the protein levels of transcription factors, we reasoned this to be an advantage since examples of transcription factors that are regulated by CHIP-dependent mono-ubiquitylation without degradation have been reported (142).

We carried out an analysis of relative DNA binding activities in nuclear extracts of control vs. CHIP-overexpressing ErbB2+ BT474 breast cancer cell line, and expressed the results as fold difference in binding activity (based on the intensity of spots on the arrays), where the intensities of control spots were found to show the expected invariance. As expected, the DNA-binding activities of most transcription factors did not change beyond an arbitrary cu-off of 3-fold (Figure 4.4A). However, smaller subsets of transcription factors present in the nuclear extracts of CHIP-overexpressing vs. control cells showed more substantial increase or decrease in DNA-binding activities (Figure 4.4A), and we consider these as likely targets of CHIP, either as direct targets of CHIPE3 ubiquitin ligase or as being regulated by other transcription factors or signaling pathways that change the abundance or activities of these transcription factors. Consistent with the robustness of our assay, the transcription factors identified as CHIP-depndent in our analysis (Table 4.4) included many transcription factors shown to be downregulated by CHIP, such as p-53 and NFkB (143, 144).

4.5 MZF-1 is a direct target of CHIP-mediated ubiquitination and degradation

Among the transcription factors identified by our screen, we focused on MZF-1 for a number of reasons, a primary one being its recent linkage to invasion signaling downstream of ErbB2 (145). Myeloid zinc finger 1 (MZF-1) is a physiological regulator of myeloid lineage development but has been linked to leukemia and more recently to solid tumors (146-149). P55PIK transcriptionally activated by MZF-1 promotes colorectal cancer cell proliferation (146). The MZF-1/c-MYC axis mediates lung adenocarcinoma progression caused by wild-type lkb1 loss (148). Osteopontin mediates an MZF-1-TGF-beta1-dependent transformation of mesenchymal stem cells into cancer-associated fibroblasts in breast cancer (149).

Efforts to identify mechanisms by which ErbB2 signaling leads to breast cancer cell invasiveness in a 3D matrix culture identified a novel pathway in which ErbB2 signaling, via MZF-1, leads to transcriptional upregulation of cathepsin B (CTSB) and L (CTSL). In this study, Cdc42-binding protein kinase beta, extracellular regulated kinase 2, p21-activated protein kinase 4, and protein kinase C alpha were identified as essential mediators of ErbB2-induced cysteine cathepsin expression and breast cancer cell invasiveness. This identified signaling network activates the transcription of cathepsin B gene (CTSB) via myeloid zinc finger-1 transcription factor that binds to an ErbB2-responsive enhancer element in the first intron of CTSB (145).

Our screen identified MZF-1 as one of the CHIP targets whose DNA-binding activity was reduced upon CHIP overexpression in ErbB2-overexpressing breast cancer c ell line BT474(Figure 4.4A; MZF-1 is highlighted as a red dot). To validate MZF-1 is a transcription factor regulated by CHIP, we performed electrophoresis mobility shift assay (EMSA) using double-stranded oligonucleotide probes corresponding to MZF-1 binding sites on the promoters of CD34 genes (150). The level of binding, as seen in the intensity of shifted bands on gels, between MZF-1 and its consensus DNA sequence was indeed decreased in CHIP-overexpressing BT474 cells compared to control cells

(Figure 4.4B). We further analyzed the mRNA and protein levels of MZF-1 in CHIP-overexpressing vs. control cells. Upon CHIP overexpression, both mRNA and protein level of MZF-1 were decreased (Figure 4.4C and 4.4D). This result suggested that at least part of the mechanism by which the DNA-binding activity of MZF-1 was reduced in CHIP-overexpressing cells was indirect, via regulation of upstream modulators of MZF-1 transcription. However, to assess whether or not MZF-1 is also a target of direct ubiquitination and degradation by CHIP we assessed the level of mZF-1 protein level and its ubiquitination upon CHIP overexpression. We transfected MZF-1 and/or CHIP plasmids into HEK-293T cells and analyzed the ubiquitination and degradation of MZF-1. Immunoprecipitation of MZF-1 showed increased ubiquitination to be directly proportional to ectopic CHIP levels (Figure 4.4E, upper). Correspondingly, the total level of MZF-1 decreased upon increased expression of CHIP (Figure 4.4E, upper). All these results therefore demonstrated that MZF-1 is ubiquitinated and degraded by CHIP. We further assessed this question by testing the impact of expressing mutations in CHIP, CHIPK30A (mutation in TPR domain and hence incapable of associating with Hsp90/Hsc70) and CHIPH260Q (mutation in U-box domain and hence E3 deficient) (75), on its ability to promote MZF-1 degradation. These analyses showed that intact TPR and U-box domains were required for CHIP to reduce MZF-1 protein levels. These results support the conclusion that MZF-1 is a bona-fide target of CHIP-dependent degradation.

In addition, we examined the extracellular matrix degradation by culturing cells on FITC-labeled gelatins, which was a critical step for tumor metastasis. The degradation of florescent gelatin was significantly decreased in $CHIP^{OE}$ cells (Figure 4.3E and 4.3F).

4.6 CHIP is a critical negative regulator of MZF-1-dependent Cathepsin B/L matrix degradation axis

Previously CTSB/L, key regulators of tumor progression and metastasis, have been reported to be downstream transcriptional targets of MZF-1 and this axis has been shown to hyperactivated by ErbB2 signaling (145). We therefore asked if the negative regulation of MZF-1 by CHIP translates into altered expression of CTSB/L. We first used the EMSA with DNA sequences corresponding to known MZF-1 binding site in the CTSB promoter region as a probe. The binding activity of CTSB/L promoter region was decreased in the nuclear extracts of CHIP-overexpressing cells compared to control cells (Figure 4.5A). Importantly, both the mRNA and protein levels of CTSB and CTSL were decreased upon CHIP overexpression (Figure 4.5B and 4.5C). Next, we used a commercial kit (the Magic Red Kit) to test the functional enzymatic activity of CTSB and CTSL in the CHIP-overexpressing vs. control ErbB2+ 21MT1 cell lines. CHIP-overexpressing cells showed reduced red fluorescence, which represents substrate cleavage by CTSB/L, compared to control cells (Figure 4.5D). Quantification of red fluorescence signals revealed that the levels of CTSB and CTSL activity were lower in CHIP-overexpressing cells compared to control cells (Figure 4.5E). Overall, these results establish that MZF-1/CTSB/L pro-invasion signaling axis is negatively regulated by CHIP.

The novel findings described above suggested that one mechanism by which loss of CHIP promotes tumor progression is through upregulation of this key pro-invasion/metastasis signaling pathway. We therefore investigated whether CTSB/L inhibition would prevent or alleviate tumor progression and invasion. We utilized 21MT1 cells to test the impact of chemical inhibition of CTSB on cell invasion. The matrix degradation assay using fluorescent collagen showed that CTSB inhibitor CA074 (151) prevented matrix degradation (Figure 4.6A and 4.6B). Further, the colorimetric trans-well invasion assay showed marked inhibition of cell invasion by CA074 (Figure 4.6C).

Next we tested the efficacy of CA074 in BT474 xenograft model, by treating mice with CA074, Trastuzumab or their combination, since Trastuzumab is a standard

targeted therapeutic antibody clinically used for ErbB2+ breast cancer. Treatment of mice with CA074 resulted in a marked inhibition of tumor growth, comparable to that seen with Trastuzumab, although the combination did not show a significant additive/synergistic effect (Figure 4.6D). The likely explanation for the latter result includes the fact that both drugs are being used at their optimal doses based on previous studies (151). These results support the idea that one mechanism by which loss of CHIP functions to promote ErbB2+ breast tumor progression (based on our clinical-pathological studies) is by allowing increased MZF-1 dependent cathepsin expression. Our results also support the potential targeting of cathepsin B, and potentially CTSB/L together, as a future therapeutic approach against ErbB2+ breast cancer where CHIP is downregulated, especially under metastatic settings.

4.7 Discussion

In this chapter, we used TMAs derived from the largest cohort studied for analyses of CHIP protein expression in breast cancer to demonstrate that CHIP expression is downregulated in nearly two-thirds ErB2+ and triple-negative subtypes of breast cancers and in about a third of ER+ breast cancers. Analyses in cell lines confirmed the predominant loss of CHIP expression in the former two subtypes of breast cancer, and as in previous studies (83) suggested that loss of CHIP expression is regulated at the level of mRNA levels. It will be of interest to examine if this is due to suppression of transcription possibly due to hypermethylation of CHIP gene, due to influence of altered regulatory RNAs such as microRNAs (152), or both. Since the ER+ subtype is the largest subtype of breast cancer, numerically the CHIP-low ER+ tumors add to similar ErbB2+ and triple-negative cases with nearly half of all patients with breast cancer exhibiting a loss of CHIP expression. Our clinical-pathological analyses suggest that patients within this group carry an intrinsically poorer survival and increased tumor

progression and metastasis. This is consistent with poorer intrinsic patient outcomes and higher metastatic odds of patients with triple-negative and ErbB2+ breast cancers (83). It will be of considerable future interest to further assess if the ER+ patients with low CHIP expression belong to a particular molecular sub-classification of ER+ tumors; in this regard, a potential candidate is the luminal B subtype of breast cancers which has considerably poor survival and therapeutic responses compared to luminal A or normal-like breast cancers (83). Thus, our clinical-pathological analyses, together with other recent reports (83, 92), strongly supports the idea that CHIP is a tumor suppresser whose expression is a barrier to tumor progression and metastasis in breast cancer.

Our study revealed a novel finding in that it is the loss of nuclear CHIP instead of cytoplasmic CHIP that correlates with tumor progression markers and poorer survival. We used this novel clinically-driven insight as a basis for an unbiased protein/DNA array screen to identify a substantial group of transcription factors whose DNA-binding activity is directly or indirectly regulated by CHIP (Figure 4.4A). This screen vastly expands the list of potential targets of CHIP, beyond a few described in the literature (143, 144), whose unregulated activity may contribute to oncogenesis in breast and other cancers. As an in-depth analysis of all or most of the identified transcription factors would be unfeasible within this study, we focused on a particularly novel and relevant candidate MZF-1.

MZF-1 is a physiological regulator of myeloid lineage development but has been linked to leukemia and more recently to solid tumors. A previous report exploring mechanistic basis of ErbB2-driven invasion signaling in a 3D matrix culture identified a novel pathway in which ErbB2 signaling impinges on via MZF1 to upregulate its ability to transcribe specific invasion-mediated gene targets cathepsin B (CTSB) and L (CTSL) (153). CTSB and CTSL have been shown to be overexpressed in primary breast cancer tissues and knockdown of CTSB or MZF1 abrogated invasiveness in vitro. Since our

study revealed MZF1 as one of the transcription factors whose DNA-binding activity was downregulated by CHIP, we considered it as a particularly pertinent candidate for further elucidation as a potential target of CHIP in ErbB2+ breast cancer.

Further analysis confirmed that MZF-1 was a direct target of CHIP for ubiquitination (Figure 4.4D) but also revealed that MZF-1 levels may be regulated by CHIP at the mRNA level, likely due to an impact of CHIP on upstream regulators of MZF-1 expression, such as FOXM1, which is known to function upstream of MZF-1 and showed reduced DNA-binding activity in CHIP-overexpressing cells. It remains possible that additional CHIP-dependent negative regulation of MZF-1 activity may emanate from negative regulation of upstream kinases, including ErbB2 itself, by CHIP as shown in Chapter 3 and in previous studies (74, 75).

Consistent with a key role of CHIP in controlling the MZF-1-dependent transcriptional network leading to CTSB/L expression, ErbB2+ breast cancer cell lines express lower levels of CHIP compared to normal or ER+ breast cancer cell lines (such as MCF-7) and correspondingly express high CTSB levels, which were markedly reduced upon CHIP overexpression (Figure 4.5C). Conversely, knockdown of CHIP in an ER+ breast cancer cell line, MCF7, markedly increased the CTSB levels (Figure 4.5D). The latter result is of interest as it suggests that the MZF-1/CTSB/L axis may be activated by non-ErbB2 oncogenic drives as well, consistent with loss of CHIP expression in triple-negative and a subset of ER+ breast cancers. Future studies to identify oncogenic drivers distinct from ErbB2 that connect to MZF-1/CTSB/L pathway will be of great significance.

Cathepsin B is a well-established downstream mediator of invasive/metastatic signaling in various cancers, including breast cancer (145, 151). Targeting CTSB, using a specific inhibitor CA074, decreased extracellular matrix degradation and cell invasion in vitro and tumor growth in vivo (Figure 4.6). Thus, our studies using both genetic

manipulations and pharmacological tools demonstrate that upregulation of MZF-1/CTSB1/L axis is an important pro-oncogenic mechanism unleashed as a result of loss of CHIP expression in ErbB2+ breast cancer. Given the well-established roles of cathepsins in matrix remodeling, invasion, angiogenesis and metastatic spread of tumors (145), we suggest that loss of CHIP expression promotes tumor progression into an invasive/metastatic disease in part through cathepsin upregulation.

Metastasis is the ultimate cause of death among a vast majority of cancer patients (154). Mechanisms that promote metastases are intricately linked to therapeutic resistance (155), reflecting successful tumor cell adaptations (154, 156, 157). A major adaptive mechanism is the upregulation of the HSP90/HSC70-depndent molecular chaperone pathways that helps maintain protein folding and function in the face of increased metabolic needs (34). This chapter identifies the mechanisms by which alterations of this pathway provide a decisive component of this adaptation, involving loss of expression of a negative co-chaperone CHIP to relax the protein quality control in tumor cells in order to maintain the oncogenic drive. Our unbiased screen in ErbB2+ breast cancer cells has defined a previously known transcriptional pathway involved in promoting metastatic signaling in ErbB2+ breast cancer cells as well as in other malignancies. This transcriptional axis provides a novel therapeutic approach by targeting its key metastasis-relevant downstream targets, such as CTSB/CTSL. Thus, the use of CTSB inhibitor CA074 could suggest a new approach to prevent or treat metastases in ErbB2+ breast cancers, and help to prevent or overcome therapeutic resistance. Expression of CHIP may also serve as a biomarker to select patients likely to benefit from such therapy. Current antibody-based therapy of ErbB2+ cancers is ineffective against brain metastases and availability of small molecules against CTSB/L could help address this key issue. While this study focused on ErbB2+ breast cancer, loss of CHIP expression is also a key event in two-thirds of triple-negative and one-third

of ER+ (which together outnumber the CHIP-lo ErbB2+ breast cancers). Together, the ErbB2+ and triple-negative breast cancers, while a minority of all breast cancers, account for the majority of deaths due to breast cancer, the most common malignancy and the second leading cause of cancer deaths among women. Loss of CHIP expression is also becoming identified as a mechanism of oncogenic progression in other cancers such as colorectal, pancreas and lung cancer (84, 96, 144, 158, 159). Thus mechanisms we identified in this study will impact a broad range of human malignancies.

Figure 4.1. Decreased nuclear CHIP staining in breast cancer patients.

(A) Representative IHC staining patterns of CHIP. (B) Kaplan-Meier curves survival analysis of CHIP expression in breast cancer. (C) The CHIP mRNA level in the whole panel of breast cancer cell lines. Total RNA was extracted from cells and followed by RT-PCR reactions. GAPDH was used as a normalization control. (D) The CHIP protein level in the whole panel of breast cancer cell lines by western blotting. Hsc70 was loading the control. (E) Generation of stable $CHIP^{OE}$ breast cancer cell lines.

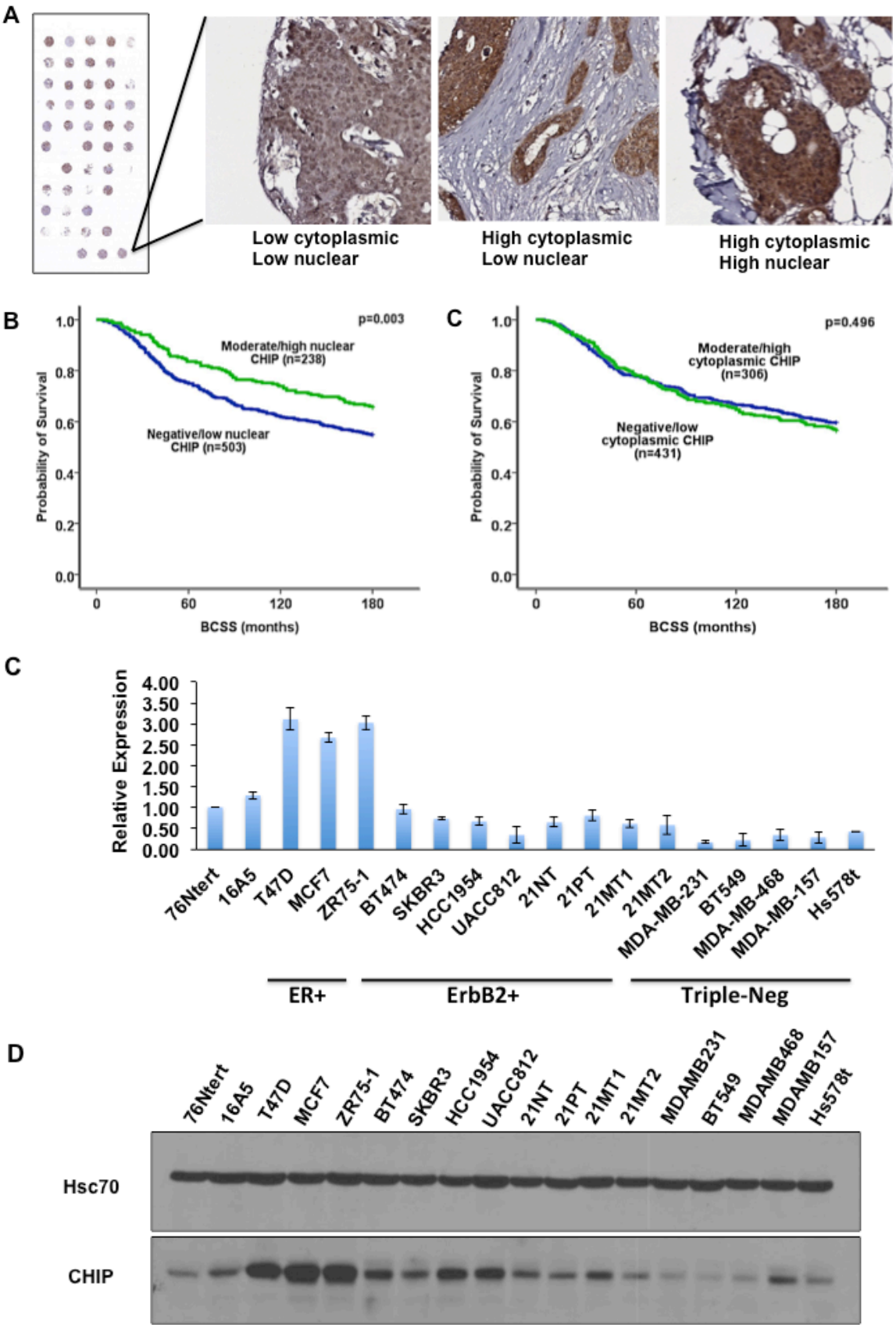
A
Low cytoplasmic
Low nuclear
High cytoplasmic
Low nuclear
High cytoplasmic
High nuclear
B
p=0.003
Moderate/high nuclear CHIP (n=238)
Negative/low nuclear CHIP (n=503)
Probability of Survival
BCSS (months)
C
p=0.496
Moderate/high cytoplasmic CHIP (n=306)
Negative/low cytoplasmic CHIP (n=431)
Probability of Survival
BCSS (months)
C
Relative Expression
76Ntert
16A5
T47D
MCF7
ZR75-1
BT474
SKBR3
HCC1954
UACC812
21NT
21PT
21MT1
21MT2
MDA-MB-231
BT549
MDA-MB-468
MDA-MB-157
Hs578t
ER+
ErbB2+
Triple-Neg
D
Hsc70
CHIP

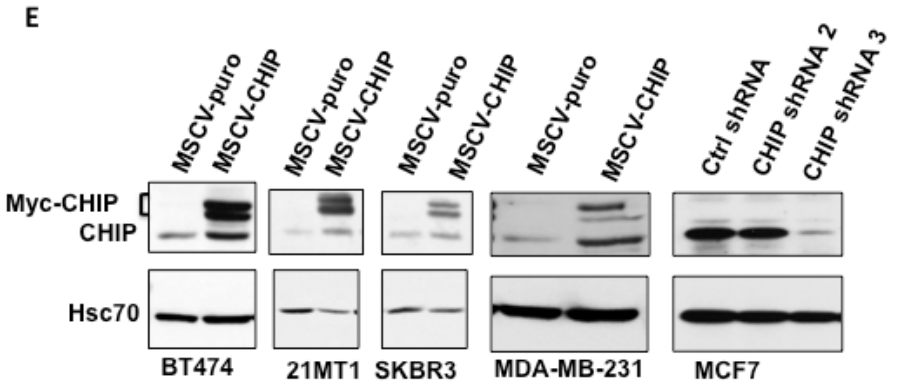
E
MSCV-puro
MSCV-CHIP
MSCV-puro
MSCV-CHIP
MSCV-puro
MSCV-CHIP
MSCV-puro
MSCV-CHIP
Ctrl shRNA
CHIP shRNA 2
CHIP shRNA 3
Myc-CHIP
CHIP
Hsc70
BT474
21MT1
SKBR3
MDA-MB-231
MCF7

Figure 4.2. CHIP overexpression suppresses tumor growth in a mouse xenograft model.

(A) Tumor growth curves in nude mice inoculated with control and $CHIP^{OE}$ BT474 cells. (B) Representative tumors were shown, upper panel from control cells, lower panel from $CHIP^{OE}$ cells. (C) Expression level of CHIP in xenograft tumor cells was analyzed by immunoblotting. (D, E) Sections of tumor from mice injected with control and $CHIP^{OE}$ cells were stained with hematoxylin and eosin (H&E, E) or labeled with Ki67 (brown staining) and cleaved caspase 3 (red staining) (Ki67 and CC3, D). (F, G) Quantification of Ki67 (F) and CC3 (G) positive cells in Figure D and E. Bars represents mean $\pm$ S.D. (n=6).

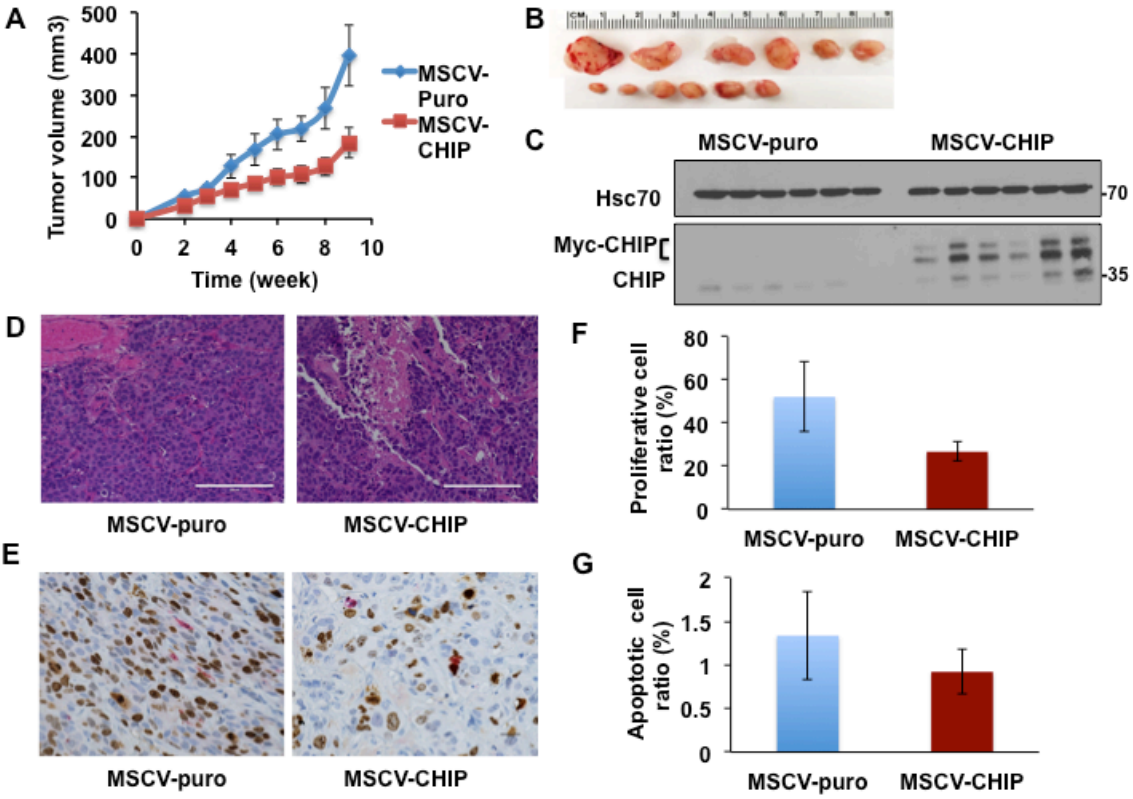
A
Tumor volume (mm3)
500
400
300
200
100
0
0 2 4 6 8 10
Time (week)
MSCV-Puro
MSCV-CHIP
B
C
MSCV-puro
MSCV-CHIP
Hsc70
Myc-CHIP
CHIP
70
35
D
MSCV-puro
MSCV-CHIP
E
MSCV-puro
MSCV-CHIP
F
Proliferative cell ratio (%)
80
60
40
20
0
MSCV-puro
MSCV-CHIP
G
Apoptotic cell ratio (%)
2
1.5
1
0.5
0
MSCV-puro
MSCV-CHIP

Figure 4.3. CHIP overexpression suppresses oncogenesis in ErbB2+ cells.

(A) Accumulative proliferation of control and $CHIP^{OE}$ 21MT1 cells. Growth rate were measured by MTT assay. (B) Decreased anchorage-independent cell growth in $CHIP^{OE}$ cells. Cells were seed in soft agar plates and incubated for 3 weeks. Colonies were stained, imaged and analyzed under microscope. (C, D) Decreased migration and invasion by CHIP overexpression. Cells were seed onto filters with 8-μm pore size in uncoated (C, migration) or Matrigel- coated (D, invasion) upper chambers. Average numbers of cells that migrated or invaded are shown. (E) Decreased extracellular matrix degradation in $CHIP^{OE}$ cells. Cells were seed on top of FITC-labeled gelatin in glass chamber and incubated for 48 hours. Cells were fixed and stained with invadipodia and DAPI and imaged under fluorescent microscope. The black hole represents degraded extracellular matrix. (F) Quantification of degraded extracellular matrix. Data represent mean $\pm$ S.D., n=3.

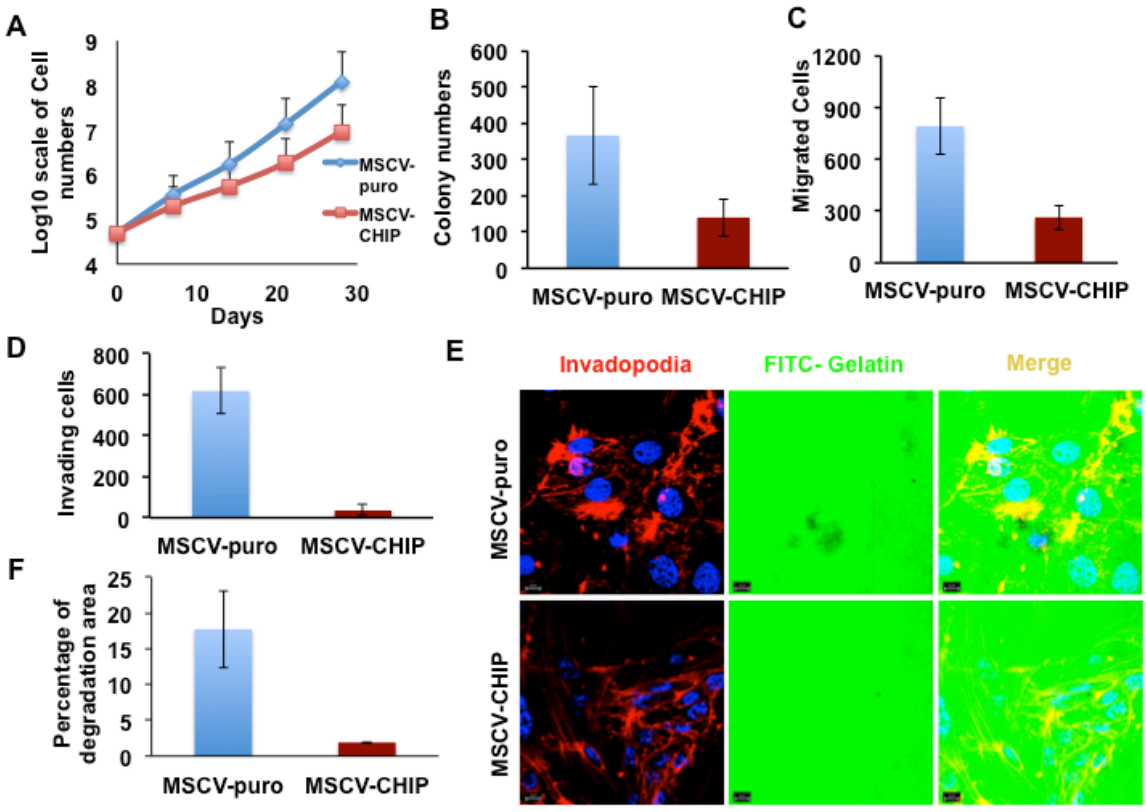
A
Log10 scale of Cell numbers
9
8
7
6
5
4
0
10
20
30
Days
MSCV-puro
MSCV-CHIP
B
Colony numbers
600
500
400
300
200
100
0
MSCV-puro
MSCV-CHIP
C
Migrated Cells
1200
900
600
300
0
MSCV-puro
MSCV-CHIP
D
Invading cells
800
600
400
200
0
MSCV-puro
MSCV-CHIP
E
Invadopodia
FITC- Gelatin
Merge
MSCV-puro
MSCV-CHIP
F
Percentage of degradation area
25
20
15
10
5
0
MSCV-puro
MSCV-CHIP

Figure 4.4. CHIP regulates transcription factor activity and MZF-1 is one of the targets.

(A) Analysis of DNA-binding activities of 345 transcription factors in control vs. $CHIP^{OE}$ ErbB2+ BT474 cell line by Panomics Combo-array (Affymatrix). Y-axis represents log-fold binding in $CHIP^{OE}$ over control cells. MZF-1 is highlighted in red. (B) MZF-1 binding activity decreased in $CHIP^{OE}$ cells. Biotin-labeled MZF-1 consensus DNA sequence was used as probe and loaded with nuclear extracts from $CHIP^{OE}$ and control cells to carry out EMAS. 200 fold higher non-biotin-labeled consensus sequence served as competitor. (C, D) MZF-1 mRNA and protein level decreased in $CHIP^{OE}$ cells. Total RNA was prepared from BT474 cells and MZF-1 mRNA level was quantified using real-time RT-PCRs (C), protein level was analyzed by immunoblotting (D). (E) Ubiquitination and degradation of MZF-1 is induced by CHIP. GFP-tagged MZF-1 and Myc-tagged CHIP (0, 0.5, 4ug) were transfected into HEK293t cells. MZF-1 was immuoprecipitated by using anti-MZF-1 antibody, ubiquitin and MZF-1 was detected in immuoprecipitants (upper panel) and MZF-1, CHIP and Hsc70 were detected in whole cell lysates (lower panel).

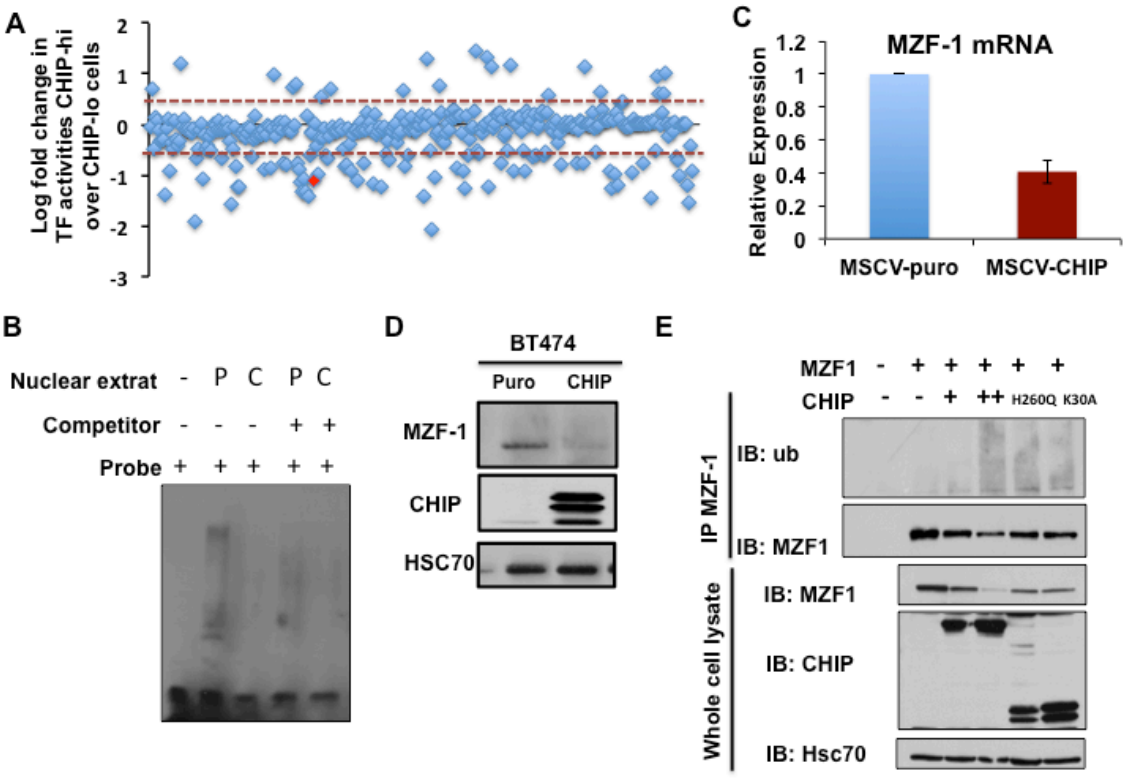
A
Log fold change in TF activities CHIP-hi over CHIP-lo cells
2
1
0
-1
-2
-3
C
MZF-1 mRNA
Relative Expression
1.2
1
0.8
0.6
0.4
0.2
0
MSCV-puro
MSCV-CHIP
B
Nuclear extrat - P C P C
Competitor - - - + +
Probe + + + + +
D
BT474
Puro
CHIP
MZF-1
CHIP
HSC70
E
MZF1 - + + + + +
CHIP - - + ++ H260Q K30A
IP MZF-1
IB: ub
IB: MZF1
Whole cell lysate
IB: MZF1
IB: CHIP
IB: Hsc70

Figure 4.5. CTSB/L is the downstream target of CHIP-MZF-1 axis.

(A) The binding activity of CTSB promoter region is decreased in $CHIP^{OE}$ BT474 cells. Biotin-labeled CTSB promoter region DNA sequence was used as probe and loaded with nuclear extracts from $CHIP^{OE}$ and control cells to carry out EMAS. 200 fold higher non-biotin-labeled consensus sequence served as competitor. (B, C) CTSB/L mRNA and protein level decreased in $CHIP^{OE}$ cells. Total RNA was prepared from BT474 cells and CTSB/L mRNA level was quantified using real-time RT-PCRs (C), protein level was analyzed by immunoblotting. (D) CTSB/L activity decreased in $CHIP^{OE}$ cells. Cells were seed on cover slips and incubated with CTSB/L substrates for 1 hour, fixed and stained with DAPI, imaged were took under fluorescent microscope. Red fluorescence represents CTSB/L cleavage products. (E, F) Quantification of red fluorescence in Figure D. Data represents mean$\pm$ S.D., n=3.

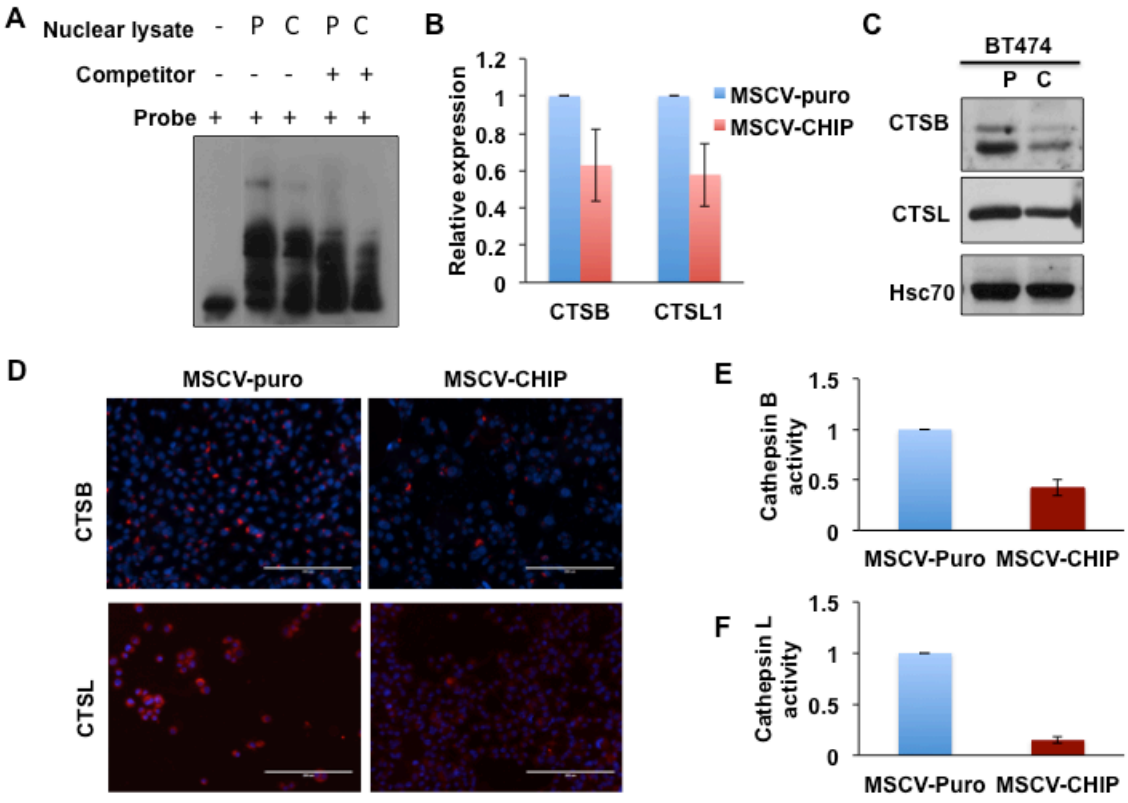
A
Nuclear lysate - P C P C
Competitor - - - + +
Probe + + + + +
B
Relative expression
1.2
1
0.8
0.6
0.4
0.2
0
MSCV-puro
MSCV-CHIP
CTSB
CTSL1
C
BT474
P C
CTSB
CTSL
Hsc70
D
MSCV-puro
MSCV-CHIP
CTSB
CTSL
E
Cathepsin B activity
1.5
1
0.5
0
MSCV-Puro MSCV-CHIP
F
Cathepsin L activity
1.5
1
0.5
0
MSCV-Puro MSCV-CHIP

Figure 4.6. CTSB inhibition decreased ErbB2+ cell progression.

(A) CTSB inhibition decreased extracellular matrix degradation in 21MT1 cells. Cells were seed on top of FITC-labeled gelatin in glass chamber and incubated with DMSO or CA074 for 48 hours. Cells were fixed and stained with invadipodia and DAPI and imaged under fluorescent microscope. The black hole represents degraded extracellular matrix. (B) Quantification of degraded extracellular matrix. Data represent mean $\pm$ S.D., n=3. (C) CTSB inhibition decreased 21MT1 cell invasion. Cells were seed on top of marigel-coated membrane in 96-well plated, and incubated with DMSO or CA074 for 24 hours. Invading cells were trypsinized, stained and read under fluorescent reader. (D) CTSB inhibition decreased tumor growth in xenograft model. BT474 cells were inculcated under fatpad of nude mice. Saline/Trastuzumab was injected through tail vein at the dose of 4mg/kg every four days. CA074 was intraperitoneally injected daily at 25mg/kg. Tumor volumes were monitored every other day. Data represents mean $\pm$ S.E., n=4.

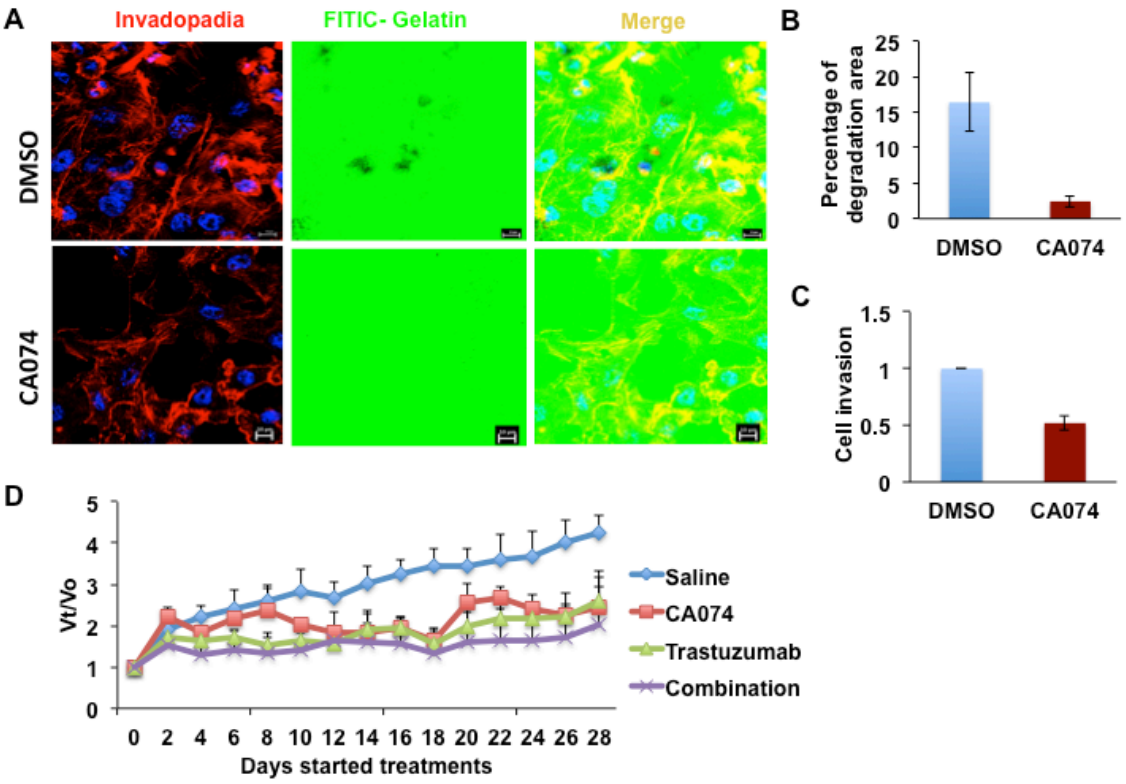
A
Invadopadia
FITIC- Gelatin
Merge
DMSO
CA074
B
Percentage of degradation area
25
20
15
10
5
0
DMSO
CA074
C
Cell invasion
1.5
1
0.5
0
DMSO
CA074
D
Vt/Vo
5
4
3
2
1
0
0 2 4 6 8 10 12 14 16 18 20 22 24 26 28
Days started treatments
Saline
CA074
Trastuzumab
Combination

Table 4.1 The association between Nuclear (N) CHIP and clinicopathological variables in the whole series.

Clinicopathological variables	N-CHIP		
	Negative/ low expression, N (%)	High expression, N (%)	p-value
Age (years)			
<50	231(35.1%)	100(31.8%)	**0.316**
≥50	427(64.9%)	214(68.2%)	
Menopausal status			
Pre	248(37.8%)	121(38.7%)	**0.798**
Post	408(62.2%)	192(61.3%)	
Tumour Size			
<2 CM	89(44.5%)	168(53.5%)	**0.008**
≥2CM	361(55.5%)	146(46.5%)	
Tumour Grade			
1	66(10.2%)	72(22.9%)	**1×10^{-7}**
2	194(29.9%)	126(40.1%)	
3	388(59.9%)	116(36.9%)	
Tubule formation			
1	23(3.7%)	23(7.5%)	**4×10^{-4}**
2	187(29.8%)	117(38.1%)	
3	417(66.5%)	167(54.4%)	
Pleomorphism			
1	11(1.8%)	6(2.0%)	**1×10^{-7}**
2	196(31.4%)	155(50.5%)	
3	418(66.9%)	146(47.6%)	
Mitosis			
1	157(25.0%)	148(48.2%)	**1×10^{-7}**
2	117(18.7%)	63(20.5%)	
3	353(56.3%)	96(31.3%)	
Lymph Node Stage			
1	398(61.4%)	192(61.1%)	**0.558**
2	195(30.1%)	101(32.2%)	
3	55(8.5%)	21(6.7%)	
Lymphovascular invasion (LVI)			
No	418(64.5%)	202(64.5%)	**0.993**
Definite	230(35.5%)	111(35.5%)	
Nottingham Prognostic Index			
Mild	147(23.8%)	126(41.7%)	**1×10^{-7}**
Moderate	368(59.5%)	144(47.7%)	
High	103(16.7%)	32(10.6%0	

Table 4.2: The association between Nuclear (N) CHP and different proteins related to ER and HER2 pathways in the whole series.

	N-CHIP		
	Negative/low expression, N (%)	**High expression, N (%)**	**p-value**
Hormon receptors			
Oestrogen receptor (ER) Negative Positive	 207(31.7%) 447(68.3%)	 44(14.2%) 266(85.8%)	**1×10^{-7}**
Progesterone receptor (PgR) Negative Positive	 296(47.0%) 334(53.0%)	 97(32.1%) 205(67.9%)	**1×10^{-5}**
Androgen receptor (AR) Negative Positive	 272(6.5%) 313(53.5%)	 65(23.7%) 209(76.3%)	**1×10^{-7}**
Triple negative status Non TN TN	 497(78.1%) 139(21.9%)	 276(89.9%) 31(10.1%)	**1×10^{-5}**
Basal phenotype Negative Positive	 528(82.8%) 110(17.2%)	 285(92.5%) 23(7.5%)	**5×10^{-5}**
Other ER related proteins			
CK7/8 Negative Positive	 12(1.9%) 621(98.1%)	 3(1.0%) 297(99.0%)	**0.310**
CK18 Negative Positive	 2(16.2%) 476(83.8%)	 22(7.9%) 258(92.1%)	**0.001**
CK19 Negative Positive	 63(10.2%) 554(89.8%)	 16(5.4%) 283(94.6%)	**0.014**
E-Cadherin Negative Positive	 235(38.1%) 382(61.9%)	 104(35.0%) 193(65.0%)	**0.368**
p-Cadherin Negative Positive	 229(43.8% 294(56.2%)	 144(56.9%) 109(43.1%)	**0.001**
N-Cadherin Negative Positive	 107(22.3%) 372(77.7%)	 78(34.7%) 147(65.3%)	**0.001**
Tumour suppressor proteins			
p53 Negative/low Positive	 423(67.9%) 200(32.1%)	 228(77.3%) 67(22.7%)	**0.003**
BRCA1 Negative/low High	 266(52.3%) 243(47.7%0	 87(34.0%) 169(66.0%)	**2×10^{-6}**
Proliferation markers KI67-LI Negative/low High	 171(33.5%) 339(66.5%)	 138(54.8%) 114(45.2%)	**1×10^{-7}**
Apoptosis related markers BCL2 Negative/low High	 219(44.6%) 272(55.4%)	 71(32.7%) 146(67.3%)	**0.003**

HER family proteins			
HER1 Negative Positive	 482(76.0%) 152(24.0%)	 254(83.6%) 50(16.4%)	**0.009**
HER2 Negative Positive	 521(82.6%) 110(17.4%)	 273(90.7%) 28(9.3%)	**0.001**
HER3 Negative Positive	 44(7.5%) 539(92.5%)	 30(10.8%) 248(89.2%)	**0.112**
HER4 Negative Positive	 65(10.4%) 560(89.6%)	 50(16.4%) 254(83.6%)	**0.009**

Table 4.3 The association between cytoplasmic CHIP and the clinicopathological variables in the whole series

	C-CHIP		
	Negative/low expression, N (%)	High expression, N (%)	p-value
Hormon receptors			
Oestrogen receptor (ER) Negative Positive	 151(28.0%) 388(72.0%)	 98(23.4%) 320(76.6%0	0.110
Progesterone receptor (PgR) Negative Positive	 216(41.7%) 302(58.3%)	 175(43.0%) 232(57.0%)	0.691
Androgen receptor (AR) Negative Positive	 193(40.9%) 279(59.1%)	 142(37.4%) 238(62.6%)	0.296
Triple negative status Non TN TN	 415(79.3%) 108(20.7%)	 352(85.2%) 61(14.8%)	0.020
Basal phenotype	 375(71.0%) 153(29.0%)	 321(77.7%) 92(22.3%)	0.024
CK7/8 Negative Positive	11(2.1%) 509(97.9%)	4(1.0%) 402(99.0%)	0.176
CK18 Negative Positive	78(16.9%) 384(83.1%)	34(9.0%) 345(91.0%)	0.001
CK19 Negative Positive	47(9.3%) 461(90.7%)	31(7.7%) 3709(92.3%)	0.416
E-Cadherin Negative Positive	 186(36.7%) 321(63.3%)	 153(38.3%) 247(61.8%)	0.629
p-Cadherin Negative Positive	 190(46.0%) 223(54.0%)	 182(50.8%) 176(49.2%)	0.180
N-Cadherin Negative Positive	 107(28.1%) 274(71.9%)	 75(23.7%) 242(76.3%)	0.185
p53 Negative/low Positive	 350(68.8%) 159(31.2%)	 297(73.9%) 105(26.1%)	0.091
BRCA1 Negative/low High	 187(45.3%) 226(54.7%)	 165(47.6%) 182(52.4%)	0.532
Proliferation markers KI67-LI Negative/low	 176(41.4%) 249(58.6%)	 130(39.3%) 201(60.7%)	0.553

High			
Apoptosis related markers BCL2 Negative/low High	 165(40.8%) 239(59.2%)	 123(41.3%) 175(58.7%)	 0.908
HER1 Negative Positive	 419(80.0%) 105(20.0%)	 311(76.4%) 96(23.6%)	 0.192
HER2 Negative Positive	 455(87.7%) 64(12.3%)	 333(82.0%) 73(18.0%)	 0.016
HER3 Negative Positive	 50(10.5%) 428(89.5%)	 24(6.4%) 352(93.6%)	 0.036
HER4 Negative Positive	 67(13.0%) 450(87.0%)	 47(11.6%) 358(88.4%)	 0.535

Table 4.4: The list of transcription factors which activity were downregulated by CHIP overexpression in ErbB2+ BT474 cells

.

ACPBP	E12/E47	L-lll BP	NF-E6/CP1
ADD-1	E2	Lactoferrin-BP	NF-Y
ADR-1	EGR-1	LF-A1	NFkB
ALF-1	EKLF	LSF	p-53
alpha-PAL	ETF	LXRF-1	PAX-2
AML-1	Freac-2	MEF-1	PAX-4
ARP	Freac-4	MRE	PAX-5
ATF	GAG	MT-box	PAX-6
ATF adelta	GBF-1/2/3/HY5	MTF	PBGD BP
ATF-a	H4TF-1	MUSF-1	Pbx1
c-Rel	HFH-1	MyoD	PCF
CACC	HFH-3	MZF-1	PEBP-2
CCAAT	HFH-8	NF-1	PPUR
CEBP	HIF-1	NF-1/2	PPUR
CEF-2	HNF-3	NF-4FA	PRDll-BF1
COUP-TF	HNF-4a	NF-Atx	PUR
CTCF	ISGF	NF-E1/YY1	RAR/DR-5
E12	Isl-1	NF-E2	RB

Chapter 5: Conclusions and future directions

5.1 Conclusions

Taken all together, we demonstrated a novel role of E3 ubiquitin ligase CHIP in regulating ErbB2-mediated oncogenesis in breast cancer. Previously our laboratory reported that CHIP was the E3 ligase that mediated ErbB2 degradation upon Hsp90 inhibition. However, further analysis of CHIP KD in cells did not abolish ErbB2 degradation when treated with Hsp90 inhibitor 17AAG. Instead, we observed higher cell surface ErbB2 level in CHIP KD cells. A functional role of CHIP in protein quality control suggested that CHIP may regulate ErbB2 during its maturation. In support of this hypothesis, we show that CHIP downregulates immature ErbB2 by enforcing its ERAD pathway (Figure 5.1). In addition, loss of CHIP promotes an increase in ER stress in ErbB2+ breast cancer cells, which sensitizes these tumor cells to further ER stress induction by a clinically-used drug, the proteasome inhibitor bortezomib. Notably, the combination of bortezomib with trastuzumab, a FDA-proved standard therapeutic monoclonal antibody targeted against ErbB2+ breast cancer, showed synergistic growth inhibition in ErbB2+ breast cancer cells.

Consistent with recent and our clinical studies, which support a tumor suppressor function of CHIP in ErbB2+ breast cancers, we constructed stable CHIP overexpressing breast cancer cell lines and illustrated CHIP as a suppressor of ErbB2+ tumor growth and metastasis in vitro and in vivo. We undertook an extensive clinical-pathological study of an extensively well-annotated breast cancer tissue bank to address the variant conclusions of previous studies on whether CHIP is a prognosticator of poor or better survival (83, 92, 93). Given the size of our study, our findings conclusively demonstrate that loss of CHIP is a key pro-tumor progression adaptation in breast cancer. Importantly, our studies showed that it is the loss of nuclear staining of CHIP, observed in two thirds of ErbB2+ and triple-negative and one third of ER+ patients, that significantly correlated with poor patient outcome, notably increased tumor grade, tumor

size, mitosis, vascular invasion and lower breast cancer-specific survival at 15 years. To explore the mechanism of how nuclear CHIP functions in ErbB2+ breast cancer, we conducted an unbiased screen of DNA-binding activity of 345 transcription factors using a commercial Protein/DNA array. Myeloid zinc finger 1(MZF-1) was identified and validated as one of the direct target of CHIP. Further analysis of MZF-1downstream target genes CTSB/CTSL revealed the novel CHIP-MZF-1-CTSB/CTSL pro-invasion signaling axis recently identified downstream of ErbB2 (145) to be a key pathway controlled by the levels of expression of CHIP in ErbB2+ breast cancer (Figure 5.1). Targeting CTSB by using a specific chemical inhibitor CA074 in an ErbB2+ breast cancer xenograft model demonstrated that targeting MZF1-CTSB/L axis in CHIP-low ErbB2+ breast cancer is a potential therapeutic strategy. Given our findings that MZF-1-CTSB/L axis is also unleashed by loss of CHIP in ER+ breast cancer cells, it is likely that our findings and their therapeutic implications will be directly applicable to other malignancies in which CHIP expression is downregulated as a tumor adaptation. Overall, mechanistic and initial preclinical analyses presented in this thesis should provide a basis for future strategies to improve therapeutics of ErbB2+ and other breast cancers with downregulation of CHIP E3 expression by targeting a novel pathway identified here to be regulated by CHIP.

5.2 Future directions

In this thesis, we investigated the tumor suppressor role of E3 ubiquitin ligase CHIP in ErbB2+ breast cancer. We identified a novel MZF-1-CTSB/L pathway in ErbB2-mediated tumor progression and metastasis from an unbiased transcription factor screen (Figure 4.4A). Aside from MZF1, which was analyzed here, the large subset of analyzed transcription factors that was downregulated by CHIP included HNF-3 (FoxM1) an

important candidate of clinical relevance. FoxM1 overexpression has been linked to EMT, metastasis and resistance to chemotherapy, trastuzumab and lapatinib in ErbB2+ breast cancers (155, 160-163), and is overexpressed in breast tumor tissues. It is reasonable to anticipate that transcription activity of FoxM1 is also regulated by CHIP and its upregulation upon loss of CHIP expression may be a key factor in breast cancer progression. It will be of considerable interest to explore this avenue.

Cancer stem cells (CSCs) have several distinct characteristics, including high metastatic potential, tumor-initiating potential and properties that resemble normal stem cells such as self-renewal, differentiation and chemotherapy drug efflux (143, 164). Because of these characteristics, CSCs are considered to be responsible for cancer initiation, progression and metastasis. Recently, CHIP was reported to be reduced CSCs in a population of breast cancer cells (165). CHIP depletion resulted in an increased proportion of CSCs among breast cancer cells. The molecular mechanism of how CHIP regulates CSC properties in breast cancer is unknown. However, from our protein/DNA array screening PAX2, c-Myc and p53 transcription factors provide potential candidates as these have been identified to be downregulated by CHIP. These transcription factors are thought to positively regulate CSCs. (166-170). Hence, further validating these factors in breast cancers and performing tumor spheres assays may elucidate the relationship between CHIP and CSCs.

As the link of MZF-1 to breast cancer is relatively new, it will be of great interest to assess the importance of this transcription factor in breast cancer oncogenesis and metastasis using human cell line and genetically-modified mouse models of breast cancer.

Our studies revealed a key role of CHIP in regulating ErbB2 ERAD, but curiously revealed the block to ErbB2 transport to be primarily at the Golgi. It will be of great interest to further examine if indeed the ERAD-associated biochemical cascade is

indeed involved in CIP-dependent degradation of ErbB2 in the ER as well as potentially at the Golgi. Such studies will require fractionation of different pools of ErbB2 and assessment of their CHIP-dependent ubiquitination, and interaction with Hsp90/Hsc70 molecular chaperones as ERAD apparatus.

Finally, it will be of considerable importance to further validate the findings presented here in a broader panel of human breast cancer cell line models and in genetically-modified mouse models where the impact of MZF-1-CTSB/L pro-invasion/metastasis axis can be more critically examined in an environment of an intact immune system in models that show various components of metastatic disease aside from primary tumorigenesis.

Figure 5.1 The working model of how CHIP regulates ErbB2 mediated oncogenesis

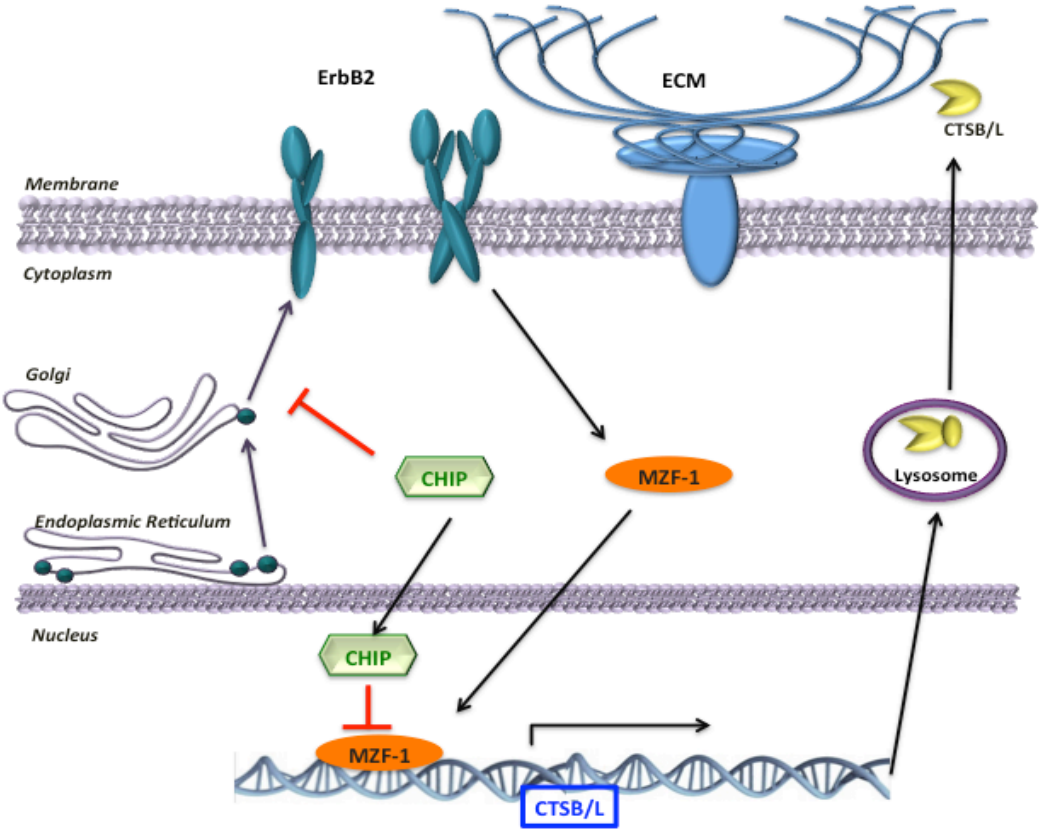
ErbB2
ECM
CTSB/L
Membrane
Cytoplasm
Golgi
CHIP
MZF-1
Lysosome
Endoplasmic Reticulum
Nucleus
CHIP
MZF-1
CTSB/L

Chapter 6: References

References

1. Rapoport TA. Transport of proteins across the endoplasmic reticulum membrane. Science 1992;258(5084):931-6.

2. Singh I, Doms RW, Wagner KR, Helenius A. Intracellular transport of soluble and membrane-bound glycoproteins: Folding, assembly and secretion of anchor-free influenza hemagglutinin. EMBO J 1990;9(3):631-9.

3. Gething MJ, Sambrook J. Transport and assembly processes in the endoplasmic reticulum. Semin Cell Biol 1990;1(1):65-72.

4. Barlowe C. COPII: A membrane coat that forms endoplasmic reticulum-derived vesicles. FEBS Lett 1995;369(1):93-6.

5. Gaynor EC, Emr SD. COPI-independent anterograde transport: Cargo-selective ER to golgi protein transport in yeast COPI mutants. J Cell Biol 1997;136(4):789-802.

6. Hegde RS, Ploegh HL. Quality and quantity control at the endoplasmic reticulum. Curr Opin Cell Biol 2010;22(4):437-46.

7. Hershko A. Ubiquitin: Roles in protein modification and breakdown. Cell 1983;34(1):11-2.

8. Peng J, Schwartz D, Elias JE, et al. A proteomics approach to understanding protein ubiquitination. Nat Biotechnol 2003;21(8):921-6.

9. Xu M, Skaug B, Zeng W, Chen ZJ. A ubiquitin replacement strategy in human cells reveals distinct mechanisms of IKK activation by TNFalpha and IL-1beta. Mol Cell 2009;36(2):302-14.

10. Deshaies RJ, Joazeiro CA. RING domain E3 ubiquitin ligases. Annu Rev Biochem 2009;78:399-434.

11. Ye Y, Rape M. Building ubiquitin chains: E2 enzymes at work. Nat Rev Mol Cell Biol 2009;10(11):755-64.

12. Hochstrasser M. Lingering mysteries of ubiquitin-chain assembly. Cell 2006;124(1):27-34.

13. Finley D. Recognition and processing of ubiquitin-protein conjugates by the proteasome. Annu Rev Biochem 2009;78:477-513.

14. Borissenko L, Groll M. 20S proteasome and its inhibitors: Crystallographic knowledge for drug development. Chem Rev 2007;107(3):687-717.

15. Groll M, Ditzel L, Lowe J, et al. Structure of 20S proteasome from yeast at 2.4 A resolution. Nature 1997;386(6624):463-71.

16. Joo HY, Dai Q, Jones AE, Zhai L, Wang H. In vitro and in vivo assays for studying histone ubiquitination and deubiquitination. Methods Mol Biol 2015;1288:213-30.

17. Richly H, Rape M, Braun S, Rumpf S, Hoege C, Jentsch S. A series of ubiquitin binding factors connects CDC48/p97 to substrate multiubiquitylation and proteasomal targeting. Cell 2005;120(1):73-84.

18. Alexandru G, Graumann J, Smith GT, Kolawa NJ, Fang R, Deshaies RJ. UBXD7 binds multiple ubiquitin ligases and implicates p97 in HIF1alpha turnover. Cell 2008;134(5):804-16.

19. Meyer H. P97 complexes as signal integration hubs. BMC Biol 2012;10:48,7007-10-48.

20. Mayer MP, Bukau B. Hsp70 chaperones: Cellular functions and molecular mechanism. Cell Mol Life Sci 2005;62(6):670-84.

21. Kang PJ, Ostermann J, Shilling J, Neupert W, Craig EA, Pfanner N. Requirement for hsp70 in the mitochondrial matrix for translocation and folding of precursor proteins. Nature 1990;348(6297):137-43.

22. Kampinga HH, Craig EA. The HSP70 chaperone machinery: J proteins as drivers of functional specificity. Nat Rev Mol Cell Biol 2010;11(8):579-92.

23. Rudiger S, Germeroth L, Schneider-Mergener J, Bukau B. Substrate specificity of the DnaK chaperone determined by screening cellulose-bound peptide libraries. EMBO J 1997;16(7):1501-7.

24. Schlecht R, Erbse AH, Bukau B, Mayer MP. Mechanics of Hsp70 chaperones enables differential interaction with client proteins. Nat Struct Mol Biol 2011;18(3):345-51.

25. Marcinowski M, Holler M, Feige MJ, Baerend D, Lamb DC, Buchner J. Substrate discrimination of the chaperone BiP by autonomous and cochaperone-regulated conformational transitions. Nat Struct Mol Biol 2011;18(2):150-8.

26. Muller P, Ruckova E, Halada P, et al. C-terminal phosphorylation of Hsp70 and Hsp90 regulates alternate binding to co-chaperones CHIP and HOP to determine cellular protein folding/degradation balances. Oncogene 2013;32(25):3101-10.

27. Smith DF, Toft DO. Minireview: The intersection of steroid receptors with molecular chaperones: Observations and questions. Mol Endocrinol 2008;22(10):2229-40.

28. Borkovich KA, Farrelly FW, Finkelstein DB, Taulien J, Lindquist S. Hsp82 is an essential protein that is required in higher concentrations for growth of cells at higher temperatures. Mol Cell Biol 1989;9(9):3919-30.

29. Young JC, Moarefi I, Hartl FU. Hsp90: A specialized but essential protein-folding tool. J Cell Biol 2001;154(2):267-73.

30. Welch WJ, Feramisco JR. Purification of the major mammalian heat shock proteins. J Biol Chem 1982;257(24):14949-59.

31. Csermely P, Schnaider T, Soti C, Prohaszka Z, Nardai G. The 90-kDa molecular chaperone family: Structure, function, and clinical applications. A comprehensive review. Pharmacol Ther 1998;79(2):129-68.

32. Langer T, Rosmus S, Fasold H. Intracellular localization of the 90 kDA heat shock protein (HSP90alpha) determined by expression of a EGFP-HSP90alpha-fusion protein in unstressed and heat stressed 3T3 cells. Cell Biol Int 2003;27(1):47-52.

33. Felts SJ, Owen BA, Nguyen P, Trepel J, Donner DB, Toft DO. The hsp90-related protein TRAP1 is a mitochondrial protein with distinct functional properties. J Biol Chem 2000;275(5):3305-12.

34. Dai C, Whitesell L. HSP90: A rising star on the horizon of anticancer targets. Future Oncol 2005;1(4):529-40.

35. Whitesell L, Lindquist SL. HSP90 and the chaperoning of cancer. Nat Rev Cancer 2005;5(10):761-72.

36. Prigent SA, Lemoine NR. The type 1 (EGFR-related) family of growth factor receptors and their ligands. Prog Growth Factor Res 1992;4(1):1-24.

37. Warren CM, Landgraf R. Signaling through ERBB receptors: Multiple layers of diversity and control. Cell Signal 2006;18(7):923-33.

38. Siegel PM, Dankort DL, Hardy WR, Muller WJ. Novel activating mutations in the neu proto-oncogene involved in induction of mammary tumors. Mol Cell Biol 1994;14(11):7068-77.

39. Peles E, Yarden Y. Neu and its ligands: From an oncogene to neural factors. Bioessays 1993;15(12):815-24.

40. Riese DJ,2nd, Stern DF. Specificity within the EGF family/ErbB receptor family signaling network. Bioessays 1998;20(1):41-8.

41. Baulida J, Kraus MH, Alimandi M, Di Fiore PP, Carpenter G. All ErbB receptors other than the epidermal growth factor receptor are endocytosis impaired. J Biol Chem 1996;271(9):5251-7.

42. Tzahar E, Yarden Y. The ErbB-2/HER2 oncogenic receptor of adenocarcinomas: From orphanhood to multiple stromal ligands. Biochim Biophys Acta 1998;1377(1):M25-37.

43. Normanno N, Selvam MP, Qi CF, et al. Amphiregulin as an autocrine growth factor for c-ha-ras- and c-erbB-2-transformed human mammary epithelial cells. Proc Natl Acad Sci U S A 1994;91(7):2790-4.

44. Yarden Y, Pines G. The ERBB network: At last, cancer therapy meets systems biology. Nat Rev Cancer 2012;12(8):553-63.

45. Komatsu M, Yee L, Carraway KL. Overexpression of sialomucin complex, a rat homologue of MUC4, inhibits tumor killing by lymphokine-activated killer cells. Cancer Res 1999;59(9):2229-36.

46. Chaturvedi P, Singh AP, Batra SK. Structure, evolution, and biology of the MUC4 mucin. FASEB J 2008;22(4):966-81.

47. Workman HC, Sweeney C, Carraway KL,3rd. The membrane mucin Muc4 inhibits apoptosis induced by multiple insults via ErbB2-dependent and ErbB2-independent mechanisms. Cancer Res 2009;69(7):2845-52.

48. Zheng YS, Tong TJ. The effect of epidermal growth factor on the expression of erb B2/neu oncogene in mouse embryo fibroblast cells. Shi Yan Sheng Wu Xue Bao 1992;25(4):413-6.

49. Jepson S, Komatsu M, Haq B, et al. Muc4/sialomucin complex, the intramembrane ErbB2 ligand, induces specific phosphorylation of ErbB2 and enhances expression of p27(kip), but does not activate mitogen-activated kinase or protein kinaseB/Akt pathways. Oncogene 2002;21(49):7524-32.

50. Ramsauer VP, Carraway CA, Salas PJ, Carraway KL. Muc4/sialomucin complex, the intramembrane ErbB2 ligand, translocates ErbB2 to the apical surface in polarized epithelial cells. J Biol Chem 2003;278(32):30142-7.

51. Fox SB, Harris AL. The epidermal growth factor receptor in breast cancer. J Mammary Gland Biol Neoplasia 1997;2(2):131-41.

52. Di Marco E, Pierce JH, Fleming TP, et al. Autocrine interaction between TGF alpha and the EGF-receptor: Quantitative requirements for induction of the malignant phenotype. Oncogene 1989;4(7):831-8.

53. Siegel PM, Ryan ED, Cardiff RD, Muller WJ. Elevated expression of activated forms of Neu/ErbB-2 and ErbB-3 are involved in the induction of mammary tumors in transgenic mice: Implications for human breast cancer. EMBO J 1999;18(8):2149-64.

54. Slamon DJ, Godolphin W, Jones LA, et al. Studies of the HER-2/neu proto-oncogene in human breast and ovarian cancer. Science 1989;244(4905):707-12.

55. Slamon DJ. Studies of the HER-2/neu proto-oncogene in human breast cancer. Cancer Invest 1990;8(2):253.

56. Press MF, Pike MC, Hung G, et al. Amplification and overexpression of HER-2/neu in carcinomas of the salivary gland: Correlation with poor prognosis. Cancer Res 1994;54(21):5675-82.

57. Gusterson BA, Gullick WJ, Venter DJ, et al. Immunohistochemical localization of c-erbB-2 in human breast carcinomas. Mol Cell Probes 1987;1(4):383-91.

58. Krainer M, Brodowicz T, Zeillinger R, et al. Tissue expression and serum levels of HER-2/neu in patients with breast cancer. Oncology 1997;54(6):475-81.

59. Andrulis IL, Bull SB, Blackstein ME, et al. neu/erbB-2 amplification identifies a poor-prognosis group of women with node-negative breast cancer. toronto breast cancer study group. J Clin Oncol 1998;16(4):1340-9.

60. Paterson MC, Dietrich KD, Danyluk J, et al. Correlation between c-erbB-2 amplification and risk of recurrent disease in node-negative breast cancer. Cancer Res 1991;51(2):556-67.

61. Gullick WJ, Love SB, Wright C, et al. c-erbB-2 protein overexpression in breast cancer is a risk factor in patients with involved and uninvolved lymph nodes. Br J Cancer 1991;63(3):434-8.

62. Matsushita C, Tamagaki H, Miyazawa Y, Aimoto S, Smith SO, Sato T. Transmembrane helix orientation influences membrane binding of the intracellular juxtamembrane domain in neu receptor peptides. Proc Natl Acad Sci U S A 2013;110(5):1646-51.

63. Kwong KY, Hung MC. A novel splice variant of HER2 with increased transformation activity. Mol Carcinog 1998;23(2):62-8.

64. Chan R, Muller WJ, Siegel PM. Oncogenic activating mutations in the neu/erbB-2 oncogene are involved in the induction of mammary tumors. Ann N Y Acad Sci 1999;889:45-51.

65. Ballinger CA, Connell P, Wu Y, et al. Identification of CHIP, a novel tetratricopeptide repeat-containing protein that interacts with heat shock proteins and negatively regulates chaperone functions. Mol Cell Biol 1999;19(6):4535-45.

66. Lamb JR, Tugendreich S, Hieter P. Tetratrico peptide repeat interactions: To TPR or not to TPR? Trends Biochem Sci 1995;20(7):257-9.

67. Meacham GC, Patterson C, Zhang W, Younger JM, Cyr DM. The Hsc70 co-chaperone CHIP targets immature CFTR for proteasomal degradation. Nat Cell Biol 2001;3(1):100-5.

68. McDonough H, Patterson C. CHIP: A link between the chaperone and proteasome systems. Cell Stress Chaperones 2003;8(4):303-8.

69. Demand J, Alberti S, Patterson C, Hohfeld J. Cooperation of a ubiquitin domain protein and an E3 ubiquitin ligase during chaperone/proteasome coupling. Curr Biol 2001;11(20):1569-77.

70. Murata S, Minami Y, Minami M, Chiba T, Tanaka K. CHIP is a chaperone-dependent E3 ligase that ubiquitylates unfolded protein. EMBO Rep 2001;2(12):1133-8.

71. Jiang J, Ballinger CA, Wu Y, et al. CHIP is a U-box-dependent E3 ubiquitin ligase: Identification of Hsc70 as a target for ubiquitylation. J Biol Chem 2001;276(46):42938-44.

72. Cyr DM, Hohfeld J, Patterson C. Protein quality control: U-box-containing E3 ubiquitin ligases join the fold. Trends Biochem Sci 2002;27(7):368-75.

73. Wang X, DeFranco DB. Alternative effects of the ubiquitin-proteasome pathway on glucocorticoid receptor down-regulation and transactivation are mediated by CHIP, an E3 ligase. Mol Endocrinol 2005;19(6):1474-82.

74. Xu W, Marcu M, Yuan X, Mimnaugh E, Patterson C, Neckers L. Chaperone-dependent E3 ubiquitin ligase CHIP mediates a degradative pathway for c-ErbB2/Neu. Proc Natl Acad Sci U S A 2002;99(20):12847-52.

75. Zhou P, Fernandes N, Dodge IL, et al. ErbB2 degradation mediated by the co-chaperone protein CHIP. J Biol Chem 2003;278(16):13829-37.

76. Belova L, Sharma S, Brickley DR, Nicolarsen JR, Patterson C, Conzen SD. Ubiquitin-proteasome degradation of serum- and glucocorticoid-regulated kinase-1 (SGK-1) is mediated by the chaperone-dependent E3 ligase CHIP. Biochem J 2006;400(2):235-44.

77. Younger JM, Ren HY, Chen L, et al. A foldable CFTR{delta}F508 biogenic intermediate accumulates upon inhibition of the Hsc70-CHIP E3 ubiquitin ligase. J Cell Biol 2004;167(6):1075-85.

78. Alberti S, Bohse K, Arndt V, Schmitz A, Hohfeld J. The cochaperone HspBP1 inhibits the CHIP ubiquitin ligase and stimulates the maturation of the cystic fibrosis transmembrane conductance regulator. Mol Biol Cell 2004;15(9):4003-10.

79. Connell P, Ballinger CA, Jiang J, et al. The co-chaperone CHIP regulates protein triage decisions mediated by heat-shock proteins. Nat Cell Biol 2001;3(1):93-6.

80. Dai Q, Zhang C, Wu Y, et al. CHIP activates HSF1 and confers protection against apoptosis and cellular stress. EMBO J 2003;22(20):5446-58.

81. Page RC, Pruneda JN, Amick J, Klevit RE, Misra S. Structural insights into the conformation and oligomerization of E2~ubiquitin conjugates. Biochemistry 2012;51(20):4175-87.

82. Xu Z, Kohli E, Devlin KI, Bold M, Nix JC, Misra S. Interactions between the quality control ubiquitin ligase CHIP and ubiquitin conjugating enzymes. BMC Struct Biol 2008;8:26,6807-8-26.

83. Kajiro M, Hirota R, Nakajima Y, et al. The ubiquitin ligase CHIP acts as an upstream regulator of oncogenic pathways. Nat Cell Biol 2009;11(3):312-9.

84. Jang KW, Lee KH, Kim SH, et al. Ubiquitin ligase CHIP induces TRAF2 proteasomal degradation and NF-kappaB inactivation to regulate breast cancer cell invasion. J Cell Biochem 2011;112(12):3612-20.

85. Kang SA, Cho HS, Yoon JB, Chung IK, Lee ST. Hsp90 rescues PTK6 from proteasomal degradation in breast cancer cells. Biochem J 2012;447(2):313-20.

86. Schulz R, Marchenko ND, Holembowski L, et al. Inhibiting the HSP90 chaperone destabilizes macrophage migration inhibitory factor and thereby inhibits breast tumor progression. J Exp Med 2012;209(2):275-89.

87. Su CH, Lan KH, Li CP, et al. Phosphorylation accelerates geldanamycin-induced akt degradation. Arch Biochem Biophys 2013;536(1):6-11.

88. Lv Y, Song S, Zhang K, Gao H, Ma R. CHIP regulates AKT/FoxO/Bim signaling in MCF7 and MCF10A cells. PLoS One 2013;8(12):e83312.

89. Paul I, Ahmed SF, Bhowmik A, Deb S, Ghosh MK. The ubiquitin ligase CHIP regulates c-myc stability and transcriptional activity. Oncogene 2013;32(10):1284-95.

90. Bento CF, Fernandes R, Ramalho J, et al. The chaperone-dependent ubiquitin ligase CHIP targets HIF-1alpha for degradation in the presence of methylglyoxal. PLoS One 2010;5(11):e15062.

91. Ferreira JV, Fofo H, Bejarano E, et al. STUB1/CHIP is required for HIF1A degradation by chaperone-mediated autophagy. Autophagy 2013;9(9):1349-66.

92. Jan CI, Yu CC, Hung MC, et al. Tid1, CHIP and ErbB2 interactions and their prognostic implications for breast cancer patients. J Pathol 2011;225(3):424-37.

93. Patani N, Jiang W, Newbold R, Mokbel K. Prognostic implications of carboxyl-terminus of Hsc70 interacting protein and lysyl-oxidase expression in human breast cancer. J Carcinog 2010;9:9,3163.72505.

94. Soga S, Akinaga S, Shiotsu Y. Hsp90 inhibitors as anti-cancer agents, from basic discoveries to clinical development. Curr Pharm Des 2013;19(3):366-76.

95. Ruckova E, Muller P, Nenutil R, Vojtesek B. Alterations of the Hsp70/Hsp90 chaperone and the HOP/CHIP co-chaperone system in cancer. Cell Mol Biol Lett 2012;17(3):446-58.

96. Wang S, Wu X, Zhang J, et al. CHIP functions as a novel suppressor of tumour angiogenesis with prognostic significance in human gastric cancer. Gut 2013;62(4):496-508.

97. Ellgaard L, Helenius A. ER quality control: Towards an understanding at the molecular level. Curr Opin Cell Biol 2001;13(4):431-7.

98. Yoshida Y, Tanaka K. Lectin-like ERAD players in ER and cytosol. Biochim Biophys Acta 2010;1800(2):172-80.

99. Band V, Zajchowski D, Stenman G, et al. A newly established metastatic breast tumor cell line with integrated amplified copies of ERBB2 and double minute chromosomes. Genes Chromosomes Cancer 1989;1(1):48-58.

100. Mirza S, Rakha EA, Alshareeda A, et al. Cytoplasmic localization of alteration/deficiency in activation 3 (ADA3) predicts poor clinical outcome in breast cancer patients. Breast Cancer Res Treat 2013;137(3):721-31.

101. Zhao X, Mirza S, Alshareeda A, et al. Overexpression of a novel cell cycle regulator ecdysoneless in breast cancer: A marker of poor prognosis in HER2/neu-overexpressing breast cancer patients. Breast Cancer Res Treat 2012;134(1):171-80.

102. Britsch S. The neuregulin-I/ErbB signaling system in development and disease. Adv Anat Embryol Cell Biol 2007;190:1-65.

103. Falls DL. Neuregulins and the neuromuscular system: 10 years of answers and questions. J Neurocytol 2003;32(5-8):619-47.

104. Pentassuglia L, Sawyer DB. ErbB/integrin signaling interactions in regulation of myocardial cell-cell and cell-matrix interactions. Biochim Biophys Acta 2013;1833(4):909-16.

105. Emde A, Kostler WJ, Yarden Y, Association of Radiotherapy and Oncology of the Mediterranean arEa (AROME). Therapeutic strategies and mechanisms of tumorigenesis of HER2-overexpressing breast cancer. Crit Rev Oncol Hematol 2012;84 Suppl 1:e49-57.

106. Prat A, Ellis MJ, Perou CM. Practical implications of gene-expression-based assays for breast oncologists. Nat Rev Clin Oncol 2011;9(1):48-57.

107. Dent S, Oyan B, Honig A, Mano M, Howell S. HER2-targeted therapy in breast cancer: A systematic review of neoadjuvant trials. Cancer Treat Rev 2013;39(6):622-31.

108. Larsen PB, Kumler I, Nielsen DL. A systematic review of trastuzumab and lapatinib in the treatment of women with brain metastases from HER2-positive breast cancer. Cancer Treat Rev 2013;39(7):720-7.

109. Bailey TA, Luan H, Clubb RJ, et al. Mechanisms of trastuzumab resistance in ErbB2-driven breast cancer and newer opportunities to overcome therapy resistance. J Carcinog 2011;10:28,3163.90442. Epub 2011 Nov 30.

110. Rexer BN, Arteaga CL. Optimal targeting of HER2-PI3K signaling in breast cancer: Mechanistic insights and clinical implications. Cancer Res 2013;73(13):3817-20.

111. Tsai YC, Weissman AM. The unfolded protein response, degradation from endoplasmic reticulum and cancer. Genes Cancer 2010;1(7):764-78.

112. Carraway KL,3rd. E3 ubiquitin ligases in ErbB receptor quantity control. Semin Cell Dev Biol 2010;21(9):936-43.

113. Fry WH, Simion C, Sweeney C, Carraway KL,3rd. Quantity control of the ErbB3 receptor tyrosine kinase at the endoplasmic reticulum. Mol Cell Biol 2011;31(14):3009-18.

114. Needham PG, Brodsky JL. How early studies on secreted and membrane protein quality control gave rise to the ER associated degradation (ERAD) pathway: The early history of ERAD. Biochim Biophys Acta 2013;1833(11):2447-57.

115. Zuiderweg ER, Bertelsen EB, Rousaki A, Mayer MP, Gestwicki JE, Ahmad A. Allostery in the Hsp70 chaperone proteins. Top Curr Chem 2013;328:99-153.

116. Chavany C, Mimnaugh E, Miller P, et al. p185erbB2 binds to GRP94 in vivo. dissociation of the p185erbB2/GRP94 heterocomplex by benzoquinone ansamycins precedes depletion of p185erbB2. J Biol Chem 1996;271(9):4974-7.

117. Mimnaugh EG, Chavany C, Neckers L. Polyubiquitination and proteasomal degradation of the p185c-erbB-2 receptor protein-tyrosine kinase induced by geldanamycin. J Biol Chem 1996;271(37):22796-801.

118. Xu W, Yuan X, Xiang Z, Mimnaugh E, Marcu M, Neckers L. Surface charge and hydrophobicity determine ErbB2 binding to the Hsp90 chaperone complex. Nat Struct Mol Biol 2005;12(2):120-6.

119. Raja SM, Clubb RJ, Bhattacharyya M, et al. A combination of trastuzumab and 17-AAG induces enhanced ubiquitinylation and lysosomal pathway-dependent ErbB2 degradation and cytotoxicity in ErbB2-overexpressing breast cancer cells. Cancer Biol Ther 2008;7(10):1630-40.

120. Modi S, Saura C, Henderson C, et al. A multicenter trial evaluating retaspimycin HCL (IPI-504) plus trastuzumab in patients with advanced or metastatic HER2-positive breast cancer. Breast Cancer Res Treat 2013;139(1):107-13.

121. Ellgaard L, Helenius A. Quality control in the endoplasmic reticulum. Nat Rev Mol Cell Biol 2003;4(3):181-91.

122. Chauhan D, Singh A, Brahmandam M, et al. Combination of proteasome inhibitors bortezomib and NPI-0052 trigger in vivo synergistic cytotoxicity in multiple myeloma. Blood 2008;111(3):1654-64.

123. Mujtaba T, Dou QP. Advances in the understanding of mechanisms and therapeutic use of bortezomib. Discov Med 2011;12(67):471-80.

124. Brem GJ, Mylonas I, Bruning A. Eeyarestatin causes cervical cancer cell sensitization to bortezomib treatment by augmenting ER stress and CHOP expression. Gynecol Oncol 2013;128(2):383-90.

125. Kato H, Nishitoh H. Stress responses from the endoplasmic reticulum in cancer. Front Oncol 2015;5:93.

126. Li X, Zhang K, Li Z. Unfolded protein response in cancer: The physician's perspective. J Hematol Oncol 2011;4:8,8722-4-8.

127. Okiyoneda T, Barriere H, Bagdany M, et al. Peripheral protein quality control removes unfolded CFTR from the plasma membrane. Science 2010;329(5993):805-10.

128. Ren HY, Patterson C, Cyr DM, Rosser MF. Reconstitution of CHIP E3 ubiquitin ligase activity. Methods Mol Biol 2011;787:93-103.

129. Taxis C, Vogel F, Wolf DH. ER-golgi traffic is a prerequisite for efficient ER degradation. Mol Biol Cell 2002;13(6):1806-18.

130. Rajkumar SV. Myeloma today: Disease definitions and treatment advances. Am J Hematol 2015.

131. Vu T, Sliwkowski MX, Claret FX. Personalized drug combinations to overcome trastuzumab resistance in HER2-positive breast cancer. Biochim Biophys Acta 2014;1846(2):353-65.

132. Hanahan D, Weinberg RA. Hallmarks of cancer: The next generation. Cell 2011;144(5):646-74.

133. Miyata Y, Nakamoto H, Neckers L. The therapeutic target Hsp90 and cancer hallmarks. Curr Pharm Des 2013;19(3):347-65.

134. Neckers L, Neckers K. Heat-shock protein 90 inhibitors as novel cancer chemotherapeutic agents. Expert Opin Emerg Drugs 2002;7(2):277-88.

135. Raja SM, Clubb RJ, Ortega-Cava C, et al. Anticancer activity of celastrol in combination with ErbB2-targeted therapeutics for treatment of ErbB2-overexpressing breast cancers. Cancer Biol Ther 2011;11(2):263-76.

136. Barrott JJ, Haystead TA. Hsp90, an unlikely ally in the war on cancer. FEBS J 2013;280(6):1381-96.

137. Morrow PK, Zambrana F, Esteva FJ. Recent advances in systemic therapy: Advances in systemic therapy for HER2-positive metastatic breast cancer. Breast Cancer Res 2009;11(4):207.

138. Stankiewicz M, Nikolay R, Rybin V, Mayer MP. CHIP participates in protein triage decisions by preferentially ubiquitinating Hsp70-bound substrates. FEBS J 2010;277(16):3353-67.

139. Kundrat L, Regan L. Balance between folding and degradation for Hsp90-dependent client proteins: A key role for CHIP. Biochemistry 2010;49(35):7428-38.

140. Paul I, Ghosh MK. A CHIPotle in physiology and disease. Int J Biochem Cell Biol 2015;58:37-52.

141. Wang J, Bai Y, Li T, Lu Z. DNA microarrays with unimolecular hairpin double-stranded DNA probes: Fabrication and exploration of sequence-specific DNA/protein interactions. J Biochem Biophys Methods 2003;55(3):215-32.

142. Ronnebaum SM, Wu Y, McDonough H, Patterson C. The ubiquitin ligase CHIP prevents SirT6 degradation through noncanonical ubiquitination. Mol Cell Biol 2013;33(22):4461-72.

143. Cicalese A, Bonizzi G, Pasi CE, et al. The tumor suppressor p53 regulates polarity of self-renewing divisions in mammary stem cells. Cell 2009;138(6):1083-95.

144. Wang Y, Ren F, Wang Y, et al. CHIP/Stub1 functions as a tumor suppressor and represses NF-kappaB-mediated signaling in colorectal cancer. Carcinogenesis 2014;35(5):983-91.

145. Rafn B, Nielsen CF, Andersen SH, et al. ErbB2-driven breast cancer cell invasion depends on a complex signaling network activating myeloid zinc finger-1-dependent cathepsin B expression. Mol Cell 2012;45(6):764-76.

146. Deng Y, Wang J, Wang G, et al. p55PIK transcriptionally activated by MZF1 promotes colorectal cancer cell proliferation. Biomed Res Int 2013;2013:868131.

147. Gaboli M, Kotsi PA, Gurrieri C, et al. Mzf1 controls cell proliferation and tumorigenesis. Genes Dev 2001;15(13):1625-30.

148. Tsai LH, Wu JY, Cheng YW, et al. The MZF1/c-MYC axis mediates lung adenocarcinoma progression caused by wild-type lkb1 loss. Oncogene 2014.

149. Weber CE, Kothari AN, Wai PY, et al. Osteopontin mediates an MZF1-TGF-beta1-dependent transformation of mesenchymal stem cells into cancer-associated fibroblasts in breast cancer. Oncogene 2014.

150. Perrotti D, Melotti P, Skorski T, Casella I, Peschle C, Calabretta B. Overexpression of the zinc finger protein MZF1 inhibits hematopoietic development from embryonic stem cells: Correlation with negative regulation of CD34 and c-myb promoter activity. Mol Cell Biol 1995;15(11):6075-87.

151. Withana NP, Blum G, Sameni M, et al. Cathepsin B inhibition limits bone metastasis in breast cancer. Cancer Res 2012;72(5):1199-209.

152. Guo J, Ren F, Wang Y, et al. miR-764-5p promotes osteoblast differentiation through inhibition of CHIP/STUB1 expression. J Bone Miner Res 2012;27(7):1607-18.

153. Rafn B, Kallunki T. A way to invade: A story of ErbB2 and lysosomes. Cell Cycle 2012;11(13):2415-6.

154. Brewster AM, Chavez-MacGregor M, Brown P. Epidemiology, biology, and treatment of triple-negative breast cancer in women of african ancestry. Lancet Oncol 2014;15(13):e625-34.

155. Peake BF, Nahta R. Resistance to HER2-targeted therapies: A potential role for FOXM1. Breast Cancer Manag 2014;3(5):423-31.

156. Tomao F, Papa A, Zaccarelli E, et al. Triple-negative breast cancer: New perspectives for targeted therapies. Onco Targets Ther 2015;8:177-93.

157. Hirshfield KM, Ganesan S. Triple-negative breast cancer: Molecular subtypes and targeted therapy. Curr Opin Obstet Gynecol 2014;26(1):34-40.

158. Liang ZL, Kim M, Huang SM, Lee HJ, Kim JM. Expression of carboxyl terminus of Hsp70-interacting protein (CHIP) indicates poor prognosis in human gallbladder carcinoma. Oncol Lett 2013;5(3):813-8.

159. Wang T, Yang J, Xu J, et al. CHIP is a novel tumor suppressor in pancreatic cancer through targeting EGFR. Oncotarget 2014;5(7):1969-86.

160. Carr JR, Park HJ, Wang Z, Kiefer MM, Raychaudhuri P. FoxM1 mediates resistance to herceptin and paclitaxel. Cancer Res 2010;70(12):5054-63.

161. Chen PM, Cheng YW, Wang YC, Wu TC, Chen CY, Lee H. Up-regulation of FOXM1 by E6 oncoprotein through the MZF1/NKX2-1 axis is required for human papillomavirus-associated tumorigenesis. Neoplasia 2014;16(11):961-71.

162. Francis RE, Myatt SS, Krol J, et al. FoxM1 is a downstream target and marker of HER2 overexpression in breast cancer. Int J Oncol 2009;35(1):57-68.

163. Kambach DM, Sodi VL, Lelkes PI, Azizkhan-Clifford J, Reginato MJ. ErbB2, FoxM1 and 14-3-3zeta prime breast cancer cells for invasion in response to ionizing radiation. Oncogene 2014;33(5):589-98.

164. Korkaya H, Kim GI, Davis A, et al. Activation of an IL6 inflammatory loop mediates trastuzumab resistance in HER2+ breast cancer by expanding the cancer stem cell population. Mol Cell 2012;47(4):570-84.

165. Tsuchiya M, Nakajima Y, Hirata N, et al. Ubiquitin ligase CHIP suppresses cancer stem cell properties in a population of breast cancer cells. Biochem Biophys Res Commun 2014;452(4):928-32.

166. Choijamts B, Jimi S, Kondo T, et al. CD133+ cancer stem cell-like cells derived from uterine carcinosarcoma (malignant mixed mullerian tumor). Stem Cells 2011;29(10):1485-95.

167. Park EK, Lee JC, Park JW, et al. Transcriptional repression of cancer stem cell marker CD133 by tumor suppressor p53. Cell Death Dis 2015;6:e1964.

168. Lawson DA, Bhakta NR, Kessenbrock K, et al. Single-cell analysis reveals a stem-cell program in human metastatic breast cancer cells. Nature 2015;526(7571):131-5.

169. Hou Y, Li W, Sheng Y, et al. The transcription factor Foxm1 is essential for the quiescence and maintenance of hematopoietic stem cells. Nat Immunol 2015;16(8):810-8.

170. Gong AH, Wei P, Zhang S, et al. FoxM1 drives a feed-forward STAT3-activation signaling loop that promotes the self-renewal and tumorigenicity of glioblastoma stem-like cells. Cancer Res 2015;75(11):2337-48.